Wireless Transmission of Power for Sensors in Context Aware Spaces

by

Jorge Ulises Martinez Araiza

B.S. Telecommunications Engineering
National Autonomous University of Mexico (2000)

Submitted to the Program in Media Arts and Sciences, School of Architecture and Planning
in partial fulfillment of the requirements for the degree of

Master of Sciences in Media Arts and Sciences

at the

MASSACHUSETTS INSTITUTE OF TECHNOLOGY

June 2002

Author .....
Program in Media Arts and Sciences, School of Architecture and Planning
May 10, 2002

Certified by .....
Edwin J. Selker
Associate Professor of Media Arts and Sciences
Thesis Supervisor

Accepted by .....
Andrew B. Lippman
Chairperson
Department Committee on Graduate Students

Wireless Transmission of Power for Sensors in Context Aware Spaces

by

Jorge Ulises Martinez Araiza

Submitted to the Program in Media Arts and Sciences, School of Architecture and Planning
on May 10, 2002, in partial fulfillment of the
requirements for the degree of
Master of Sciences in Media Arts and Sciences

Abstract

In the present thesis I create and use wireless power as an alternative to replace wiring and batteries in certain new scenarios and environments. Two specific scenarios will be highlighted and discussed that motivated this research: The Interactive Electromechanical Necklace and the Wireless-Batteryless Electronic Sensors.

The objective is to wirelessly gather energy from one RF source and convert it into usable DC power that is further applied to a set of low-power-demanding electronic circuits. This idea improves the accomplishments of Radio Frequency Identification (RFID) tags systems. The RF-to-DC conversion objective is accomplished by designing and characterizing an element commonly known as a Rectenna, which consists of an antenna and an associated rectification circuitry. The rectenna is fully characterized in this dissertation and it is used for powering electronic lights, sounds, transmitters, and different types of sensors as well.

The wireless power transmission system is presented in the first place with the development of a special set of wearable beads for an interactive necklace. These beads allow physical interaction between the necklace and electronic elements placed in the environment. This scenario demonstrates that passive electronics without batteries are possible. Next I also design and implement low-power sensors that will use the energy delivered from the rectennas to perform active tasks. The switching sensor provides visual/audio feedback to the user when there's a change in the state of the sensed object (i.e. LEDs lit when a stapler runs out of staples); the humidity sensor permits monitoring the humidity in the soil of a flower pot. The sensor actively transmits the information of any of two possible stages (dry soil/humid soil) to its environment. This scenario extends the capabilities of common RFID tags, where not only they transmit information but also can react to their environment in an active fashion.

Thesis Supervisor: Edwin J. Selker
Title: Associate Professor of Media Arts and Sciences

The following people served as readers of this dissertation:

Thesis Reader .....

Joseph Paradiso

Principal Research Scientist

MIT Media Laboratory

Technology Director, Things That Think Consortium

Thesis Reader .....

Yumi Mori

Visiting Scientist

MIT Media Laboratory

Acknowledgments

To **Ted Selker**, for his invaluable guide throughout my graduate studies. It was certainly a short period but it was a significant one. Thank you Ted for sharing your experiences, your thoughts and thanks for those always interesting talks.

To my readers **Joe Paradiso** and **Yumi Mori**. Thank you for the suggestions and invaluable comments. Thanks Joe for the constructive critique. Thanks Yumi for the short but interesting talks and advice.

Thanks to **Matt Reynolds**, for having trusted in me, for your invaluable guide and comments in the always-interesting field of RF. *Gracias* Mr. Reynolds!

To **Barbara Dormady**, **Susan Knightly**, and **Linda Peterson**, infinite thanks for your infinite patience and help. You girls rock!

To the **Media Lab** for being such a unique place, for I realized here that life has a wide variety of interesting colors. To **MIT** for being the top best institute in the world to study Engineering Sciences, also thanks to its professors that with their lectures I have gained a little bit more of knowledge about what to be an engineer means. Special thanks to professor **Jin Au Kong**.

To my beloved **UNAM**, that prepared me for being here. Thanks to **Telmex**, especially to **Carlos Slim**, **Javier Elguea** and many more that made this possible, so we could show that Mexicans also know how to play with Science.

To my teacher, mentor, roommate and friend **Ante Salcedo**. Thanks for having me started into this beautiful world known as Electromagnetic Theory... Maxwell rules!

To the **Mexican Mafia**, also known as the mischievous Pepetl band, for being there in the good ones, the bitter ones and in the other ones: **Ray** the little Dictator, all the **Jorges** and all the **Juanes**, Mr. nicknames **Marquinho**, **Georgina** Pellizcona, **Willy** and his always accurate comments, **Chema** with the characteristic laugh and **Ernestin** with his extreme adventures.

To **Andrea Lockerd**, **Edison Thomaz**, **Surj Patel**, **Win Burleson**, **Teresa Hyun-Yeul Lee** and to those graduate students that slip from my memory, thanks.

To the **Holly Muffin Band**, because no matter what the distance was they always trusted in me and supported me with their emails and talks. **Gustavin**, **Hunter**, **Adriana**, **Edita**, **Saulinho** (**Saul**), **Marcela**, **Waldasco**, **Enriqueta**... long live the *Pumas*!

Thank you so much, **holly muffin**. To my beloved **Keisha**, thanks also.

To my brother, **Omar**, for I have realized here, at the distance, that there is no other single best friend than he. My dear brother, you are the best, I am proud to be your brother, your blood. There are still many experiences to have, and now I know that it doesn't matter how bitter or sweet the future is, because it feels good to know that I can always count on you no matter what.

To my father, **José**, for showing me the way, for his precise comments and because I will never get tired of saying that you are the best father anyone could have had. Some times, a man has to face huge changes in his life, but with guidance such as yours, the path is easier to face. I am proud to be your son, *Papá*.

To my mother, **Teresa**, because no words are enough to describe what I feel, and how grateful I am for all you have given me. To my mother because her tears and laughs always gave me strength to keep going, and because since I was a baby she prepared me for this moment. And there is no slight doubt in my mind that you are the best mom I could have ever asked for, therefore *muchas gracias Ma'*.

To **Ana**, thank you. I will never get tired to say that I am really glad to have met you. I am also glad that we have grown up at the same time, sometimes together and sometimes not. I can't stop marvelling about the things you do and who you are, and I can't stop marvelling myself on how much I have learned to love you. My dear little best friend, *gracias Enana*.

To **Rocio**. Because I may or may not know exactly when, or where, or why, or in which moment I started to love you this much, but the point is that I do. Thank you for everything, for being there and for sometimes not being there, for having given me the hugs, the virtual slaps on the face, for all the advice you gave me, for your voice and all the rest you have shared with me. Thank you for being unique in the world, for being so special, thank you for having accepted me for what I am. Thank you

Rocio, because without you I wouldn't have had the strength to survive some days to accomplish this errand. And maybe I can do steal to the future a piece of a dream, and then maybe inside that little piece these own dreams can fit in. And because the best part of loving you is to know that you have been there, always, *gracias Rocio*.

And, as a few years ago, I won't thank Elvis, neither the Pope nor God.

And it all started here:

$$\nabla\times\overline{H}(\overline{r},t) = \frac{\partial}{\partial t}\overline{D}(\overline{r},t) + \overline{J}(\overline{r},t)$$
$$\nabla\times\overline{E}(\overline{r},t) = -\frac{\partial}{\partial t}\overline{B}(\overline{r},t)$$
$$\nabla\cdot\overline{D}(\overline{r},t) = \rho(\overline{r},t)$$
$$\nabla\cdot\overline{B}(\overline{r},t) = 0$$

Thank you, Mr. Maxwell

Contents

List of Figures

List of Tables

Chapter 1

Introduction

1.1 Motivation

The technological revolution has shown us a future of devices that can integrate disparate Media (voice, data, images, etc.). Moreover, trends flood to the wireless world, where huge amounts of data are transported by electromagnetic waves. Today there is a plethora of such devices; if they don't yet fully cover all the expectations they seem to be on the right track. PDA's, cellular telephones, laptop computers: all these technologies try to integrate and to take advantage of various media.

At the same time, at the Media Lab we talk about and work on new intelligent environments and context-aware spaces, which both try to make human lives easier. These intelligent environments store information and use it afterwards; somewhere they have stored a task user model, and with the help of an external sensor array, they acquire data and create a representation of the ongoing events. This representation is compared to the model that is stored in memory, allowing the system to react accordingly, making the system more context-aware. In other words, these are computers that respond in an implicit way to the user needs, given the context in which they're involved.

From the point of view that new technologies move towards portability, they require the use of an onboard power supply, usually batteries. Batteries have allowed us to build systems that are mobile, and more portability yields, among other things,

less hassle with cables. Running power lines back and forth is usually a demanding task under certain circumstances. It is common these days to run power cords to virtually any electronic system laying on a desk, namely computers, PDA's, etc. Using this idea of wireless power transmission, it is possible to get rid of bulky cords, and also remove the complications associated with the power interconnections and the amount of cables needed.

Nevertheless wiring is the most confusing element of things; also batteries are often the heaviest part and the most difficult to maintain (recharging them or replacing them). We know how to make circuits that are less power consuming, which extends battery life in a significant way. Accordingly, in this thesis the idea of battery-less circuits will be explored, and also the notion of wireless power as an aide to existing power sources will be presented and discussed.

Inside the broad radio electric spectrum, the ISM band (Industrial, Scientific and Medical band located around the 2.4GHz frequency) is very popular given the amount of equipment, services and standards that operate within it: wireless LAN networks (IEEE 802.11), Bluetooth devices, wireless telephones, and even microwave ovens! Today it is of common practice to have a wireless communication system that works in this frequency range: examples range from such diverse environments as universities, offices, and laboratories, even inside homes. Within 2.4GHz, the availability of components is important and their efficiencies have been improved over the years.

Therefore, from this rather strange combination of the need to provide energy to small, low power-demanding devices such as certain types of sensors, and the need to transmit radio frequencies through the air, the motivation for the present thesis work arises: to use RF frequencies, in particular the ISM 2.4GHz band, to transmit and provide power to electronic circuits (i.e. sensors) in a wireless fashion. Even today, systems already use this wireless power transmission concept for RFID tag purposes. An RFID tag is a device that is electronically programmed with unique information, and a base station (reader) retrieves the information from the tag in a wireless fashion. RFID Systems operating within the 2.4GHz band are categorized as

either active or passive. Active RFID tags are powered by an internal battery and are typically read/write. Passive RFID tags operate without a separate external power source and obtain operating power generated from the reader, by converting the RF signal to DC voltage to supply the tag with energy.

1.2 The history of power transmission by Radio Waves

Radio power transmission is defined as a three-step process in which:

- DC electrical power is converted into RF power
- The RF power is then transmitted through space to some distant point
- The power is collected and converted back into DC power at the receiving point.

Because the overall efficiency is necessarily the product of the individual efficiencies associated with the three elements of the system, a premium is placed upon efficiency conversion technology as well as upon aperture-to-aperture transfer efficiency. In many respects the modern history of free space power transmission has been the development of components for the transmitting and receiving ends of the system that have sought to achieve the combined objectives of high efficiency, low cost, high reliability, and low mass.

1.2.1 Early History

Power transmission by radio waves dates back to the early work of Heinrich Hertz [1]. Not only did he demonstrated electromagnetic wave propagation in free space by using a complete system with a spark gap to generate high-frequency power and to detect it at the receiving end, but he also used parabolic reflectors at both he transmitting and receiving ends of the system.

Nikola Tesla carried out his experiments on power transmission by radio waves at the turn of the century [2] [3]. He became interested in the broad concept of resonance

and sought to apply the principle to the transmission of electrical power from one point to another without wires. By means of the alternating surges of current running up and down a mast. Tesla hoped to set up oscillations of electrical energy over large areas of the surface of the Earth, thus generate standing waves into which he would immerse his receiving antennas at the optimum points.

Tesla carried out his first attempt to transmit power without wires at Colorado Springs, Colorado, in 1899. He built a gigantic coil in a large square building over which rose a 200-ft mast with a 3-ft diameter copper ball positioned at the top. The Tesla coil was resonated at a frequency of 150,000 Hz and fed with 300 kW of low-frequency power obtained from the Colorado Springs Electric Company. When the RF output of the Tesla coil was fed to the mast an RF potential was produced on the sphere that approached 100,000,000 V, according to Tesla. Such a high potential with respect to the earth's surface resulted in very long and very visible discharges from the sphere. There is, however, no clear record of how much of this power was radiated into space and whether any significant amount of it was collected at a distant point.

Not until the early 1930's was another attempt made to transmit power without wires, and this time experiments were cautiously made within the confines of a laboratory. This experiment, performed in the Westinghouse Laboratory by H.V. Noble, consisted of identical transmitting and receiving 100 MHz dipoles located about 25 ft from each other. No attempts were made to focus the energy, but several hundred watts of power were transferred between the dipoles.

The major reason for the lack of serious interest in wireless power transmission during the first fifty years of this century was that knowledgeable people realized that efficient point-to-point transmission of power depended upon concentrating the electromagnetic energy into a narrow beam. The only practical manner in which this could be done would be to use electromagnetic energy of very short wavelengths and collect energy over large diameters via optical reflectors or lenses. For the first thirty five years of this century, devices did not exist to provide even a few milliwatts of energy at these wavelengths. Sufficient power was not even available for experimental work in communications and radar systems until the magnetron was developed during

World War II [4].

1.2.2 The modern history

The modern history of free-space power transmission as it relates to microwaves includes not only the development of the technology of microwave power transmission but also several proposed applications, ranging from RFID tags [5] to unmanned vehicles [6].

Another disciplinary consideration are those factors that have confined the frequency used in the development of the technology, and thus far its applications to the 2.4–2.5 GHz band, reserved for industrial, scientific, medical (ISM) application. Although this frequency was originally used because of the designation of the ISM band for experimental purposes and the availability of components there, it is also a frequency where the efficiencies of microwave components are very high. If the Earth's atmosphere is involved, it constitutes an excellent compromise between greater propagation attenuation in heavy rainfall at higher frequencies, and the larger aperture dimensions necessary for efficient transmission at lower frequencies.

1.3 Basic Principles

Besides, modern times present certain facts that motivated the present research. The evolving needs for ubiquitous computing and sensorial spaces could provide a good platform for such types of wireless power transmission systems. A few important driving facts are:

- High frequency electronics are now very accessible, cheap, low power, small and more reliable. In the past, access to this kind of technology was restricted to military industry and high-end companies. Every day, more electronic components are capable of handling radio frequency signals, and high frequencies are now more accessible because the packaged RF front-ends are becoming more transparent to the end users that take advantage of them in the most diverse

applications, from remote-controlled electronic doors up to advanced telecommunication systems.

- The use of low power electronics employing the latest CMOS[1] technology is in evidence almost everywhere. The trend now is to design new Integrated Circuits (IC's) that are extremely low power consuming and, at the same time, powerful and capable of doing complex tasks. Power saving issues arise almost everywhere and the new electronic systems that run with batteries tend to last longer thanks to the low power drain these circuits have.

- From the design point of view, thanks to modern computers and processing capabilities it is relatively easy to design high quality high frequency electronics and, even more, to custom-make antennas that can solve specific problems. In the past such design problems were delegated to research environments and academic institutions, but now there is software that significatively simplifies the design process, where with just a few parameters, complex electronic circuits such as filters and antennas can be designed with a high level of confidence and reliability.

As means of transferring energy from one point to another, beamed microwave power transmission has these features:

- No mass, either in the form of wires or ferrying vehicles, is required between the source of energy and the point of consumption.

- Energy can be transferred at the velocity of light

- The direction of energy transfer can be rapidly changed

- Little energy is lost in the Earth's atmosphere at longer microwave wavelengths

[1]CMOS stands for Complementary Metal-Oxide Semiconductor. Today, CMOS technology is the dominant semiconductor technology for microprocessors, memories and application specific integrated circuits (ASICs). The main advantage of CMOS over NMOS and bipolar technology is the much smaller power dissipation. Unlike NMOS or bipolar circuits, a CMOS circuit has almost no static power dissipation. Power is only dissipated in case the circuit actually switches. This allows to integrate many more CMOS gates on an IC than in NMOS or bipolar technology, resulting in much better performance.

1.3.1 Free space transmission.

The means for transporting the energy through free space by microwaves are the transmitting and receiving apertures. The size and expense of these apertures has a direct relationship to the wavelength that is being used, the distance over which energy is being sent, and the desired efficiency of transmission. Goubau and others [7,8] have derived the following relationship between the aperture to aperture efficiency and a parameter τ given in figure 1-1.

$$\tau = \sqrt{A_t A_r}/\lambda D \tag{1.1}$$

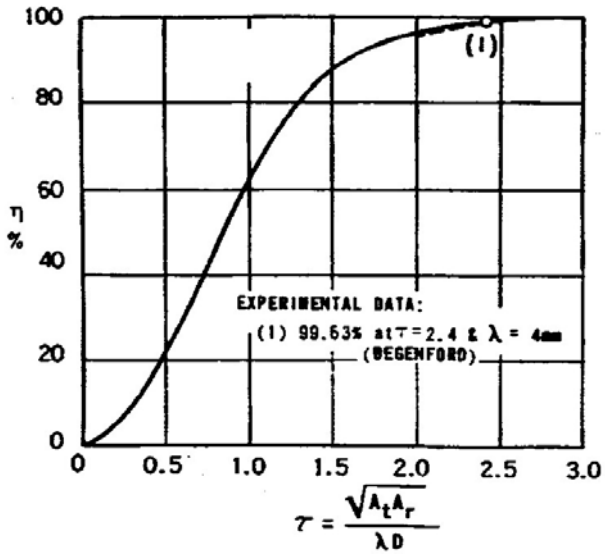

Figure 1-1: Transmission efficiency as a function of the parameter tau.

where

- A_t is the transmitting aperture area
- A_r is the receiving aperture area
- λ is the wavelength of the microwave power being transmitted
- D is the separation distance between the two apertures

From (1.1), a simple expression for the transmitter and receiver aperture areas can be derived with the assumption that the aperture sizes are equal. Under these conditions:

$$A_t = A_r = \tau\lambda D \tag{1.2}$$

This is a revealing expression because it shows that the aperture area, rather than its diameter, varies with wavelength, and the advantages of going to higher frequency are diminished if the aperture areas are approximately equal, as they tend to be for total overall economy.

However, there are applications where the reception area may be limited and where a particular intensity of the incident microwave illumination is desired. Under those circumstances we may use:

$$P_d = A_t P_t / \lambda^2 D^2 \tag{1.3}$$

where

- P_d is the power density at the center of the receiving location
- P_t is the total radiated power from the transmitter
- A_t is the total area of the transmitting antenna
- λ is the wavelength
- D is the separation between the apertures

With this situation it is seen that to achieve a desired value of P_d at the receiver site, while being constrained by a fixed transmitted power P_t, the transmitting aperture area varies as the inverse square of the wavelength of the radiation. For some applications, where the area available for a transmitter is limited, the short wavelengths are very attractive.

1.3.2 Choice of frequency.

If there were complete freedom to select the best frequency for power transmission, the items that would have to be considered are:

1. The size of the aperture as given by expression (1.3).
2. The dependency of overall system efficiency, including the components at the two ends of the system, upon frequency
3. The heat radiation losses associated with the inefficiency of components
4. The losses due to blocking and fading elements in the air
5. The existing state of the art of available components and
6. The impact of the use of the selected frequency upon other users of the electromagnetical spectrum

1.3.3 The rectenna

The rectenna is a unique device that was conceived and developed for beamed microwave power transmission [9]. It is spread out over the receiving aperture area and, as its nature suggests, combines the functions of an antenna and a rectifier. In its simple form, the rectenna consists of a collection of rectenna elements, each composed of a receiving element (usually a half wave dipole) that feeds a low pass filter circuit terminated in a rectifying diode.

The rectenna has many desirable characteristics. They include:

1. In its pure form, a relatively non-directional aperture analogous to that of a single dipole, regardless of the size of the aperture; in this form the aperture collection efficiency is independent of the illumination density distribution across the aperture
2. An overall efficiency from incident microwave power to DC power output that has been measured at over 85% [6]

3. A low specific mass of from 1 to 2 kg per kilowatt of DC power output

4. Relative insensitivity of the overall efficiency to changes in the level of power input or load impedance

5. Small amounts of the critical GaAs material required, less than 1/100 000 of that required for a solar photovoltaic array of the same area.

The term "rectenna" is now used generically for the receiving aperture of any beamed power transmission system that combines the function of capture and rectification, even though in some formats there has been a departure from the "one to one" relationship between dipoles and diodes in the original "pure" form of the device. This departure results in directional sensitivity of the rectenna, which may be tolerated for some applications.

1.4 RFID and WTPS

The Wireless Transmission of Power for Sensors (WTPS) proposed in the present dissertation improves common RFID systems, now they can have sensors, computation, and effectors. It is thus worth establishing the similarities and differences.

WTPS allows the existence of active elements (sensors) thanks to higher power densities in comparison to the classic RFID systems. The raly of information can be made in a different frequency band from that where the RF power is located. RFID systems generally respond by modulating the reflection coefficient of their antenna. Also, WTPS is centered around the far-field transmission principle, whereas RFID is classically located in the near field region.

The proposed WTPS system and an RFID system are similar because both systems collect energy from the environment. Also they can provide a base station with useful information (identification number) about the user. Finally both use Rectennas as the transducer element between RF energy and DC power.

1.5 Thesis Objectives

This thesis has developed both the system that gathers the wireless power and the sensors that will use this power to monitor certain environment variables, these devices will not be limited to just store and identity operations, as with the RFID tags. So for starters, the design of an antenna system that gathers the RF energy from the environment and transforms it to DC power will be designed, constructed, and extensively analyzed. The metrics to be analyzed are the amount of power delivered to a given load and the conversion efficiency (defined as the amount of RF power present at the receiver over DC power measured in the rectenna terminals). Chapter 2 will give a general theoretical background that is needed to understand the proposed system in more detail. Chapter 3 will present in full detail the design-ruling physics (equations) used for the development of the wireless power system, from the relations utilized in the design of the microstrip antenna to basic concepts of signal rectification using diodes. Chapter 4 presents all the experimental results obtained from the implementation and realization of the rectenna system. Finally, Chapter 5 presents the user scenarios with which the system was deployed and tested and discusses sensors used within these scenarios. Chapter 6 gives the conclusions and future work proposals for the Wireless Transmission of Power concepts.

Chapter 2

Theoretical Background

2.1 Classification of wireless systems

In the broadest sense, a wireless system allows the communication of information between two points without the use of a wired connection. This may be accomplished using sonic, infrared, optical, or radio frequency energy. While early television remote controllers used ultrasonic signals, very low data rates and poor immunity to interference make such systems a poor choice for modern applications. Infrared signals can provide moderate data rates, but the fact that infrared radiation is easily blocked by even small obstructions limits its use to short range indoor applications such as remote controllers and local area data links. Similarly, optical signals propagating in an unobstructed environment can provide moderate to high data rates, but require a line-of-sight path, and cannot be used where dust, foliage, or fog can block the signal. For these reasons, most modern wireless systems rely on RF and microwave signals, usually in the UHF (100MHz) to millimeter wave (30GHz) frequency range. Because of spectrum crowding and the need for higher bandwidth, the trend is to use higher frequencies, so that the majority of wireless systems today operate at frequencies ranging from about 800MHz to a few gigahertz. RF and microwave signals offer wide bandwidths, and have the added advantage of being able to penetrate fog, dust, foliage, and even buildings and vehicles to some extent.

One way to categorize wireless systems is according to the nature and placement

Wireless System	Operating Frequency
Advanced Mobile Phone Service (AMPS)	T: 824-849MHz R: 869-894MHz
Global System Mobile (European GSM)	T: 880-915MHz R: 925-960MHz
Personal Communication Services (PCS)	T: 1710-1785MHz R: 1805-1880MHz
US Paging	931-932MHz
Global Positioning Satellite (GPS)	L1: 1575.42MHz L2: 1227.60MHz
Direct Broadcast Satellite (DBS)	11.7-12.5GHz
Wireless Local Area Networks (WLANs)	902-928MHz 2.400-2.484GHz 5.725-5.850GHz
Local Multipoint Distribution Service (LMDS)	28GHz
US Industrial, Medical, and Scientific bands (ISM)	902-928MHz 2.400-2.484GHz 5.725-5.850GHz

Table 2.1: Wireless System Frequencies

of the users. In a point-to-point radio system, a single transmitter communicates with a single receiver. Such systems generally use high-gain antennas in fixed positions to maximize received power and minimize interference with other radios that may be operating nearby in the same frequency range. Point-to-point radios are generally used for dedicated data communications by utility companies and for connection of cellular phone sites to a central switching office. Point-to-multipoint systems connect a central station to a large number of possible receivers. The most common examples are commercial AM and FM broadcasting radio and broadcast television. Multipoint-to-multipoint systems allow simultaneous communication between individual users (who may not be in fixed locations).

Wireless systems can be grouped according to their operating frequency. Table 2.1 lists the operating frequencies of some of the most common wireless systems.

2.1.1 Wireless Local Area Networks

Wireless local area networks (WLANs) provide connections between computers over short distances. Typical indoor applications may be in hospitals, office buildings, and factories, where coverage distances are usually less than a few hundred feet. Outdoors, in the absence of obstructions and with the use of high gain antennas, ranges up to a few miles can be obtained. Wireless networks are especially useful when it is impossibly or prohibitively expensive to place wiring in or between buildings, or when only temporary access is needed between computers. Mobile computer users, of course, can only be connected to a computer network by a wireless link.

Currently most commercial WLAN products in the United States operate in the Industrial, Scientific, and Medical (ISM) frequency bands, and use either frequency-hopping or direct-sequence spread spectrum techniques in accordance with IEEE standard 802.11. Maximum bit rates range from 1 to 2 Mbps, which are much slower than the data rates that can be achieved with wired Ethernet lines.

2.1.2 Radio Frequency Identification (RFID)

Radio Frequency Identification (RFID) systems are used for inventory tracking, shipping, toll collection, personal security access, and other functions. As an example, available now in several cities, automatic toll collection (ATC) uses a small transponder in an automobile that can be interrogated by an RF system mounted at the entrance of a highway or bridge. The transponder provides the vehicle's account number, which is then debited, and a monthly bill sent to the driver. RFID systems are much more specialized than cellular or WLAN systems, and use a wide range of modulation methods, operating frequencies, and duplexing schemes.

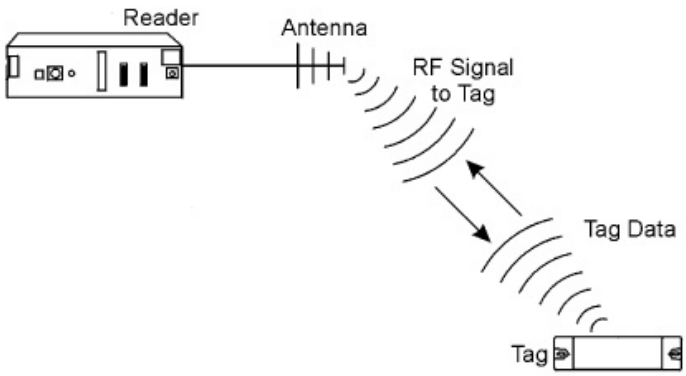

Figure 2-1: Basic Principle of microwave RFID Systems

2.2 2450 MHz RFID Systems

2.2.1 Operating Principle

Microwave RFID systems have been in widespread use for over 10 years in transportation applications (rail car tracking, toll collection and vehicular access control). Systems operating in the UHF and microwave regions are divided between "active power" and "passive power" tags. Operational range and functionality can be extended with active power (a battery in the tag), and passive power provides extended life and lower costs. In the past, microwave RFID tags have been relatively complex and expensive because of the challenge of processing microwave signals with CMOS integrated circuits. This barrier of tag construction simplification has been overcome, and the majority of present microwave RFID systems for article tracking use a single integrated circuit and passive power. This has positive implications on cost, lifetime, and environmental situation. The basic operating principle of 2450 MHz RFID systems is energy and data transmission using propagating radio signals ("E" field transmission). A basic diagram of a microwave RFID system is shown in 2-1. This is exactly the same principle as used in long-range radio communication systems. An antenna on the reader generates a propagating radio wave, which is received by the antenna in the tag. A passive power tag converts the signal to DC voltage to supply the tag with energy. Data transmission from the reader to the tag is done by changing one parameter of the transmitting field (amplitude, frequency or phase).

The return transmission from the tag is accomplished by changing the load of the tag's antenna (amplitude and/or phase). In this context, the microwave, 13.56 MHz and < 135 kHz systems use the same principle. For microwave RFID systems, this method is called modulated backscatter. Alternatively, a signal of different frequency can be generated, modulated, and transmitted to the reader. These later types of systems are referred to as using "active RF transmitter" tags.

Differing from inductive RFID systems (13.56 MHz and also < 135 kHz), UHF systems and microwave RFID systems operate in the "far field" of the reader transmission antenna. Achievable operating distances 0.5 to 12 meters is possible for passive power tags and beyond 30 meters for active power tags depending on microwave frequency, regional regulations, and antenna details (for single reader antenna configurations). Since the systems operate with the tags in the far field of the reader antennas, the field strength decreases with the first exponent of the distance, which means that the required transmission power increases with the second exponent of the distance. Limitations are set by regulations. As a reference value and depending on the chip technology, power consumption and data rate used, a passive 2.45 GHz tag at 4 W ERP (Effective Radiated Power) yield some 0.5-1 meter range and active tags range approx. up to 15-20 meter with standard power readers.

UHF and microwave signals are attenuated and reflected by materials containing water or human tissue, and are reflected by metallic objects. Unlike inductive RFID systems, it is possible to design tags that work flat on metallic objects. Line of sight transmission is not required for operation. UHF and microwave signals easily penetrate wood, paper, cardboard, clothing, paint, dry, dirt, and similar materials. Additionally, because of the short wavelength of the radio signal and reflective properties of metallic objects, reader systems can be designed to have high reliability in regions with high metallic object content.

2.2.2 Typical Tags

Today 2450 MHz tags are available in many different shapes and with different functionality, influenced by the applications' requirements. Unlike inductive RFID tags,

which require substantial surface area, many turns of wire, or magnetic core material to collect the magnetic field, UHF and microwave tags can be very small requiring length in only one dimension. Thus, in addition to having longer range over the inductive systems, the UHF and microwave tags can be easier to package and come in a wider variety of configurations. Tag lengths of 2 to 10 cm are typical. The tag's thickness is limited only by the thickness of the chip as the antenna can be fabricated on thin flexible materials. Since tags operating in the E field do not require antennas with extremely low impedances, inexpensive flexible antennas able to withstand considerable bending are achievable.

Shape

Two main classes for 2450 MHz tags can be found:

- Rigid industrial tags for logistical purposes
- Thin and flexible smart label RFID products (also disposable products)

The expectation is that all different types of tags will also be used in future. It is one of the benefits of 2450 MHz that many different shapes and sizes can be realized. An additional benefit for article tracking and supply chain applications is that UHF and microwave tags are widely used in the transportation function and thus a single reader system can read tags on rail cars, inter-modal containers, trucks, trailers and automobiles as well as parcels, packages, garments, pallets, boxes and the like.

2.2.3 Regulations

Most express delivery services, for example, use handheld terminals than can scan bar codes on packages and relay information to a central station. Compared to barcode, the impact of regulations is much greater for RFID. There are two areas that have to be considered:

Frequency	Electric Field	Magnetic Field	Power Density
125 kHz	614 V/m	130 A/m	
13.56 MHz	136 V/m	1.2 A/m	
915 MHz	-	-	3 mW/cm^2
2450 MHz	-	-	8 mW/cm^2

Table 2.2: Frequency Limits for RFID systems

Human safety

In the area of human safety compliance to the most important safety standards (world-wide) has been verified by leading manufacturers. This has been done for UHF and microwave systems as well as proximity and vicinity systems operating at 13.56 MHz. RFID systems of all frequencies can be used without any doubts or reservations and provides a safe means of RFID application. In simple words, it has been demonstrated that system performance is not linited significantly by today's radiation safety regulations and technology capabilities.

There are many standards in place. In the US, the standard ANSI C95.1-1991 was reaffirmed in 1997 and is presently undergoing revision. The latest standard is IEEE Standard C95.1, 1999 Edition that reaffirms and updates the ANSI standard and is summarized here. The standards have many facets, but the basic premise is that no adverse effects occur at a specific absorption rate (SAR) level of 4 W/kg. A safety factor of 10 is provided for 'occupational environments' and 50 for the general public. The SAR is the rate at which energy is absorbed by the human body from electromagnetic waves. The standard covers all frequencies of interest for RFID.

The standards also list the strengths of the fields permitted at the various frequencies, derived from the allowed SAR values. Table 2.2 lists the limits for several frequencies of interest (using the occupational limits):

In EUROPE, the EU Commission has issued on July 12th a Council Recommendation for the general public on the limitation on EM Fields and specified basic restrictions and reference levels. Either the reference levels or the basic restrictions must be met.

The basic restrictions for localized SAR between 100 kHz and 10 GHz is 2 W/kg

for 'head and trunk' and 4 W/kg for 'limbs'.

Frequency (f)	Electric Field (V/m)	Magnetic Field (A/m)
3 – 150 kHz	87	5
0.15 – 1 MHz	87	0.73/f
1 – 10 MHz	$87/f^{1/2}$	0.73/f
10 - 400 MHz	28	0.073
400 - 2000 MHz	$1.375f^{1/2}$	$0.0037f^{1/2}$
2 – 300 GHz	61	0.16

Table 2.3: Limits for several frequency bands

Radiation (to ensure proper use of the spectrum)

In general RFID technology does not yet face harmonized international regulations (as legislation is still an issue of the different local authorities). However, 2450MHz is one of the most advanced frequencies in terms of this allocation and harmonization process, thus offering global use under different environmental (e.g. noise level) and regulatory conditions. Operation is possible in the UHF and/or microwave regions worldwide. Operation is possible under both unlicensed and licensed conditions.

This is a short summary of the regulatory situation for radiation limits at 2450 MHz:

United States: FCC 15.247

- Frequency : 902-928 MHz, 2400-2483.5 MHz, 5725-5850 MHz
- Transmitter power : 1 W
- Antenna gain : 6 dBi
- Resulting EIRP maximum : +36 dBm
- Communication protocol : spread spectrum, DSSS or FHSS
- Licensing : unlicensed

FCC Sub Part M, 90.350-90.357

- Frequency : 902-904, 909.75-921.25 MHz
- Maximum EIRP : 30 W
- Licensing : licensed

Performance

Ranges of 0.5 to 5 meters from a single antenna are typical for passive power UHF and microwave RFID systems. The ranges of the UHF (915 MHz) systems are generally longer than the microwave systems (2450 MHz) because the wavelength is longer at the lower frequency (equation 1.3), antennas collect more energy, and parasitic effects are lower.

Compared to the low frequency inductive systems, the UHF and microwave systems can have longer range, higher data rates, smaller antennas, and more flexibility in form factors and antenna designs. On the other hand tolerance to object penetration and reading range under no-line-of-site conditions can be better with inductive systems. Date Rates with active UHF and Microwave systems are higher than inductive systems, whereas with passive systems, the difference might not be significant.

2.3 The Radio Link and The Friis equation

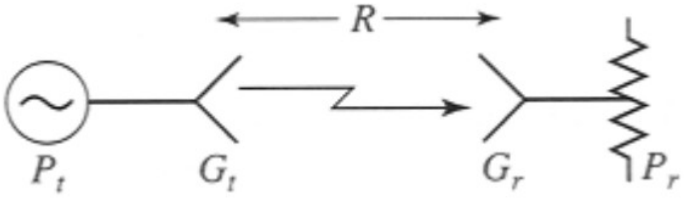

Figure 2-2: A block diagram for a general radio link

A general radio link is shown in figure 2-2, where the transmit power is P_t, the transmit antenna gain is G_t, the receive antenna gain is G_r, and the received power (delivered to a matched load) is P_r. The transmit and receive antennas are separated by the distance R.

By conservation of energy, the power density S_{avg} radiated by an isotropic antenna ($D = 1 = 0dB$) at a distance R is given by

$$S_{avg} = \frac{P_t}{4\pi R^2} W/m^2 \tag{2.1}$$

where P_t is the power radiated by the antenna. This result is deduced from the fact that we must be able to recover all of the radiated power by integrating over a sphere of radius R surrounding the antenna; since the power is distributed isotropically, and the area of a sphere is $4\pi R^2$, (2.1) follows. If the transmit antenna has a directivity greater than 0 dB, we can find the radiated power density by multipliying by the directivity, since directivity is defined as the ratio of the actual radiation intensity to the equivalent isotropic radiation intensity. Also, if the transmit antenna has losses, we can include the radiation efficiency factor, which has the effect of converting directivity to gain. Thus, the general expression for the power density radiated by an arbitrary transmit antenna is

$$S_{avg} = \frac{G_t P_t}{4\pi R^2} W/m^2 \tag{2.2}$$

2.3.1 Effective Area

For a receiving antenna, it is of interest to determine the received power for a given incident plane wave field.

We expect that received power will be proportional to the power density, or Poynting vector, of the incident wave. Since the Poynting vector has dimensions of W/m^2, and the received power P_r has dimensions of Watts, the proportionality constant must have units of area. Thus we write:

$$P_r = A_e S_{avg} \tag{2.3}$$

where A_e is defined as the *effective aperture area* of the receive antenna. The effective aperture area has dimensions of m^2, and can be interpreted as the "capture area" of a receive antenna, intercepting part of the incident power density radiated

toward the receive antenna. P_r in (2.3) is the power available at the terminal of the receive antenna, as delivered to a matched load.

The maximum effective aperture area of an antenna can be shown to be related to the directivity of the antenna as:

$$A_e = \frac{D\lambda^2}{4\pi} \tag{2.4}$$

where λ is the operating wavelength of the antenna. For electrical aperture antennas[1] the effective aperture area is often close to the actual physical aperture area. But for many other types of antennas, such as dipoles and loops, there is no simple relation between the physical cross-sectional area of the antenna and its effective aperture area. The maximum effective aperture area as defined above does not include the effect of losses in the antenna, which can be accounted for by replacing D in (2.4) with G, the gain, of the antenna.

2.3.2 Received power

If the power density obtained in (2.2) is incident on the receiver antenna, we can use the concept of effective aperture area defined above to obtain the following expression for the received power:

$$P_r = A_e S_{avg} = \frac{G_t P_t A_e}{4\pi R^2} \tag{2.5}$$

Where P_r units are Watts [W]. Next, (2.4) can be used to relate the effective area to the directivity of the receive antenna. Again, the possibility of losses in the receive antenna can be accounted for by using the gain (rather than the directivity) of the receive antenna. So the final result for the received power is

$$P_r = \frac{G_t G_r \lambda^2}{(4\pi R)^2} P_t \tag{2.6}$$

[1]Many types of antennas can be classified as *aperture antennas*, meaning that the antenna has a well-defined aperture area from which radiation occurs. Examples include reflector antennas, horn antennas, lens antennas, and array antennas.

The units of P_r are Watts [W].

(2.6) is also known as the Friis equation, which addresses the fundamental question of how much power is received by a radio antenna. In practice, the value given by (2.6) should be interpreted as the maximum possible received power, as there are a number of factors that can serve to reduce the received power in an actual radio system. These include impedance mismatch at either antenna, polarization mismatch between them, propagation effects leading to attenuation or depolarization, and multipath effects that may cause partial cancellation of the received field.

Observe in (2.6) that the received power decreases as $1/R^2$ as the separation between transmitter and receiver increases. As mentioned earlier this dependence is a result of conservation of energy. While it may seem to be prohibitively large for large distances, in fact the space decay of $1/R^2$ is much better than the exponential decrease in power due to losses in a wired communications link. This is because the attenuation of power on a transmission line varies as $e^{-2\alpha z}$ (where α is the voltage attenuation constant of the line), and at large distances the exponential function always decreases faster than an algebraic dependence like $1/R^2$. Thus for long distance communications, radio links will perform better than wired links.

2.4 Radiated Power and Safety

Safety is a legitimate concern for users of wireless equipment, particularly in regard to possible hazards caused by radiated electromagnetic fields. The body absorbs RF and microwave energy and converts it to heat; as in the case of a microwave oven, this heating occurs within the body, and may not be felt at low power levels. Such heating is most dangerous in the brain, eyes, genitals, and stomach organs. Excessive radiation can cause cataracts, cancer, or sterility. For this reason it is important to define a safe radiation level standard, so that users of wireless equipment are not exposed to harmful power levels.

ANSI/IEEE Standard C95.1-1992 [10] gives the U.S. safety standard for human exposure to electromagnetic radiation. In the RF microwave frequency range of 100MHz

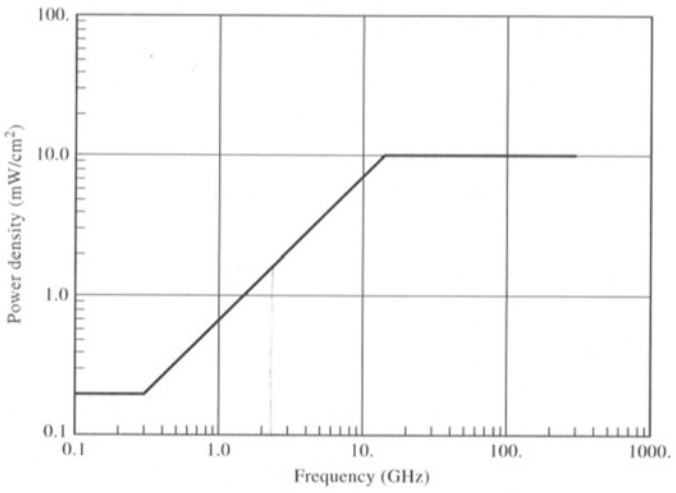

Figure 2-3: IEEE C95.1-1992 Recommended safety density levels

to 300GHz, exposure limits are set on the power density (in Watts/cm^2) as a function of frequency, as shown in figure 2-3. The recommended safe power density limit is as low as 0.2mW/cm^2 at the lower end of this frequency range, because fields penetrate the body more easily at low frequencies. At frequencies above 1.5GHz the power density limit rises to 10mW/cm^2, since most of the power absorption at these frequencies occurs near the skin surface. By comparison, the sun radiates a power density as high as 100mW/cm^2 on a clear day, but the effect of this radiation is much less severe than a corresponding level of microwave frequency radiation because the sun heats the outside of the body, with much of the generated heat being reabsorbed by the air, while microwave power heats inside the body. At frequencies below 100MHz, electric and magnetic fields interact with the body differently than at higher frequencies, hence separate limits are given for field components at these frequencies.

In addition to the above power density limits, the FCC sets limits on the total radiated power of some specific wireless equipment. Vehicle-mounted cellular phones (using an external antenna) are limited to a maximum radiated power of 3W. For handheld cellular phones, the FCC has set an exclusionary power level of 0.76W, below which phones are exempt from the ANSI standard on radiated power density. Most cellular phones radiate a maximum of 0.6W, and newer PCS phones radiate even less power. Although cellular and PCS base stations are limited to a total

effective radiated power of 500W, depending on antenna height and location, most urban base stations radiate a maximum of 10W. Wireless products using the ISM bands are limited to a maximum radiated power of 1W.

While other countries have different (sometimes lower) standards for RF and microwave exposure limits, most experts feel that the above limits represent safe levels within a reasonable margin. Some researchers, however, are concerned that health hazards may occur due to non-thermal effects of long-time exposure to even low levels of microwave radiation [11].

Chapter 3

Rectenna Design

3.1 Microstrip radiators

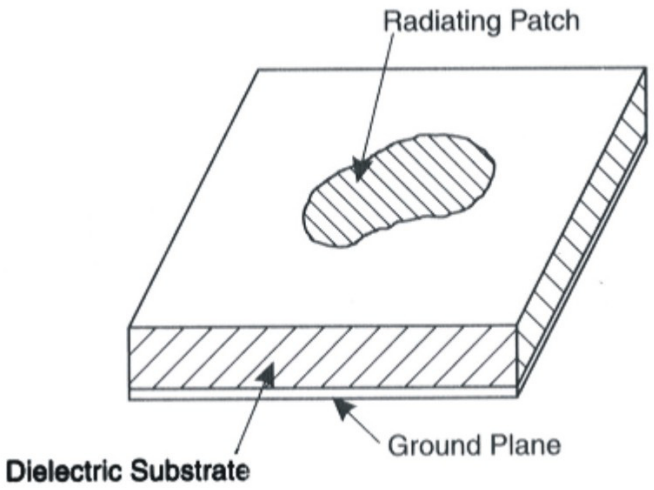

Figure 3-1: Microstrip Radiator

As shown in figure 3-1, a microstrip antenna in its simplest configuration consists of a radiating patch on one side of a dielectric substrate ($\epsilon_r \leq 10$), which has a ground plane on the other side. The Patch conductors, normally of copper or gold, can assume virtually any shape, but regular shapes are used are generally used to simplify the analysis and performance prediction. Ideally, the dielectric constant, ϵ_r, of the substrate should be low ($\epsilon_r < 2.5$), to enhance the fringe fields that account for the radiation. However, other performance requirements may dictate the use of substrate

materials whose dielectric constants can have greater values.

3.1.1 Advantages and limitations.

Microstrip antennas have several advantages compared to conventional microwave antennas, and therefore many applications cover the broad frequency range from 100MHz to 100GHz. Some of the principal advantages of microstrip antennas compared to conventional microwave antennas are:

- Light weight, low volume, and thin profile configurations, which can be made conformal
- Low fabrication cost; readily amenable to mass production
- Linear and circular polarizations are possible with simple a feed
- Dual frequency and dual-polarization antennas can be easily made
- No cavity back is required
- Can be easily integrated with microwave integrated circuits
- Feed lines and matching networks can be fabricated simultaneously with the antenna structure.

However, microstrip antennas also have some limitations compared to conventional microwave antennas:

- Narrow Bandwidth and associated tolerance problems
- Somewhat lower gain (6dB)
- Large ohmic loss in the feed structure of arrays
- Lower power handling capability (100W)

- Microstrip antennas fabricated on a substrate with a high dielectric constant are strongly preferred for easy integration with MMIC RF front-end circuitry. However, use of high dielectric constant substrate leads to poor efficiency and narrow bandwidth.

3.1.2 Microstrip patch antennas.

A microstrip patch antenna (MPA) consists of a conducting patch of any planar or non- planar geometry on one side of a dielectric substrate with a ground plane on the other side. Radiation characteristics have been calculated for a large number of patch antennas [12]. Rectangular and circular patch antennas are widely used. Typically, a patch antenna has a gain between 5 and 6 dB and exhibits a 3 dB beamwidth between 70° and 90°.

As shown in figure 3-2, the basic antenna element is a strip conductor of dimensions $L \times W$ on a dielectric substrate of dielectric constant ϵ_r and thickness h backed by a ground plane. When the patch is excited by a feed, a charge distribution is established on the underside of the patch metallization and the ground plane. At a particular instant of time, the underside of the patch is positively charged and the ground plane is negatively charged. The attractive forces between these sets of changes tend to hold a large percentage of the changes between the two surfaces. However, the repulsive force between positive charges on the patch pushes some of these charges toward the

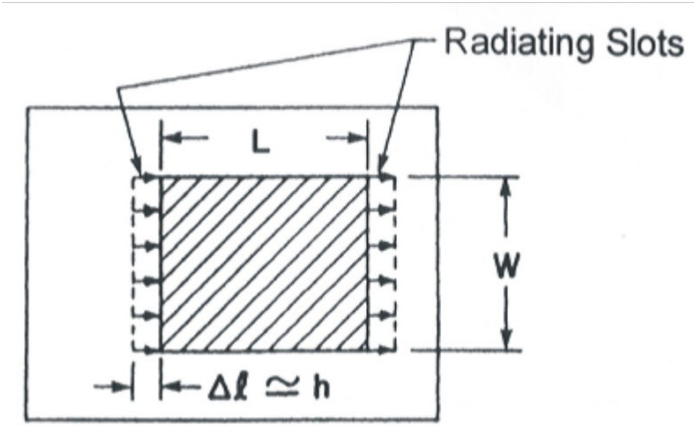

Figure 3-2: Rectangular microstrip patch antenna

edges, resulting in large charge density at the edges. These charges are the source of fringing fields and the associated radiation. Using a thicker substrate with a lower value of dielectric constant can increase the fringing field and the radiated power.

3.1.3 Design considerations for rectangular patch antennas.

Usually, the overall goal of a design is to achieve specific performance characteristics at a stipulated operating frequency. If a microstrip antenna can achieve these overall goals, then the first decision is to select a suitable antenna geometry. A rectangular patch antenna can be designed using the following considerations.

Feeding techniques.

Microstrip antennas have radiating elements on one side of a dielectric substrate, and thus early microstrip antennas were fed either by a microstrip line or a coaxial probe through the ground plane. Since then, a number of new feeding techniques have been developed: prominent among these are coaxial feed, microstrip (coplanar) feed, proximity-coupled microstrip feed, aperture-coupled microstrip feed, and coplanar waveguide feed. These feed structures are summarized in table 3.1

Substrate Selection.

An important design step is to choose a suitable dielectric substrate of appropriate thickness h and loss tangent. A thicker substrate, besides being mechanically strong, will increase the radiated power, reduce conductor loss, and improve impedance bandwidth. However, it will also increase the weight, dielectric loss, surface wave loss, and extraneous radiations from the probe feed. A rectangular patch antenna stops resonating for substrate thickness greater that $0.11\lambda_0$ ($\epsilon_r = 2.55$) due to inductive reactance on the probe feed [13]. The substrate dielectric constant ϵ_r plays a role similar to the substrate thickness. A low value of ϵ_r for the substrate will increase the fringing field at the patch periphery, and thus the radiated power. An increase in the substrate thickness has a similar effect on antenna characteristics as a decrease in the

Characteristics	**Coaxial-Probe Feed**	**Radiating Edge Coupled**	**Nonradiating Edge Coupled**	**Microstrip Gap Coupled**	**Microstrip Inset Feed**	**Proximity Coupled**	**Aperture Coupled**	**CPW Feed**
Configuration	**Nonplanar**	**Coplanar**	**Coplanar**	**Coplanar**	**Coplanar**	**Planar**	**Planar**	**Planar**
Spurious feed radiation	More	Less	Less	More	More	More	More	Less
Polarization Purity	Poor	Good	Poor	Poor	Poor	Poor	Excellent	Good
Ease of fabrication	Soldering and drilling needed	Easy	Easy	Easy	Easy	Alignment Required	Alignment Required	Alignment Required
Reliability	Poor due to soldering	Better	Better	Better	Better	Good	Good	Good
Impedance Matching	Easy	Poor	Easy	Easy	Easy	Easy	Easy	Easy
Bandwidth (achieved with Impedance Matching)	2–5%	9–12%	2–5%	2–5%	2–5%	13%	21%	3%

Table 3.1: Comparison between feeding techniques

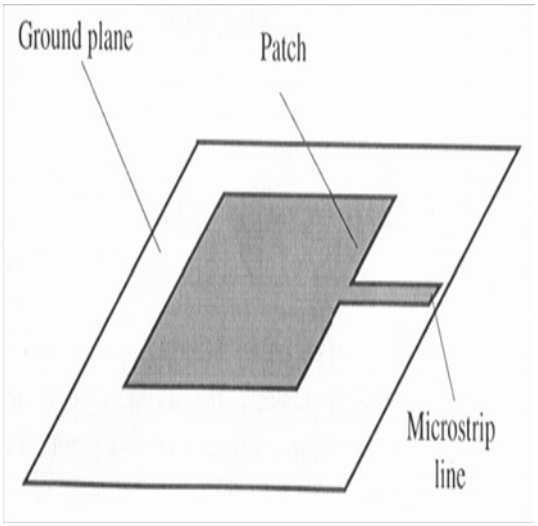

(a) Direct Feed

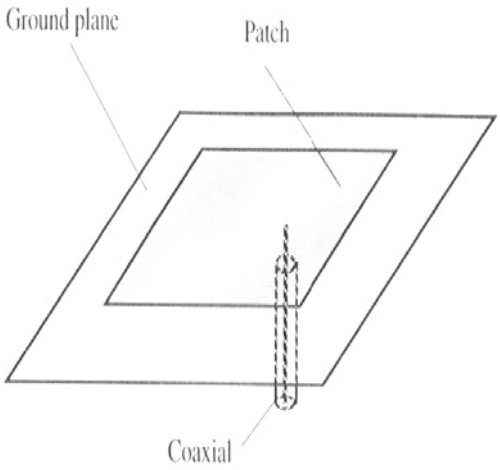

(b) Coaxial Feed

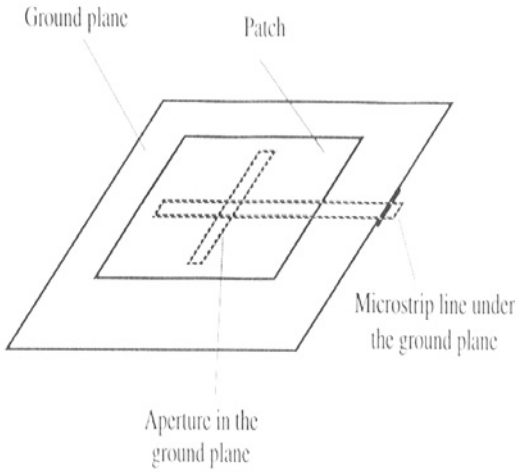

(c) Slot Feed

Figure 3-3: Examples of three typical feeding techniques

value of ϵ_r. Common dielectric materials used to fabricate microstrip antennas are FR-4 ($\epsilon_r = 4.2$), GML1000 ($\epsilon_r = 3.2$), RT/Duroid ($\epsilon_r = 2.2$), and Teflon ($\epsilon_r = 2.1$)

Element Width and Length

Patch width has a minor effect on the resonant frequency and radiation pattern of the antenna. It affects the input resistance and bandwidth to a larger extent. A larger patch width increases bandwidth, and radiation efficiency. With proper excitation one may choose a patch width W (see figure 3-2) greater than the patch length L without exciting undesired modes. It has been suggested that $1 < W/L < 2$ [14, 15].

The patch length determines the resonant frequency, and is a critical parameter in design because of the inherent narrow bandwidth of the patch. To a zeroth-order approximation, the patch length L for the TM_{10}[1] mode is given by:

$$L = \frac{c}{2f_r\sqrt{\epsilon_r}} \tag{3.1}$$

The factor $1/\sqrt{\epsilon_r}$ in (3.1) is due to the loading by the substrate and is strictly valid for a very wide patch. In practice, a fraction of the fields lie outside the physical dimensions $L\times W$ of the patch. This is called the fringing field. The effect of such a field along the edges $y = 0$ and $y = W$ can be included through the effective constant ϵ_{re} for a microstrip line of width W on the given substrate. Thus equation (3.1) becomes

$$L = \frac{c}{2f_r\sqrt{\epsilon_{re}}} \tag{3.2}$$

The next improvement is obtained by including the effect of fringing fields at the other ends of the patch, that is, along $x = 0$ and $x = L$. An additional line length ΔL on either ends of the patch can describe this effect. Consequently:

[1]An incident wave of general polarization can be decomposed into two linearly polarized waves; one with the electric field vector perpendicular to the plane of incidence which is the TE wave, and one with the electric field vector parallel to the plane of incidence which is called the transverse magnetic (TM) wave [16].

$$f_r = \frac{c}{2(L + 2\Delta L)\sqrt{\epsilon_{re}}} \tag{3.3}$$

Another way to include the effects of fringing fields is to describe these in terms of the effective dielectric constants for the width and length separately.

$$\epsilon_{re}(W) = \frac{\epsilon_r + 1}{2} + \frac{\epsilon_r - 1}{2} F(W/h) \tag{3.4}$$

$$\epsilon_{re}(L) = \frac{\epsilon_r + 1}{2} + \frac{\epsilon_r - 1}{2} F(L/h) \tag{3.5}$$

Where

$$F\left(\frac{a}{h}\right) = (1 + 12h/a)^{-1/2} + 0.04(1 - a/h)^2, \quad a/h \leq 1$$

$$F\left(\frac{a}{h}\right) = (1 + 12h/a)^{-1/2}, \quad a/h \leq 1$$

Previous studies [17] show that ΔL calculated from

$$\Delta L = 0.412h \frac{\epsilon_{re} + 0.300}{\epsilon_{re} - 0.258} \frac{W/h + 0.264}{W/h + 0.813} \tag{3.6}$$

Fits the real measured resonant frequency within 1.6% [18]

Radiation patterns and radiation resistance.

The radiation patterns of an antenna are of prime importance in determining most of its radiation characteristics, which include beamwidth, beam shape, side lobe level, directivity, polarization, and radiated power. The radiation from the patch can be derived either from the E_z field across the aperture between the patch and the ground plane (using vector electric potential) of from the currents on the surface of the patch conductor (employing vector magnetic potentials). The transmission line model and cavity model employ the aperture field approach. In the transmission line model, two slots at the radiating edges are considered. The cavity model employs four slots along

the periphery of the patch. However, the contribution of the non-radiating slots to the radiation pattern can be neglected for approximate calculations.

Radiation pattern based on a two-slot model

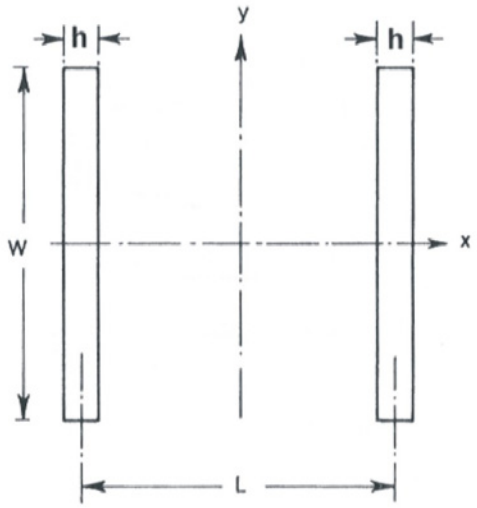

Figure 3-4: Radiating Slots Geometry

In this model, the radiation patterns for the TM_{10} mode are calculated by modelling the antenna as a combination of two parallel slots of length W, width h, and spaced a distance L apart, as suggested in figure 3-4. The radiation from the patch is linearly polarized with the electric field directed along the patch length. If the voltage across either radiating slot is taken as V_0, the radiation fields are obtained by multiplying the radiation pattern of one slot, with the array factor $2\cos(k_0 L \sin\theta\cos\phi/2)$. One obtains

$$E_\theta = -jk_0 V_0 W \frac{e^{-jk_0 r}}{4\pi r}\cos\phi F_1 F_2 \tag{3.7}$$

$$E_\phi = -jk_0 V_0 W \frac{e^{-jk_0 r}}{4\pi r}\cos\theta\sin\phi F_1 F_2 \tag{3.8}$$

where

$$F_1 = \mathrm{sinc}(k_0 h \sin\theta\cos\phi/2)\mathrm{sinc}(k_0 L \sin\theta\sin\phi/2)$$

$$F_2 = 2\cos(k_0 L \sin\theta \cos\phi/2)$$

Equations (3.7) and (3.8) yield the following expressions for the radiation field in the principal planes of a rectangular microstrip antenna operated in the TM_{10} mode.

For the $\phi = 0°$ plane or E plane:

$$E_\phi(\theta) = 0 \tag{3.9}$$

$$E_\theta(\theta) = -jk_0 V_0 W \frac{e^{-jk_0 r}}{4\pi r} F_E(\theta) \tag{3.10}$$

where

$$F_E = \text{sinc}(k_0 h \sin\theta/2)\cos(k_0 L \sin\theta/2)$$

For the $\phi = 90°$ plane or H plane

$$E_\theta(\theta) = 0 \tag{3.11}$$

$$E_\phi(\theta) = jk_0 V_0 W \frac{e^{-jk_0 r}}{4\pi r} F_H(\theta) \tag{3.12}$$

where

$$F_H = \text{sinc}(k_0 W \sin\theta/2)\cos\theta$$

The effect of the ground plane and substrate of the antenna on the radiation patterns can be included by means of factors $F_3(\theta)$ and $F_4(\theta)$. For the E-plane pattern:

$$F_3(\theta) = \frac{2\cos\theta\sqrt{\epsilon_r - \sin^2\theta}}{\sqrt{\epsilon_r - \sin^2\theta} - j\epsilon_r \cos\theta \cot(k_0 h\sqrt{\epsilon_r - \sin^2\theta})} \tag{3.13}$$

and for the H-plane pattern:

$$F_4(\theta) = \frac{2\cos\theta}{\cos\theta - j\sqrt{\epsilon_r - \sin^2\theta}\cot(k_0 h\sqrt{\epsilon_r - \sin^2\theta})} \tag{3.14}$$

The final radiation patterns are then, for the E-plane pattern

$$E_\theta(\theta) = -jk_0 V_0 W \frac{e^{-jk_0 r}}{2\pi r} F_E(\theta) F_3(\theta) \tag{3.15}$$

and for the H-plane pattern

$$E_\phi(\theta) = jk_0 V_0 W \frac{e^{-jk_0 r}}{2\pi r} F_H(\theta) F_4(\theta) \tag{3.16}$$

Radiation pattern based on the electric surface current model.

In this model the patch metallization is replaced by the surface current distribution, and the fields are solved for, taking into account the grounded substrate through an exact Green's function. The radiation patterns are found to be [19, 20]

$$E_\phi(\theta,\phi) = \sin\phi \left(\frac{j\omega\mu_0}{4\pi r}\right) e^{-jk_0 r} \tilde{J}(\theta,\phi) F_4(\theta) \tag{3.17}$$

$$E_\theta(\theta,\phi) = -\cos\phi \left(\frac{j\omega\mu_0}{4\pi r}\right) e^{-jk_0 r} \tilde{J}(\theta,\phi) F_3(\theta) \tag{3.18}$$

where $\tilde{J}(\theta,\phi)$ is the Fourier transform of the patch current. For the TM_{10} mode with [20]

$$\vec{J}(x,y) = \hat{x}\frac{V_0}{Z_0 W}\sin(\beta x) \quad \text{for } 0 < x < L,\ 0 < y < W \tag{3.19}$$

The expression for $\tilde{J}(\theta,\phi)$ is obtained as [20]

$$\tilde{J}(\theta,\phi) = \frac{V_0}{Z_0}\frac{2\sqrt{\epsilon_{re}}\cos(\pi\sin\theta\cos\phi/(2\sqrt{\epsilon_{re}}))}{k_0(\sin^2\theta\cos^2\phi - \epsilon_{re})}\text{sinc}(0.5k_0 W\sin\theta\sin\phi) \tag{3.20}$$

where $\sqrt{\epsilon_{re}} = \beta/k_0$ is the effective dielectric constant of the microstrip line of which the patch is a segment and Z_0 is the characteristic impedance corresponding

to width W. For the TM_10 mode the patch length is selected such that

$$L = \lambda_g/2 \Rightarrow k_0 L = \pi/\sqrt{\epsilon_{re}}$$

The principal plane power patterns are then obtained as follows [20]. For the $\phi = 0^\circ$ plane or E-plane:

$$E_\phi = 0 \tag{3.21}$$

$$\begin{aligned} |E_\theta(\theta)|^2 =& \epsilon_{re}[1 + \epsilon_r \cot^2(k_0 h\sqrt{\epsilon_r})]\frac{\cos^2(k_0 L \sin\theta/2)}{(\epsilon_{re} - \sin^2\theta)^2} \\ & \frac{(\epsilon_r - \sin^2\theta)\cos^2\theta}{(\epsilon_{re} - \sin^2\theta) + \epsilon_r^2 \cos^2\theta \cot^2(k_0 h\sqrt{\epsilon_r - \sin^2\theta})} \end{aligned} \tag{3.22}$$

and for the $\phi = 90^\circ$ plane or H-plane

$$E_\phi = 0 \tag{3.23}$$

$$\begin{aligned} |E_\phi(\theta)|^2 =& [1 + \epsilon_r \cot^2(k_0 h\sqrt{\epsilon_r})] \\ & \frac{\cos^2\theta}{(\epsilon_{re} - \sin^2\theta)\cot^2(k_0 h\sqrt{\epsilon_r - \sin^2\theta}) + \cos^2\theta} \mathrm{sinc}^2(k_0 W \sin\theta/2) \end{aligned} \tag{3.24}$$

The radiation patterns based on the two different radiation mechanisms described above are similar. They have been compared with measured radiation patterns for various values of substrate thickness with $\epsilon_r = 2.5$ [21]. The aperture model, without the factors $F_3(\theta)$ and $F_4(\theta)$ is found to give radiation patterns that compare well with measurements.

Beamwidth.

The half power beamwidth of an antenna its equal to the angular width between directions where the radiated field reduces to $1/\sqrt{2}$ of the maximum value. After

some approximations and algebra, one can obtain the following relationships:

$$\theta_H = 2\sin^{-1}\left(\frac{1}{2+k_0W}\right)^{1/2} \tag{3.25}$$

$$\theta_E = 2\sin^{-1}\left(\frac{7.03}{3{k_0}^2L^2+k_0h^2}\right)^{1/2} \tag{3.26}$$

Where θ_H and θ_E are the half-power beamwidths in the H and E planes, respectively. Choosing a smaller element, thus reducing L and W, can increase the beamwidth of a microstrip element.

Directivity and Gain

The directivity is a measure of the directional properties of an antenna compared of those of an isotropic antenna. The directivity is always greater that 1 since an isotropic radiator is not directional. The directivity is defined as the ratio of the maximum power density in the main beam direction to the average radiated power density. The directivity of the patch antenna is expressed as:

$$D = \frac{\frac{1}{2}Re(E_\theta H_\phi^* - E_\phi H_\theta^*)|_{\theta=0}}{P_r/4\pi r^2} = \frac{\frac{r^2}{2\eta_0}(|E_\theta|^2+|E_\phi|^2)|_{\theta=0}}{P_r/4\pi} \tag{3.27}$$

Where P_r is the radiated power, $\eta_0 = 120\pi\Omega$, and the radiation fields E_θ and E_ϕ where defined earlier. A simple approximate expression is

$$D\approx\frac{4(k_0W)^2}{\pi\eta_0 G_r} \tag{3.28}$$

Where G_r is the radiation conductance of the patch, defined later.

Radiated power and radiation resistance.

The power radiated by an antenna can be obtained by integrating the real part of the Poynting vector over the hemisphere above the patch, that is:

$$P_r = \frac{1}{2\eta_0}\int_0^{2\pi}\int_0^{\pi/2}(|E_\theta|^2+|E_\phi|^2)r^2\sin\theta d\theta d\phi \tag{3.29}$$

If (3.22) and (3.24) are used for E_θ and E_ϕ, one obtains [20]

$$\begin{aligned} P_r =& \frac{V_0^2}{Z_0^2}\frac{60\epsilon_{re}}{\pi}\int_0^{2\pi}\int_0^{\pi/2}\frac{\cos^2(\pi\sin\theta\cos\phi/(2\sqrt{\epsilon_{re}}))}{(\sin^2\theta\cos^2\phi-\epsilon_{re})^2} \\ & \cdot\sin(c^2)(k_0W\sin\theta\sin\phi/2)sin\theta d\theta d\phi \\ & \times[\frac{\cos^2\theta\sin^2\phi}{(\epsilon_r-\sin^2\theta)\cot^2(k_0h\sqrt{\epsilon_r-\sin^2\theta})+\cos^2\theta} \\ & + \frac{(\epsilon_r-\sin^2\theta)\cos^2\theta\cos^2\phi}{(\epsilon_r-\sin^2\theta)+\epsilon_r^2\cos^2\theta\cot^2(k_0h\sqrt{\epsilon_r-\sin^2\theta})}] \end{aligned} \tag{3.30}$$

A numerical integration is performed given the complexity of this equation. If the effect of the substrate is neglected, an approximate closed-form expression can be obtained for P_r. Thourode et al. [22] have obtained:

$$P_r = \frac{(E_0h)^2A\pi^4}{23040}\left[(1-B)\left(1-\frac{A}{15}+\frac{A^2}{420}\right)+\frac{B^2}{5}\left(2-\frac{A}{7}+\frac{A^2}{189}\right)\right] \tag{3.31}$$

Where $A=(\pi W/\lambda_0)^2$, and the normalized resonant length $B=(2L/\lambda_0)^2$. Equation (3.31) highlights the fact that the radiated power is directly proportional to $(k_0W)^2$ and $(k_0h)^2$.

The resonant radiation conductance G_r for a patch fed at an edge can be determined from power radiated P_r as follows:

$$P_r = \frac{1}{2}G_r(E_0h)^2 = \frac{1}{2}G_rV_0^2 \tag{3.32}$$

$$R_r = 1/G_r \tag{3.33}$$

The expressions for R_r with an estimated accuracy of 10% average for $h\leq 0.03\lambda_0$ and $\epsilon_r\leq 10$ are given by:

$$R_r = \frac{V_0^2}{2P_r} = \epsilon_{re}\frac{Z_0^2}{120I_2} \tag{3.34}$$

Where Z_0 is the characteristic impedance of the microstrip line of which the patch is a segment, and for $\epsilon_r \leq 5$,

$$I_2 = (k_0 h)^2 [0.53 - 0.03795(k_0 W/2)^2 - 0.03553/\epsilon_{re}] \tag{3.35}$$

Comparisons with numerical results for R_r have shown that (3.35) has better accuracy for thin substrates with lower ϵ_r.

The radiation resistance is found to decrease with increase in substrate thickness and patch width because radiated power increases. If the patch is fed at a distance x_f from one of the radiating edges, the input resistance is:

$$R_{in} = R_r \cos^2(\pi x_f / L) \tag{3.36}$$

The factor $\cos(\pi x_f/L)$ arises due to electric field variations for the dominant mode.

Radiation Efficiency ϵ_r

The radiation efficiency is defined as the ratio of the radiated power P_r to the input power P_i, that is,

$$\epsilon_r = \frac{P_r}{P_i} \tag{3.37}$$

The input power gets distributed in the form of radiated power, surface wave power, and dissipation in the conductors and dielectric. Therefore, (3.37) can be expressed as

$$\epsilon_r = \frac{P_r}{P_r + P_c + P_d + P_{sur}} \tag{3.38}$$

Here, P_d is the power lost in the lossy dielectric of the substrate, P_c is the power lost due to the finite conductivity of metallization (also called copper loss), P_r is the power radiated in the form of space wave, and P_{sur} is the power lost in the form of power carried away by the surface waves.

The dissipated power is generally small for low-loss substrates at microwave fre-

quencies, and one can write:

$$\epsilon_r = \frac{P_r}{P_r + P_{sur}} \tag{3.39}$$

It has been observed that radiation efficiency depends primarily on the substrate thickness and permittivity, and is not affected very much either by the patch shape or the feed [23]. Pozar has used an infinitesimal current source on the substrate and obtained the following closed-form expressions for P_r and P_{sur} [20]:

$$P_r = 40k_0^2(k_0h)^2\left(1 - \frac{1}{\epsilon_r} + \frac{2}{5\epsilon_r^2}\right) \tag{3.40}$$

$$P_{sur} = 30\pi k_0^2 \frac{\epsilon_r(x_0^2-1)}{\epsilon\left[\frac{1}{\sqrt{x_0^2-1}} + \frac{\sqrt{x_0^2-1}}{\epsilon_r - x_0^2}\right] + k_0h\left[1 + \frac{\epsilon_r^2(x_0^2-1)}{\epsilon_r - x_0^2}\right]} \tag{3.41}$$

Where x_0 is the normalized phase constant for the TM_{10} surface wave. The radiation efficiency obtained using (3.40) is found to be accurate to at least 5% for $h\sqrt{\epsilon_r} < \lambda_0/8$.

Feed point Location.

After selecting the patch dimensions L and W for a given substrate, the next task is to determine the feed point (x_0, y_0) so as to obtain a good impedance match between the generator impedance and the input impedance of the patch element. It is observed in the literature [24] that the change in feed location gives rise to a change in the input impedance and hence provides a simple method for impedance matching. If the feed is located at $x_0 = x_f$ and $0 \leq y_f \leq W$, the input resistance at resonance for the dominant TM_{10} mode can be expressed as:

$$R_{in} = R_r \cos^2(\pi x_f/L), \quad R_r \geq R_{in} \tag{3.42}$$

Where x_f is the inset distance from the radiating edge, and R_r is the radiation resistance at resonance when the patch is fed at a radiating edge. The radiation

resistance R_r has been determined previously in (3.35). The inset distance x_f is selected such that R_{in} is equal to the feed line impedance, usually taken to be 50Ω. Although the feed point can be selected anywhere along the patch width, it is better to choose $y_f = W/2$ if $W \geq L$ so that TM_{0n} (n odd) modes are not excited along with the TM_{10} mode. Kara [25] has suggested an expression for x_f that does not need calculation of radiation resistance. It is approximately given by:

$$X_f = L/2\sqrt{\epsilon_{re}(L)} \tag{3.43}$$

Where $\epsilon_{re}(L)$ is defined by (3.5).

3.2 Rectifier Design

Detectors make use of the nonlinear characteristics of a solid-state device to bring about frequency conversion to an input signal. The more nonlinear the device's *I-V* characteristic curves are, the more efficient the detection process will be, that is, a higher percentage of the signal power at the input frequency will be converted to signal power at the output frequency.

The three basic types of frequency conversion circuits are

- A rectifier
- A detector
- A mixer

Each is described briefly as follows:

A **rectifier** is a circuit that converts the RF signal into a zero frequency signal (i.e. a DC signal) with time and frequency-domain signals as shown in figure 3-5. The rectifier is used for automatic gain control (AGC) circuits or power monitor circuits, etc. A **detector** (also called a demodulator) is a circuit that demodulates a modulated

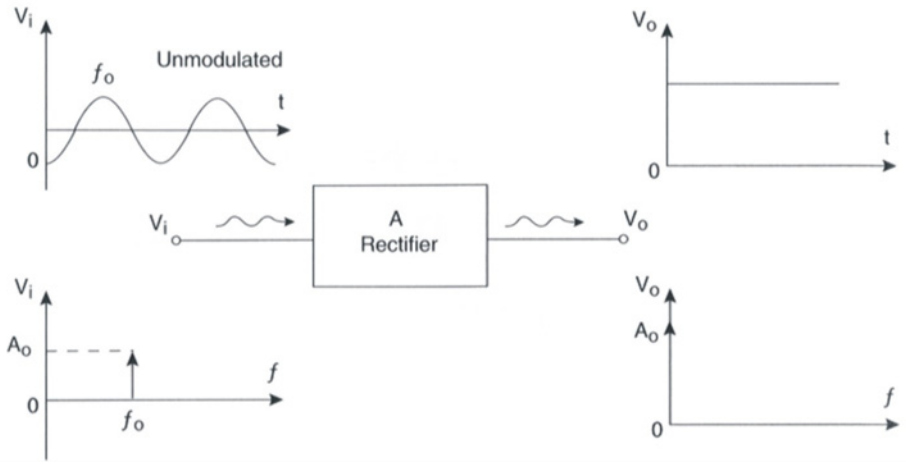

Figure 3-5: Time and Frequency Domain Signals for a Rectifier

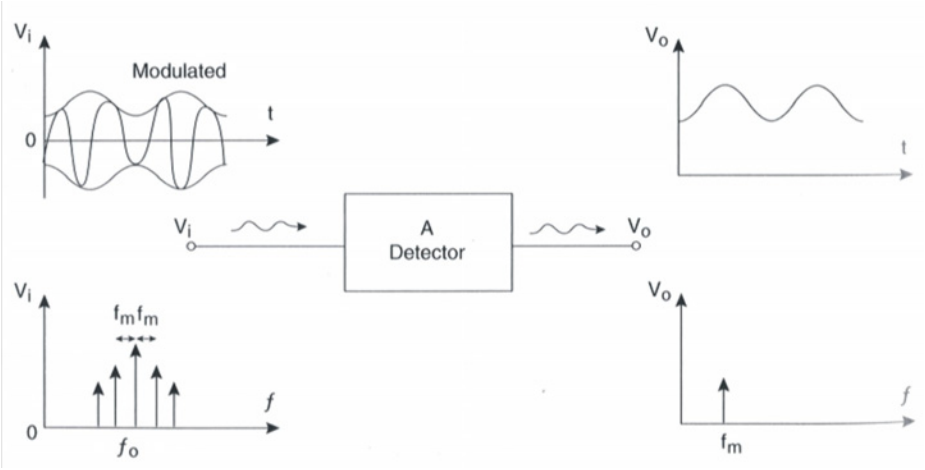

Figure 3-6: Time and Frequency Domain Signals for a Detector

carrier wave by discarding the carrier wave and outputting the modulating signal as shown in figure 3-6. Detectors are used in circuits such as AM demodulators.[2]

A **mixer** (also called a converter) is a circuit that converts an input signal to a higher-frequency signal (called an up-converter) or to a lower-frequency signal (called a down-converter) while ideally preserving all of the original signal characteristics (such as sidebands, waveshape, etc.) This frequency conversion can be readily obtained by mixing the input signal with another signal (called the Local Oscillator signal, or LO for short) as shown in figure 3-7

[2]A rectifier is a special case of a detector where proper filtering is used at the output to reject all frequencies except for the DC component.

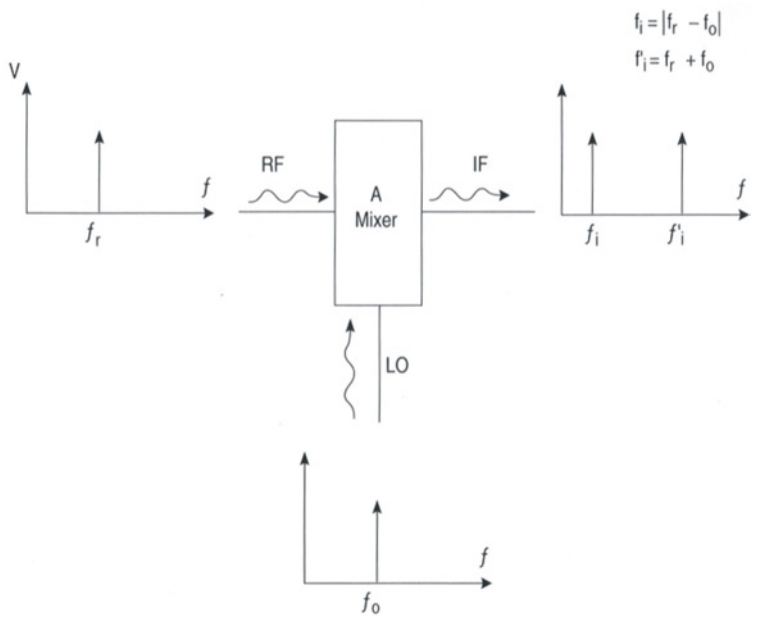

Figure 3-7: Time and Frequency Domain Signals for a Mixer

3.2.1 Small-signal Analysis of a Diode

In general, a diode can be considered to be a nonlinear resistor with its I-V characteristic curve mathematically given by:

$$I(V) = I_s \left(e^{(V/nV_t)} - 1\right) \tag{3.44}$$

where:

- $V_t = KT/q \quad (V_t = 25mV \text{ at } T = 293K)$
- $I_s =$ Diode saturation current
- $n =$Ideality factor ($1 \leq n \leq 2$) which depends on the material and physical structure of the diode. For example, for a point-contact diode $n = 2$ whereas for a Schottky barrier diode, $n = 1.2$, etc.

Figure 3-8 shows a sketch of a diode I-V characteristic curve, as described in equation (3.44).

To perform a small signal analysis, we assume that the total voltage across the diode (V) is composed of a DC bias voltage (V_0) and a small-signal RF voltage (v),

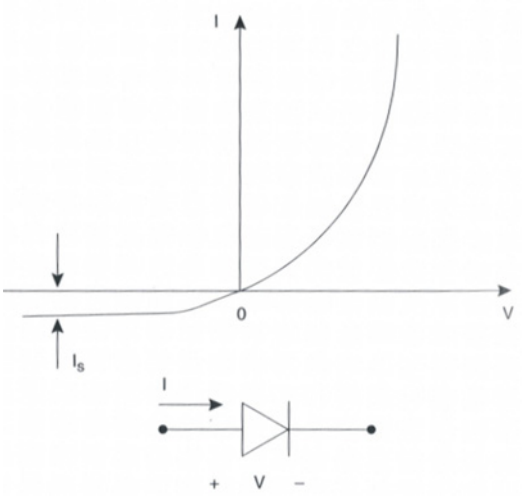

Figure 3-8: Voltage-Current Curves

that is:

$$V = V_0 + v \tag{3.45}$$

Substituting equation (3.45) in (3.44) and performing a Taylor series expansion around the Q-point (I_0, V_0) we obtain:

$$I = I(V_0 + v) = I(V_0) + v\frac{dI}{dv}|_{V_0} + \frac{1}{2}v^2\frac{d^2I}{dv^2}|_{V_0} + ... \tag{3.46}$$

where $I(V_0)$ is the DC bias current given by:

$$I_0 = I(V_0) = I_S\left(e^{(V/nV_t)} - 1\right) \tag{3.47}$$

The first order derivative corresponds to the dynamic conductance of the diode G_d (the inverse of the junction resistance, R_j) and is given by:

$$G_d = \frac{1}{R_j} = \frac{dI}{dv}|_{V_0} = \frac{I_S}{nV_T}e^{(V_0/nV_T)} = \frac{I_0 + I_S}{nV_T} \tag{3.48}$$

The second-order derivative is given by:

$$\frac{d^2I}{dv^2}|_{V_0} = \frac{dG_d}{dv} = G_d' = \frac{I_S}{(nV_T)^2}e^{(V_0/nV_T)} \tag{3.49}$$

$$G'_d = \frac{I_S + I_0}{(nV_T)^2} = \frac{G_d}{nV_T}$$

Equation (3.46) can be now written as a DC current (I_0) and an AC small signal current (i):

$$I(v) = I_0 + I \tag{3.50}$$

where

$$i = vG_d + 1/2(v^2G'd) + ... \tag{3.51}$$

The three term approximation for the diode current, as given by equation (3.50) is known as the "small signal approximation". This means that for small signals (i.e. $v/nV_T \ll 1$), higher order terms (above the second order) for i may be truncated without any loss of accuracy.

In practice, however, the diode's behavior also involves reactive effects caused by junction and parasitic capacitances and lead inductances that are directly related to the packaging as well as the structure of the diode. A typical equivalent circuit for the diode is shown in figure 3-9. In this figure, (C_p, L_p) are the parasitic elements due to packaging, R_s is the series resistance due to semiconductor neutral regions and the contact areas, and (R_j, C_j) are the junction resistance and capacitance, which are bias-dependent.

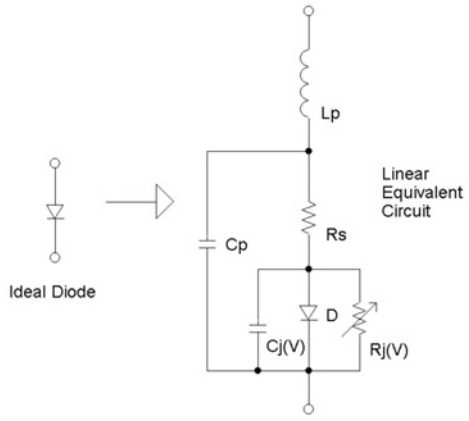

Figure 3-9: Diode Equivalent Circuit Model

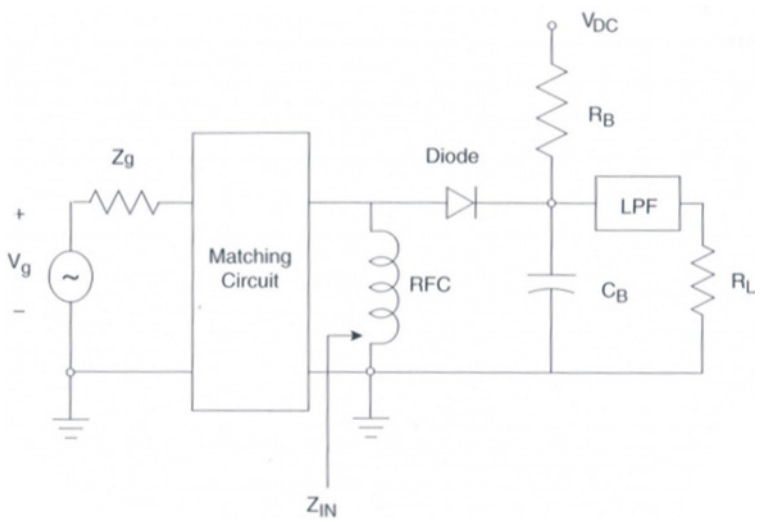

Figure 3-10: Diode Detector Configuration

3.2.2 Diode Applications in Detector Circuits

A typical diode (as analyzed previously) can be used for many different applications, particularly in a rectifier or a detector circuit, which is the primary focus of the wireless power transmission system discussed so far.

A diode converts a portion of the input RF energy to a DC current that is proportional to the input RF power. The type of detector circuit that uses an unmodulated RF signal and converts it into a DC output signal may also be referred to as a rectifier. In this section, we will explore the magnitude of the DC current relative to the input RF signal.

Let's consider a diode detector circuit (as shown in figure 3-10) and assume that the diode is biased at a Q-point (I_0, V_0) with an applied input small-signal RF voltage (v) having a frequency (ω_0) and amplitude (v_m) given by:

$$v(t) = v_m \cos(\omega_0 t) \tag{3.52}$$

From equations (3.50) and (3.51), the total current is composed of a DC bias (I_0) and an AC current given by:

$$I = I_0 + I \tag{3.53}$$

where

$$i = G_d v_m \cos(\omega_0 t) + 1/2[G'_d v_m^2 \cos^2(\omega_0 t)] \tag{3.54}$$

Using the identity

$$\cos^2(\omega_0 t) = \frac{1 + cos(2\omega_0 t)}{2}$$

we can write equation (3.54) as:

$$i = v_m^2 G'_d/4 + v_m G_d \cos(\omega_0 t) + v_m^2 G'_d \cos(2\omega_0 t)/4 \tag{3.55}$$

Thus the total DC current is given by:

$$I_{DC} = I_0 + v_m^2 G'_d/4 \tag{3.56}$$

If now the output RF signals of frequency $(\omega_0 t)$, $(2\omega_0 t)$, and other higher- order harmonics, are filtered out using a simple low-pass filter, the remaining output term will be composed of the bias current (I_0) and a term equal to $v_m^2 G'_d/4$. The DC rectified current is proportional to (v_m^2), which is the input RF power, desirable in many applications such as automatic gain control, power monitors, and virtual batteries [26]. Under this condition, the detector is said to operate in the square-law region.

3.3 Transmission-Line Impedance Matching

Transmission lines are used for the transmission of power and information. For radio frequency power transmission it is highly desirable that as much power as possible is transmitted from the generator to the load and as little power as possible is lost on the line itself. This will require that the load be matched to the characteristic impedance of the line so that the standing-wave ratio on the line is as close to unity as possible. For information transmission it is essential that the lines be matched

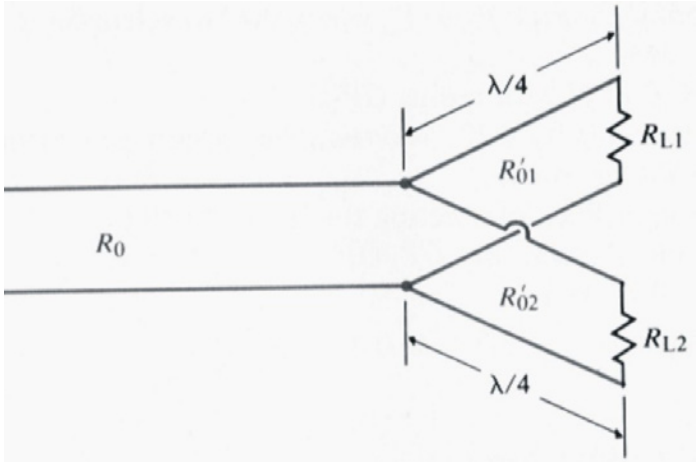

Figure 3-11: Quarter-Wave transformer Coupling Sections

because reflections from mismatched loads and junctions will result in echoes and will distort the information-carrying signal. In this section we discuss several methods for impedance matching on lossless transmission lines. We note parenthetically that the methods we develop will be of little consequence to power transmission at lower frequencies, e.g. 60Hz lines, in as much as these lines are generally very short in comparison to the millimeter wavelengths and the line losses are appreciable. Sixty-hertz power-line circuits are usually analyzed in terms of equivalent lumped electrical networks.

3.3.1 Impedance Matching by Quarter-wave Transformer

A simple method for matching a resistive load R_L to a lossless transmission line of a characteristic impedance R_0 is to insert a quarter-wave transformer (as shown in figure 3-11 with a characteristic impedance R'_0 such that

$$R'_0 = \sqrt{R_0 R_L} \tag{3.57}$$

Since the length of the quarter-wave line depends on wavelength, this matching method is frequency-sensitive. Ordinarily, the main transmission line and the matching line sections are essentially lossless. In that case, both R_0 and R'_0 are purely real, and equation (3.57) will have no solution if R_L is replaced by a complex Z_L. Hence

quarter-wave transformers are not useful for matching a complex load impedance to a low-loss line.

3.3.2 Single-stub Matching

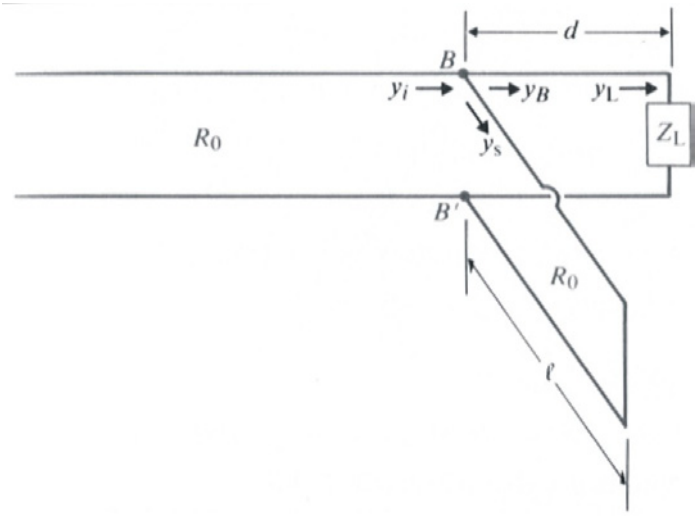

Figure 3-12: Single Stub Matching Configuration

We now tackle the problem of matching a load impedance Z_L to a lossless line that has a characteristic impedance R_0 by placing a single short-circuited stub in parallel with the line, as shown in figure 3-12. This is the *single-stub method* for impedance matching. We need to determine the length of the stub, l, and the distance from the load, d, such that the impedance of the parallel combination to the right of points $B - B'$ equals R_0. Short-circuited stubs are usually used in preference to open-circuited stubs because infinite terminating impedance is more difficult to realize than zero terminating impedance for reasons of radiation from an open end and coupling effects with neighboring objects. Moreover, a short-circuited stub of an adjustable length and a constant characteristic resistance is much easier to construct than an open-circuited one. Of course, the difference in the required length of an open-circuited stub and that for a short-circuited stub is an odd multiple of a quarter-wavelength.

The parallel combination of a line terminated in Z_L and a stub at points $B - B'$

in figure 3-12 suggests that is advantageous to analyze the matching requirements in terms of admittances. The basic requirement is

$$\begin{aligned} Y_I &= Y_B + Y_s \\ &= Y_0 = \frac{1}{R_0} \end{aligned} \tag{3.58}$$

In terms of normalized admittances, (3.58) becomes

$$1 = y_B + y_s \tag{3.59}$$

where $y_B = R_0 Y_B$ for the load section and $y_s = R_0 Y_s$ is for the short circuited stub. However, since the input admittance of a short-circuited stub is purely susceptive, y_s is purely imaginary. As a consequence, equation (3.59) can be satisfied only if

$$y_B = 1 + jb_B \tag{3.60}$$

and

$$y_s = -jb_B \tag{3.61}$$

where b_B can be positive or negative. Our objectives, then, are to find the length d such that the admittance, y_B, of the load section looking to the right of terminals $B - B'$ has a *unity real part* and to find the length l_B of the stub required to *cancel the imaginary part.*

Chapter 4

Design and Experimental Results

4.1 Antenna Design

Following the design procedures explained in chapter 3, the step-by-step procedure for designing the rectenna is presented in detail. First, the microstrip antenna design is discussed and analyzed, followed by the rectification section.

The first choice for the antenna design concerns the dielectric material. FR-4 has been selected for its ready availability and moderate relative permittivity $\epsilon_r = 4.6$. The selected substrate thickness is 0.062", so there's a good compromise between radiated power and input impedance[1]. The feeding technique was selected to be by an inset on one of the antenna's edges, so during the design process there can be more control on the input impedance of the antenna by varying the inset's width and length.

As a starting point, the antenna's length is given by

$$L = \frac{c}{2f_r\sqrt{\epsilon_r}}$$

Substituting the values $c = 3{\times}10^8 m/s$, $f_r = 2.45{\times}10^9 Hz$ and $\epsilon_r = 4.6$ into the equation we obtain:

[1] *Cfr Section 3.1*

Patch Length [cm]	Resonant Frequency [GHz]
2.80	2.5755
2.85	2.5325
2.90	2.4909
2.95	2.4507
3.00	2.4118
3.05	2.3740
3.10	2.3375
3.15	2.3020
3.20	2.2676

Table 4.1: Design values for L and resulting resonant frequencies f_r

$$\begin{aligned} L &= \frac{c}{2f_r\sqrt{\epsilon_r}} \\ &= \frac{3\times10^8 m/s}{2\times(2.45\times10^9 Hz)\sqrt{4.6}} \\ &= 0.0285m \\ &= 2.85cm \end{aligned}$$

According to what it was discussed in section 3.1, to calculate the resonant frequency with a $\pm 1.6\%$ accuracy, we have to use the following expressions:

$$f_r = \frac{c}{2(L+2\Delta L)\sqrt{\epsilon_{re}}}$$

where

$$\epsilon_{re}(L) = \frac{\epsilon_r + 1}{2} + \frac{\epsilon_r - 1}{2} F(L/h)$$

Programming this equations in MATLAB, we can select the value of L such that the resonant frequency is $2.45GHz \pm 39.2MHz$. Table 4.1 contains the corresponding values of L, and resulting f_r where $\epsilon_{re} = 4.2$.

According Table 4.1, a close resonant frequency value to the desired 2.45GHz frequency is obtained with a patch of a length $L = 2.95cm$. A more in depth analysis gives us an exact solution with $L = 2.9509cm$. In practice, such a level of accuracy is

not easily obtained with conventional fabrication methods, therefore it was decided to keep the original value of $L = 2.95cm$. If, during the lab tests, the resonant frequency is out of the expected range, the antenna can be manually tuned by adding a small tuning flag[2] at one end of it, and by trimming it consecutively the desired resonance can be achieved [24]. The width of the patch was selected to be $W = 3.7cm$ to keep a W/L relation of 1.25.

Another design issue was to select the proper feed point location (inset length) such that the antenna's input impedance was 50Ω. The proposed value is given by:

$$X_f = \frac{L}{2\sqrt{\epsilon_{re}(L)}}$$

Using $L = 2.95cm$ and a value of $\epsilon_{re} = 3.84$, obtained from 3.5, the inset's length is

$$\begin{aligned} X_f &= \frac{L}{2\sqrt{\epsilon_{re}(L)}} \\ &= \frac{0.0295m}{2\sqrt{3.84}} \\ &= 0.00752m \\ &= 7.52mm \end{aligned}$$

Summarizing, the patch antenna to be analyzed with a simulation software will have the following physical characteristics

- Length: 2.95cm
- Width: 3.7cm
- Inset length: 7.52mm

Figure 4-1 shows the dimensions of the designed antenna.

[2] A tuning flag is a piece of transmission line terminated in an open circuit connected to one end of the antenna.

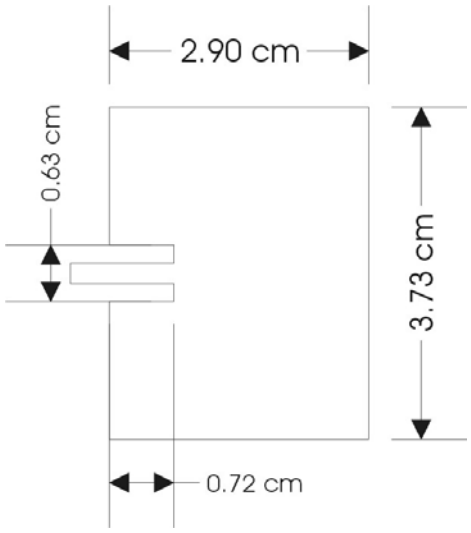

Figure 4-1: Final Antenna Design

4.1.1 Maxwell 2D Modeling

Here the results of the simulation with Maxwell 2D [27] of the antenna previously analyzed are presented. Using an edge port model, the resulting simulations for three different patches are shown: a patch with the feed point located on the edge of the patch (figure 4-2), a patch with the feed point located at the previously calculated inset length (figure 4-3) and a patch with an optimized inset length for near-resistive input impedance at 2.45GHz (figure 4-4).

The edge-fed patch results are shown in figure 4-2. It can be seen that this antenna exhibited poor performance from its extremely high VSWR[3] of 4.5, and the non purely-resistive nature of the input impedance ($Z_{in} = 43 - j70[\Omega]$) near the frequency of interest contributes to this.

The performance for the proposed microstrip antenna patch is shown in figure 4-3. Note that the resonant frequency is not located near the expected 2.45GHz value. This can be seen in the Input Return Loss (S_{11}) chart 4-3(a), where the resonance is located around 2.475GHz. Also, the input impedance at this frequency is somewhat high, about 70Ω.

Under the simulator environment, the tuning was achieved by modifying both the

[3]Voltage Standing Wave Ratio

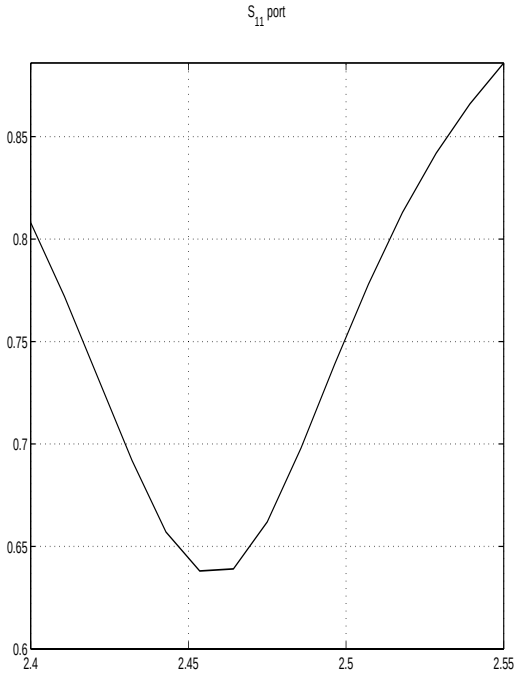

(a) S11

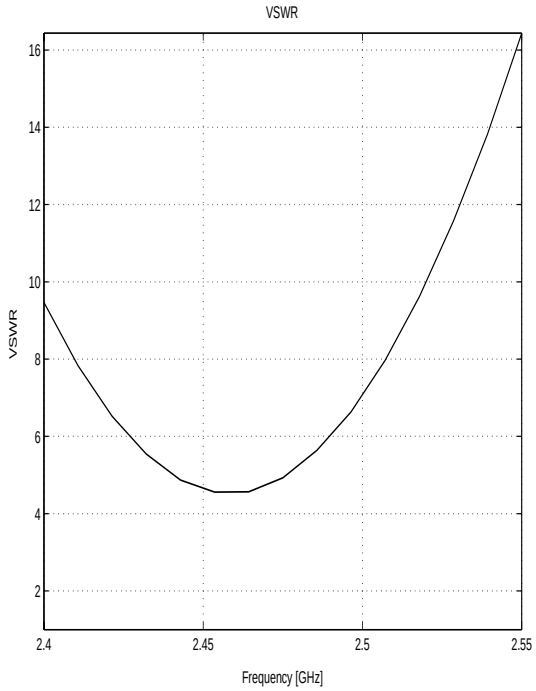

(b) VSWR

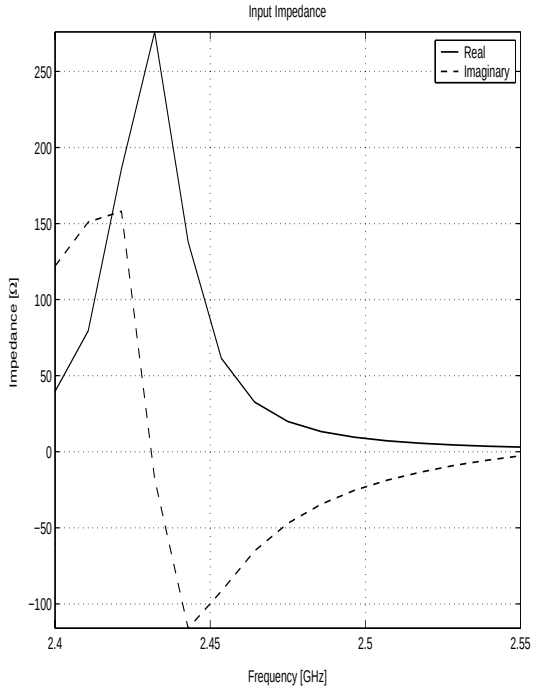

(c) Input Impedance

Figure 4-2: Simulation results for the edge-fed patch antenna

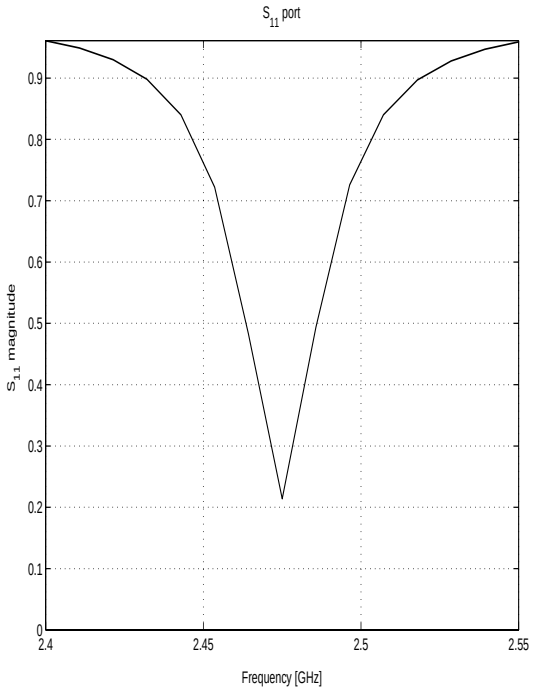

(a) S11

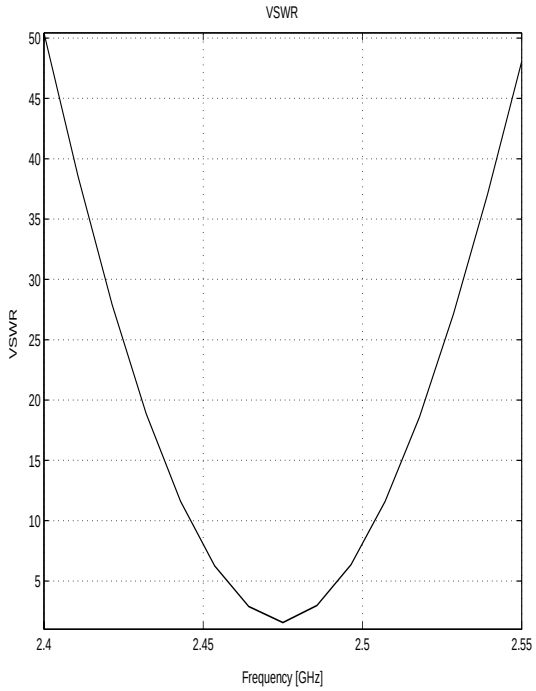

(b) VSWR

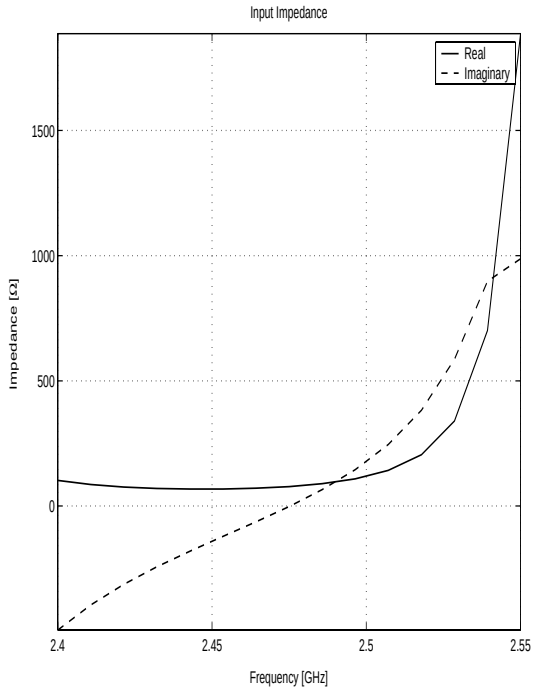

(c) Input Impedance

Figure 4-3: Simulation results for the inset-fed patch antenna

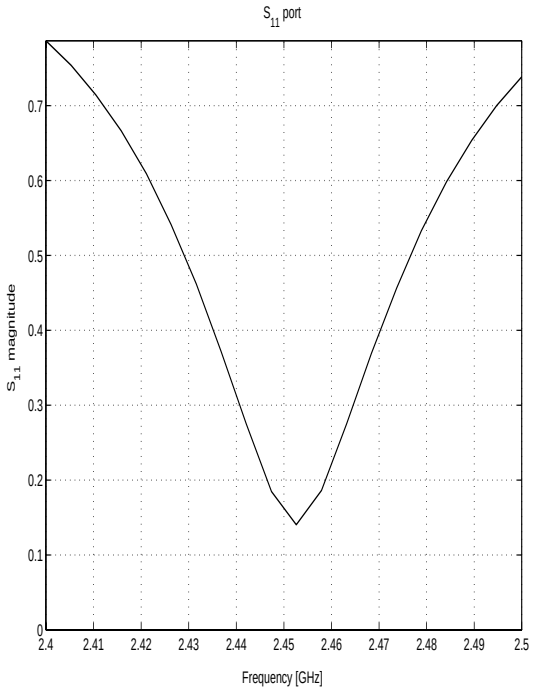

(a) S11

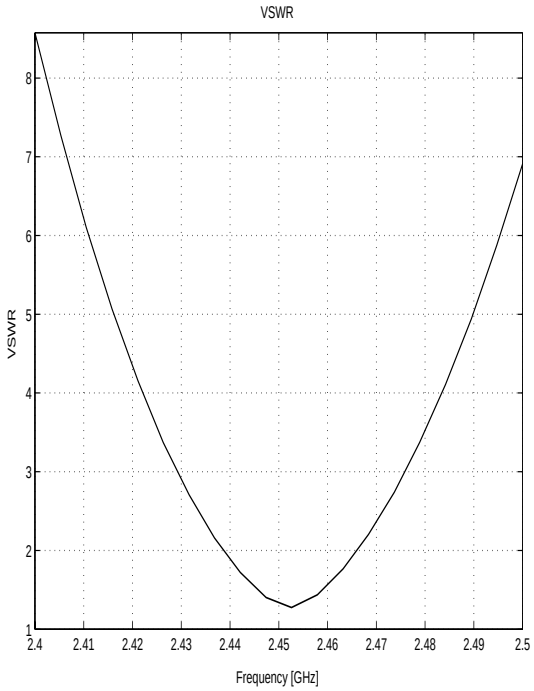

(b) VSWR

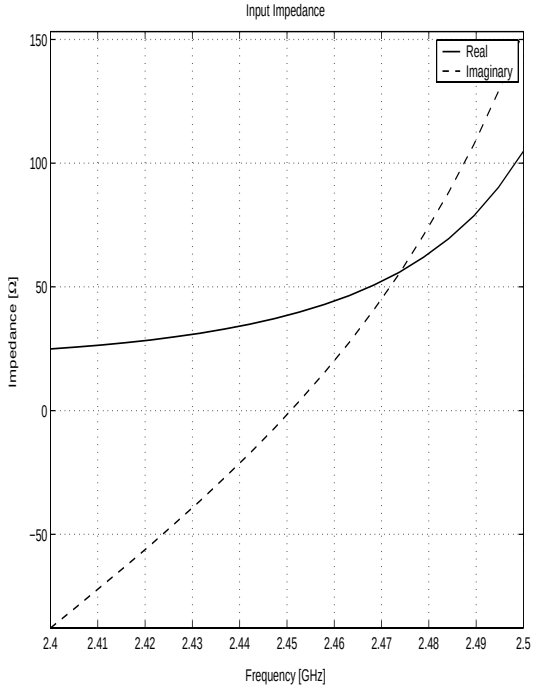

(c) Input Impedance

Figure 4-4: Simulation results for the modified inset-fed patch antenna

inset dimensions and the patch width. The results obtained from this simulation are shown in figure 4-4. The new inset length is 7.2mm, and the separation from the microstrip feeding line is about 2mm. It is important to also notice that the patch width has been slightly modified, from 3.7cm to 3.73cm. It can be seen that there is an important improvement in the resonant frequency; now the antenna is close to 2.455GHz with an acceptable VSWR of approximately 1.2:1. The expected bandwidth is about 40MHz, where the bounds are given by a VSWR of 2:1.

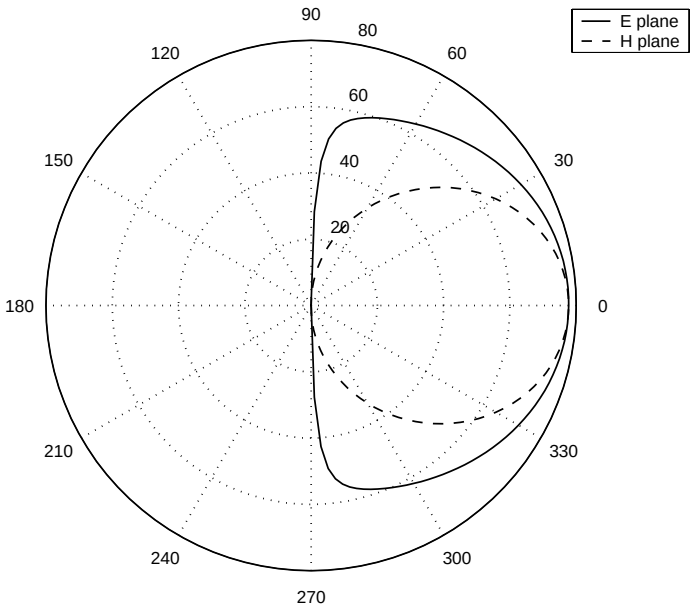

Figure 4-5: Predicted Radiation Pattern for the proposed patch antenna. The calculated beamwidth is about 90°

Summarizing, the characteristics of the final antenna to be manufactured are

- Length: 2.95cm
- Width: 3.73cm
- Inset Length: 7.2mm

The expected radiation pattern is shown in 4-5. The simulated gain of the antenna is 6dB, a value that is typical for this kind of antennas.

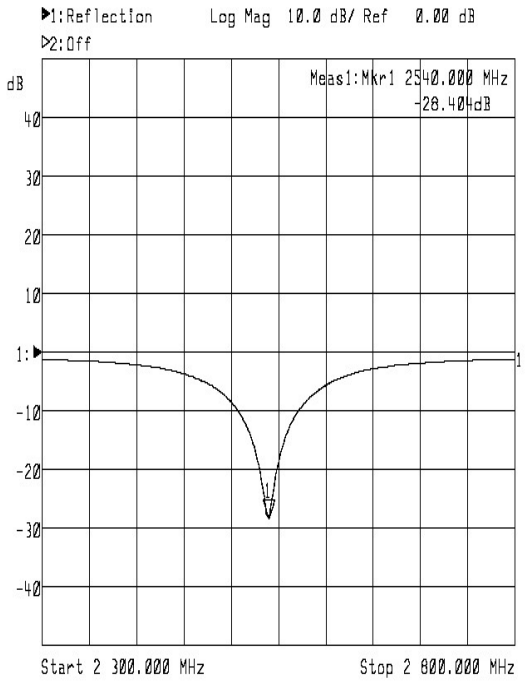

(a) Input Return Loss

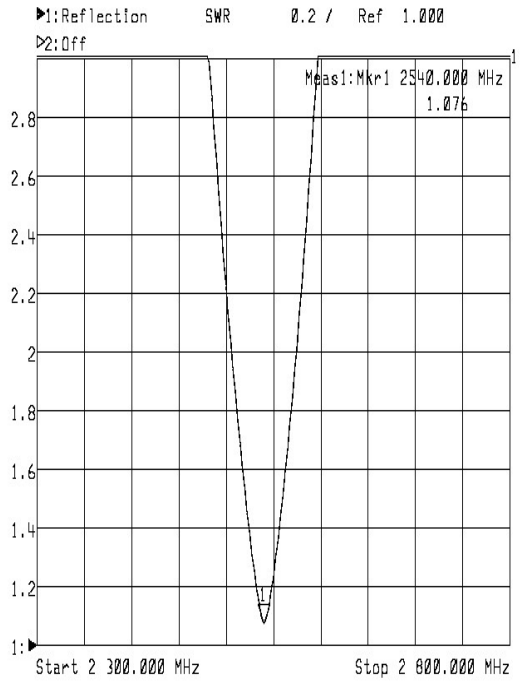

(b) VSWR

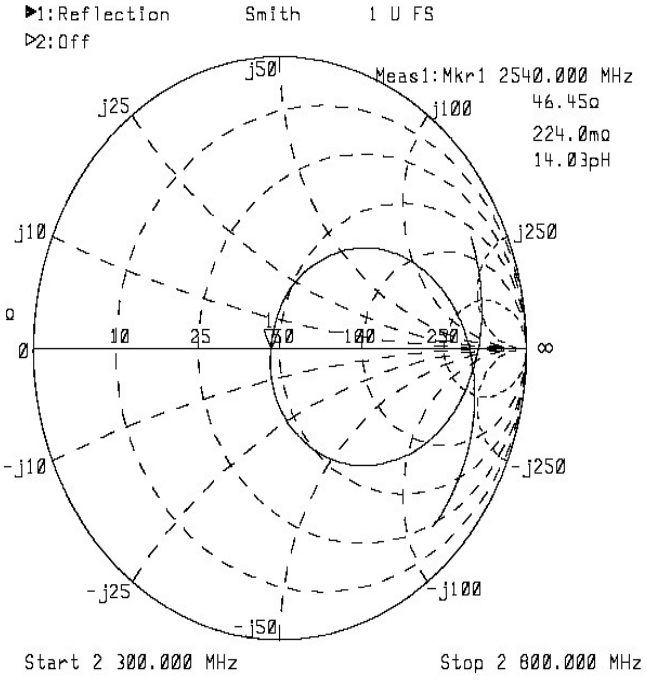

(c) Input Impedance

Figure 4-6: Measured values for the designed inset-fed patch antenna

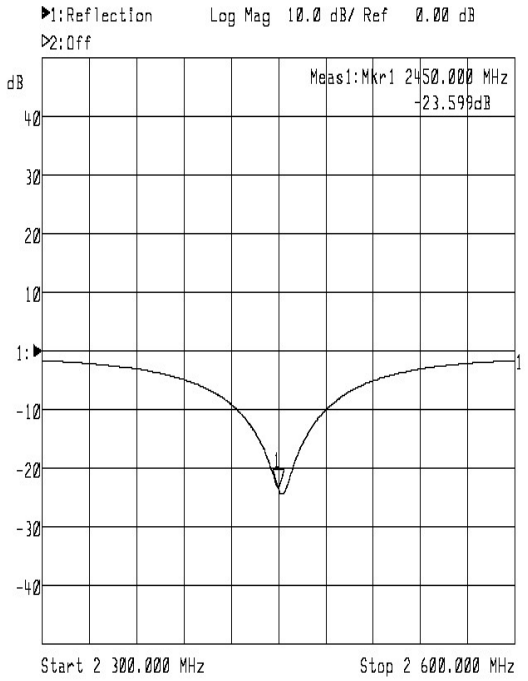

(a) Input Return Loss

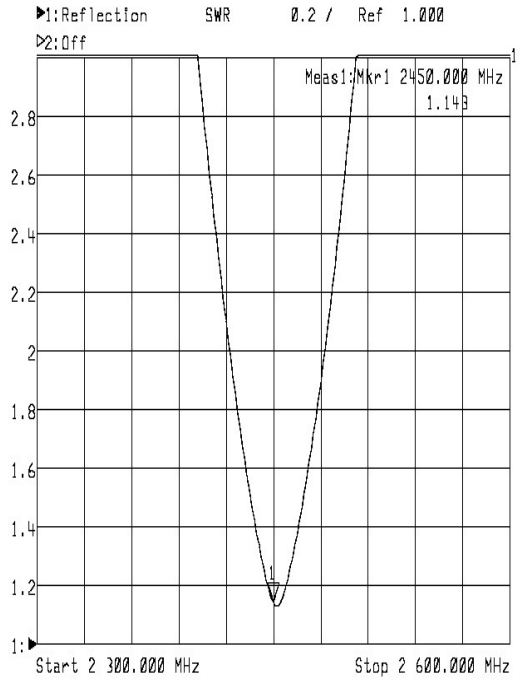

(b) VSWR

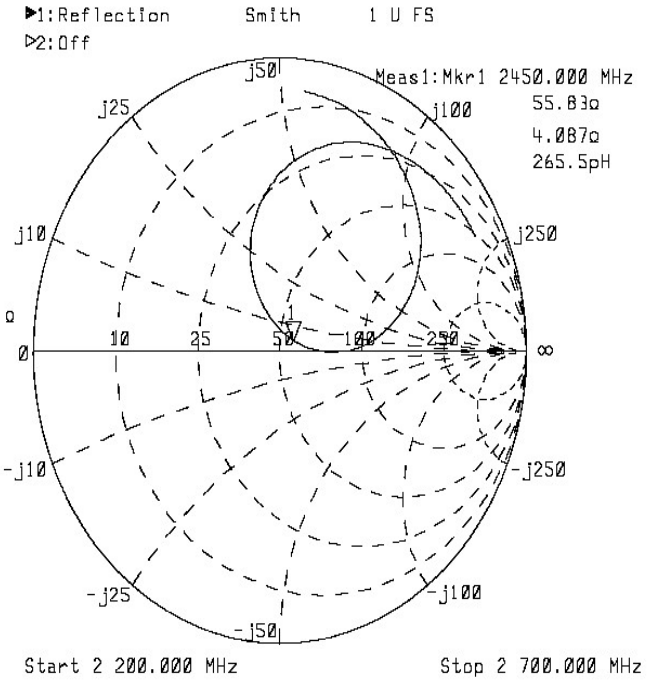

(c) Input Impedance

Figure 4-7: Measured values for the tuned inset-fed patch antenna

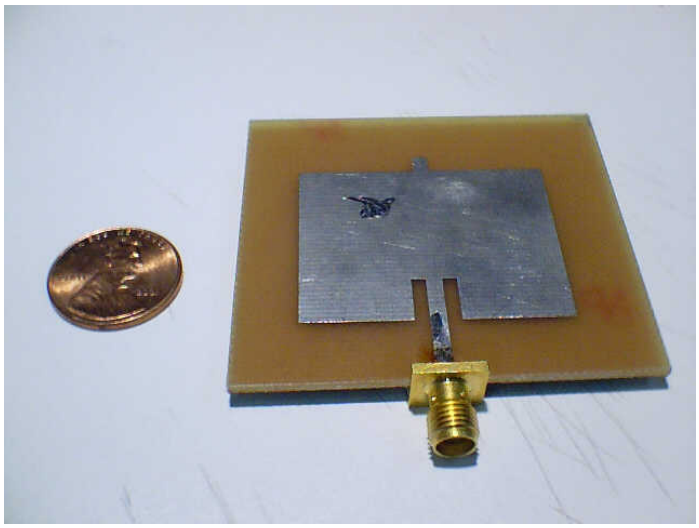

Figure 4-8: Manufactured Antenna

4.1.2 Measured Antenna Performance

The physical antenna that was built is shown in figure 4-8. Due to the lack of an RF anechoic chamber, the measurement of the antenna's radiation patterns could not be made. Both VSWR and Input Impedance were obtained using an Agilent Technologies 8714C Network Analyzer. The measurement of these data can provide useful information about the expected antenna's performance. Figure 4-6 shows the measured Input Return Loss, VSWR and complex Input Impedance of the antenna that was analyzed and discussed previously. It can be observed that the center frequency is located at 2.54GHz, not at the desired 2.45GHz value. Therefore, the need for manually tuning the antenna arises. Using a tuning flag in one end of the antenna [24] of a fixed longitude, by consecutively trimming it, the antenna can be tuned to a higher frequency. Following this procedure, the results shown in 4-7 were obtained. Now the antenna is tuned to 2.45GHz, with an Input Return Loss close to -20dB, and an approximate bandwidth of 30MHz. The input impedance at the center frequency was measured to be very close to the desired 50Ω value ($55 + 4j\Omega$).

4.2 Rectifier Design

The proposed rectification circuitry is shown in figure 4-9

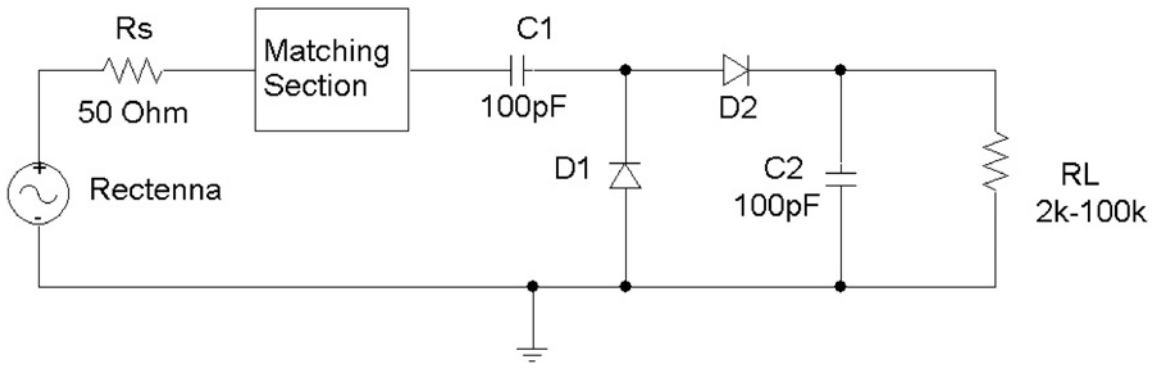

Figure 4-9: Proposed Rectification Circuit

The diodes are placed in a voltage-doubler configuration. The rectifiers are Schottky-barrier diodes, manufactured by Agilent technologies. These diodes are optimized for high-frequency operation ($f > 1GHz$). Two types of diodes will be analyzed: the HSMS8202 and the HSMS2852. They were selected following recommendations given in a few Agilent Technologies Application Notes [28–30].

To simulate the diodes, their SPICE parameters are needed. These are summarized in table 4.2

Parameter	Units	HSMS-2852	HSMS-8202
B_V	V	3.8	7.3
C_{J0}	pF	0.18	0.18
E_G	eV	0.69	0.69
I_{BV}	A	3E-4	10E-5
I_S	A	3E-6	4.6E-8
N	-	1.06	1.09
R_S	Ω	25	6
$P_B(V_J)$	V	0.35	0.5
$P_T(XTI)$	-	2	N/A
M	-	0.5	0.5

Table 4.2: SPICE parameters for the proposed diodes

Using the SPICE parameters, the first analysis of rectification properties of an HSMS8202 diode in a single detector configuration was made using Agilent Technologies AppCAD design software. The resulting performance is shown in 4-10(a). Using the HSMS2852, the obtained simulated performance is presented in 4-10(b)

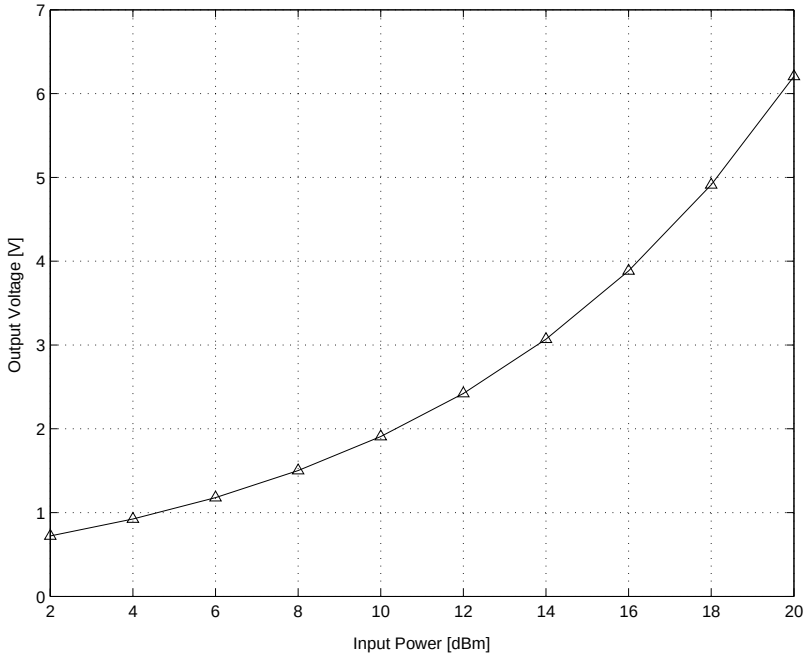

(a) HSMS8202

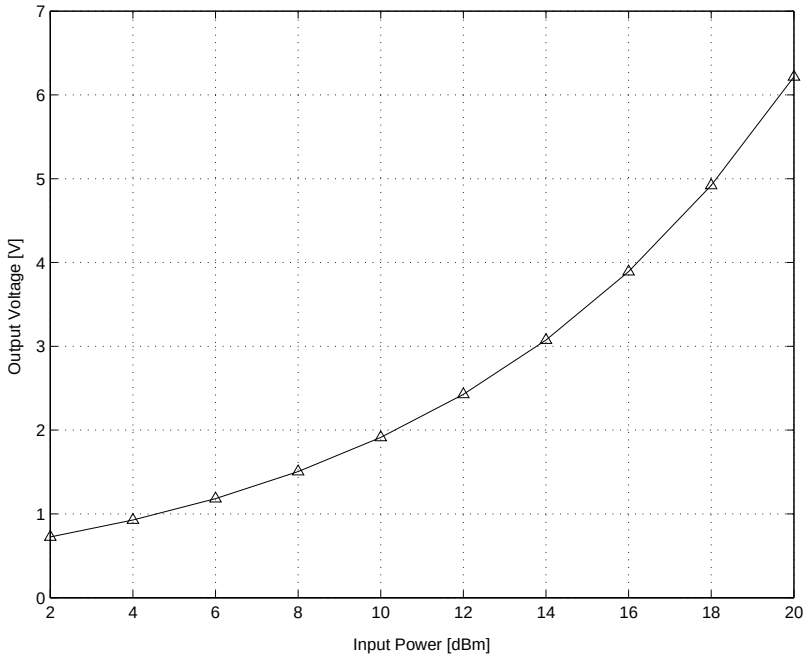

(b) HSMS2852

Figure 4-10: Voltage Outputs for the two proposed diodes

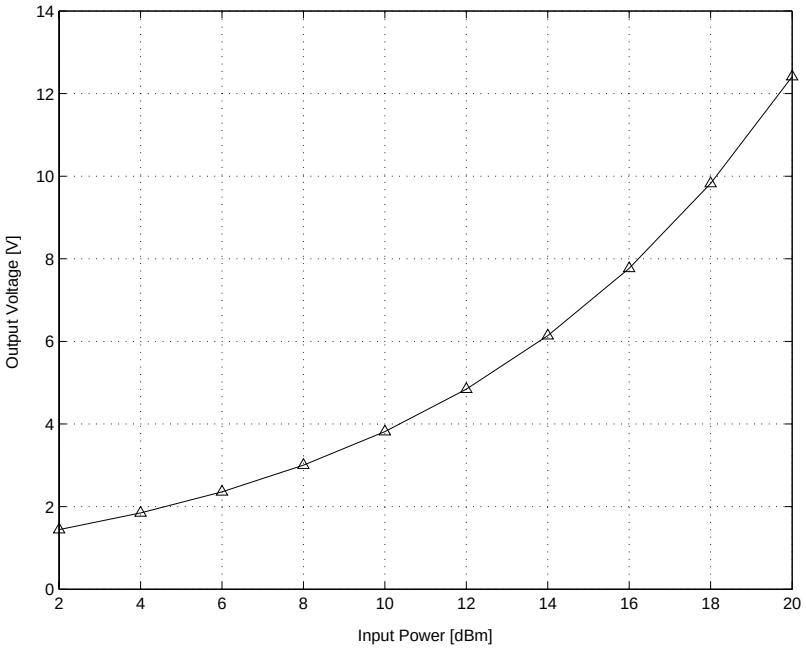

(a) HSMS8202

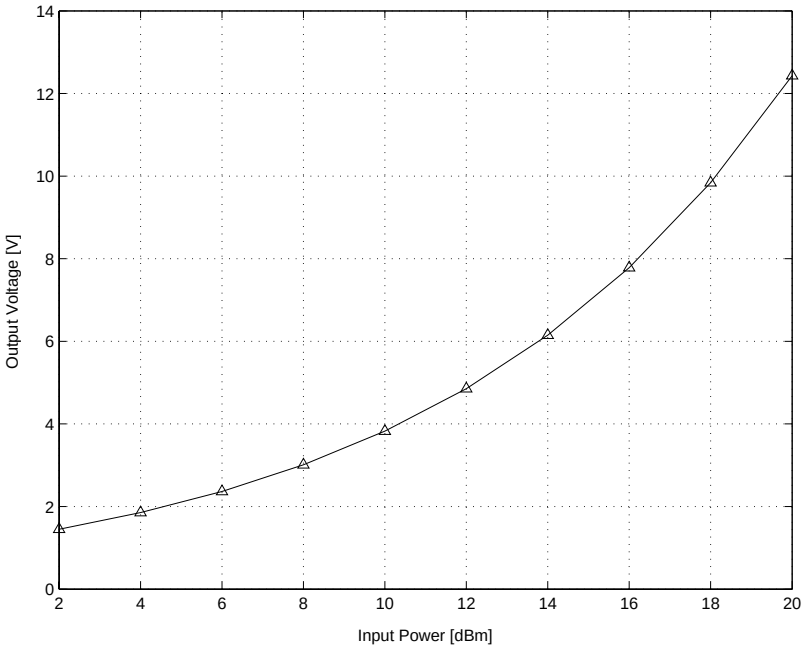

(b) HSMS2852

Figure 4-11: Voltage-doubler Outputs for the two rectifiers

Note that the presented voltage values correspond to a rectifier diode in a single configuration. In theory, the voltage-doubler configuration doubles the output voltage compared to the single configuration at the same input power [31]. Thus the expected performances are presented in figures 4-11(a) and 4-11(b). According to these results, so far no significant difference can be seen between in either one of the diodes. Thus any further analysis (unless stated otherwise) is assumed to had been made using an HSMS8202 for the sake of simplicity.

Considering that the SPICE model assumes a perfect match between the antenna and the rectification circuitry, the efficiency can be as high as 100% (ideal case) or, assuming a worst-case scenario with a poor match at the rectifier's input, the overall efficiency of the detector can be as low as 50% [6,26,32]. The resulting power outputs curves are then plotted in 4-12 for four different possible efficiencies according to literature [26].

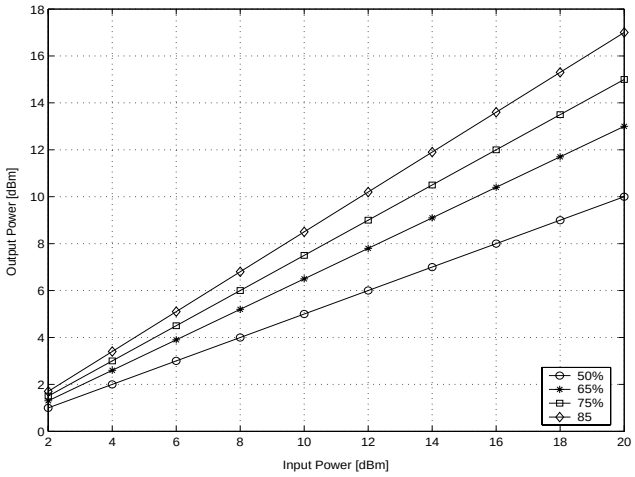

Figure 4-12: Output power for different rectification efficiencies

Combining the previously obtained output voltages and output powers, and also remembering that $P = VI$, a final set of curves related to the current that can be delivered to the matched load given a specific input power is shown in figure 4-13.

This set of curves characterizes the performance of the wireless Rectenna system.

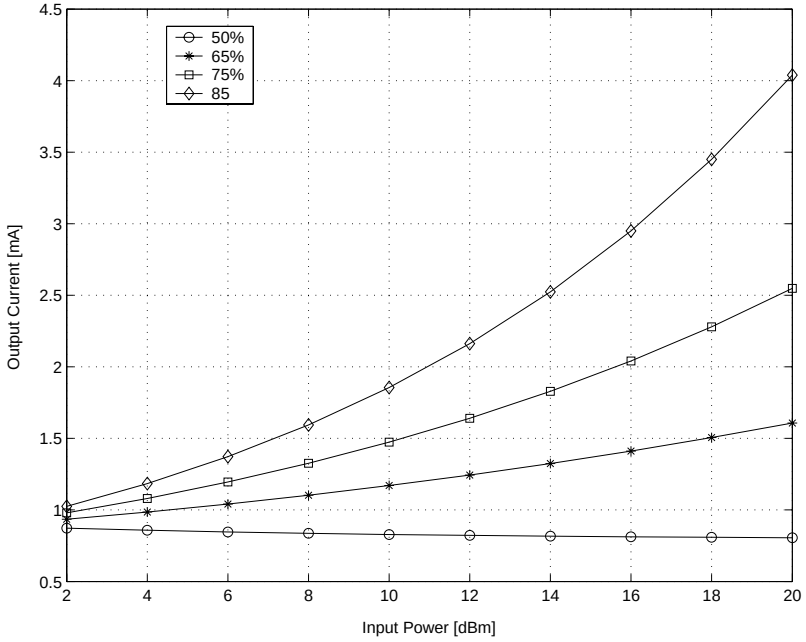

(a) Unregulated

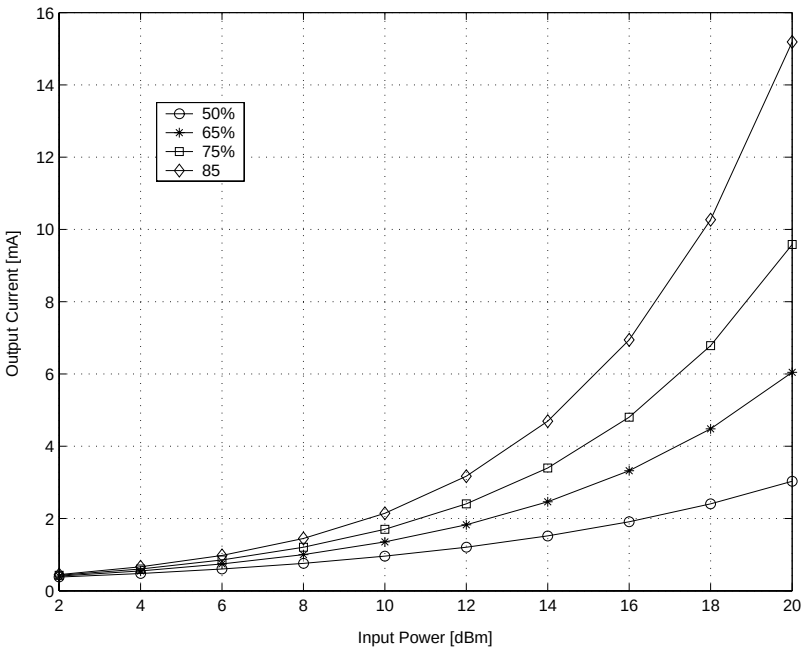

(b) Regulated ($V_{out} = 3.3V$)

Figure 4-13: Current Outputs for the proposed rectifier: a) with no voltage regulation and b) with a fixed voltage output

Frequency	0dBm	5dBm	10dBm
2435	7-88.4j	8.4-92j	9.4-95j
2440	7.5-89j	8.6-92j	9.7-95j
2445	7.6-89.3j	9-93j	10-95.8j
2450	7.9-89.7j	9.2-93.4j	10.3-96j
2455	8-90j	9.3-93j	10.5-96.7j
2460	8.2-90j	9.7-94j	10.8-97j
2465	8.5-90.8	9.9-94.5j	11-97.7j

Table 4.3: HSMS8202 Input impedances at different power input levels, $R_L = 100k\Omega$

Frequency	0dBm	5dBm	10dBm
2435	30-101j	40.8-101.8j	49.5-101j
2440	30.5-101.8j	41.4-101.6j	50-101j
2445	31.2-102.5j	42.2-102.2j	51-101j
2450	31.5-102.6j	43-102.4j	52-101.9j
2455	32.2-103.2j	43.5-102.7j	52.5-102j
2460	32.8-103.6j	44.3-103.3j	53.6-102.4j
2465	33.4-104j	45-103.3j	54.2-102.5j

Table 4.4: HSMS8202 Input impedances at different power input levels, $R_L = 2k\Omega$

4.2.1 Diode's Impedance Matching

To ensure maximum power transfer, a good impedance matching network has to be realized between the antenna and the rectifier's input. First, the diode's input impedance has to be measured at the expected frequency range (2.4-2.5GHz). For the HSMS8202 diode pair, the results obtained with two different loads are shown using two different load values: $100k\Omega$ (table 4.3) and $2k\Omega$ (table 4.4).

For the HSMS2852 the corresponding obtained impedances are:

Frequency	0dBm	5dBm	10dBm
2435	8.5-66.9j	11.0-68.7j	28.7-62.9j
2440	8.7-66.9j	11.4-68.6j	28.7-63j
2445	8.9-67j	11.6-68.9j	29-63.1j
2450	9-67.2j	11.8-68.9j	29.0-63j
2455	9.1-67.2j	12-69j	29.1-63j
2460	9.3-67.4j	12.2-69j	29.3-63.1j
2465	9.5-67.4j	12.37-69j	29.3-63j

Table 4.5: HSMS2852 Input impedances at different power input levels, $R_L = 100k\Omega$

Frequency	0dBm	5dBm	10dBm
2435	22.8-44.6j	26-45j	30-44j
2440	23.0-44.6j	26.2-44.8j	30.3-44j
2445	23.1-44.6j	26.4-44.8j	30.5-43.9j
2450	23.2-44.6j	26.6-44.8j	30.7-43.6j
2455	23.4-44.6j	26.7-44.6j	30.8-43.7j
2460	23.6-44.6j	26.9-44.7j	31-43.6j
2465	23.7-44.5j	27-44.6j	31.3-43.4j

Table 4.6: HSMS2852 Input impedances at different power input levels, $R_L = 2k\Omega$

To achieve a good impedance match between the elements, a single-stub matching network was designed using microstrip techniques, as previously discussed in section 3.3.2. Figure 4-14 shows the proposed matching networks for both rectification diodes.

Given the fact that the diode's input impedance is somewhat sensitive to the input power, as it was shown previously in 4.2.1, the design was more focused on the medium-to-low end of the power range, which is 5dBm to 0dBm. Thus, it was assumed that P_{in}=5dBm for the proposed matching sections shown in 4-14. The assumed input impedances correspond to the values obtained in tables 4.4 and 4.6, that correspond to input impedances with a 2kΩ output load. The Smith Chart in figure 4-15(a) shows the expected performance for the HSMS8202 matching section at 0dBm, whereas figures 4-15(b) and 4-15(c) show the resulting matched impedance

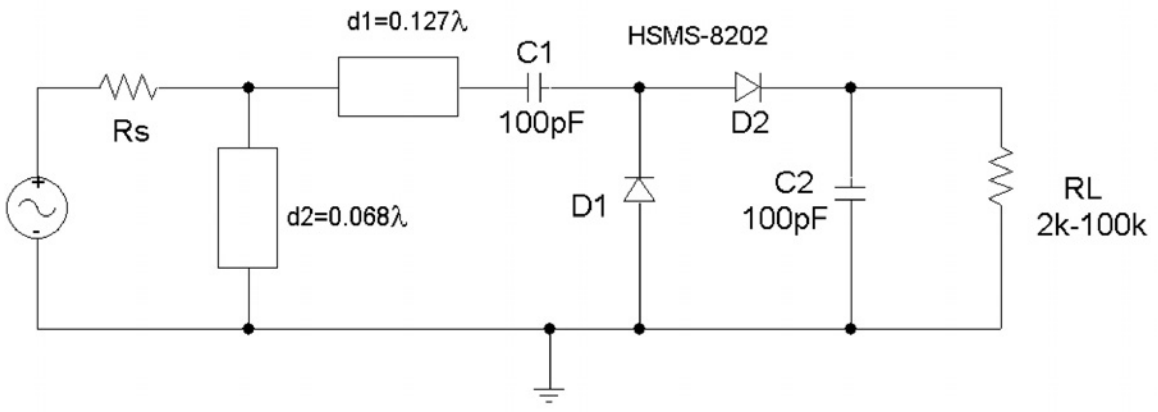

(a) HSMS8202

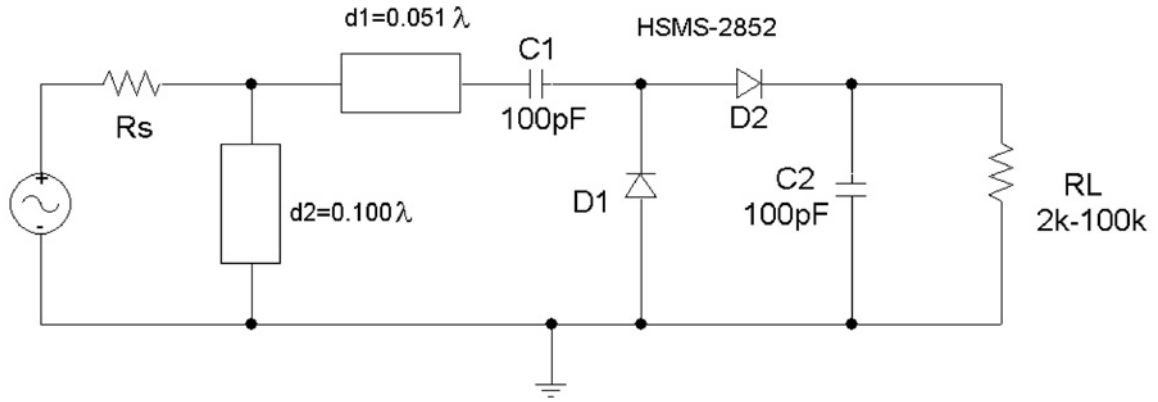

(b) HSMS2852

Figure 4-14: Proposed Matching Sections. Stub dimensions are given in wavelengths.

for the other two power levels of 5dBm and 10dBm respectively. Figure 4-16 shows the simulated impedance match for the HSMS2852.

4.2.2 Measured Rectification Data

Impedance Matching

The tuning of the matching circuit was made manually with the aide of a network analyzer. The rectification and proper tuning circuit can be seen in 4-20. Given the fact that the input impedance of the diodes is sensitive to the input power, as it was observed in the previous section, the matching had to be made with a fixed input power. It was decided then to perform manual tuning with an input power of 5dBm, as was observed that as the input power increased, the performance improved even without a proper matching section. Thus for the input power levels starting at 0dBm, the impedance match will improve as the power gets close to 5dBm, and for higher powers it should behave similarly.

For the HSMS2852 the results are shown in 4-17, 4-18, and 4-19. It is important to notice the poor matching achieved here. The graphs 4-21, 4-22, and 4-23 show the coupling obtained in the lab with the HSMS8202 diode. The VSWR obtained is 1.15:1, it also is interesting to notice that this value goes as low as 1.25:1 at the highest input power value (10dBm). This is a more than acceptable impedance match over the whole power range.

Voltage Conversion

Table 4.8 shows the obtained voltages using the HSMS8202. The rectification efficiency is higher around the medium power levels, which is expected due to the fact that the matching section is optimized at those levels. The efficiency values range from 50% in the lower power end and up to 70% near the medium-to-high power levels.

It is important to notice that the other diode pair, the HSMS2852, had a poor performance for the same levels. This results are expected, given the poor matching

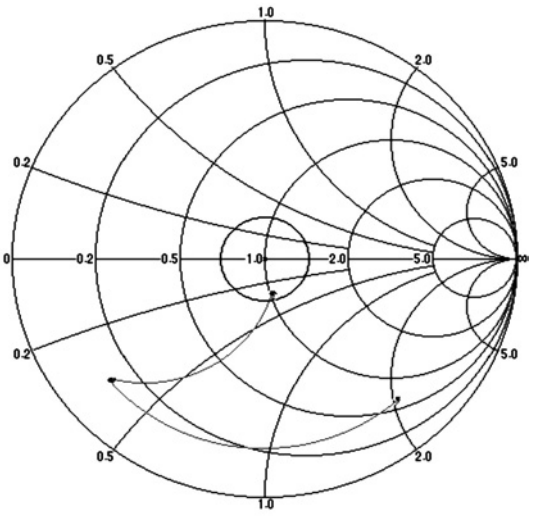

(a) 0dBm

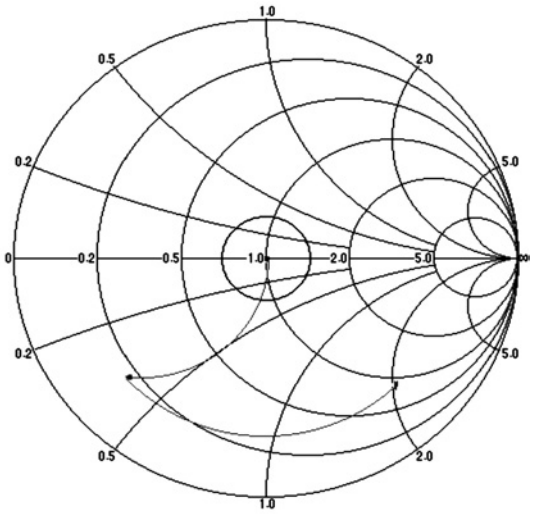

(b) 5dBm

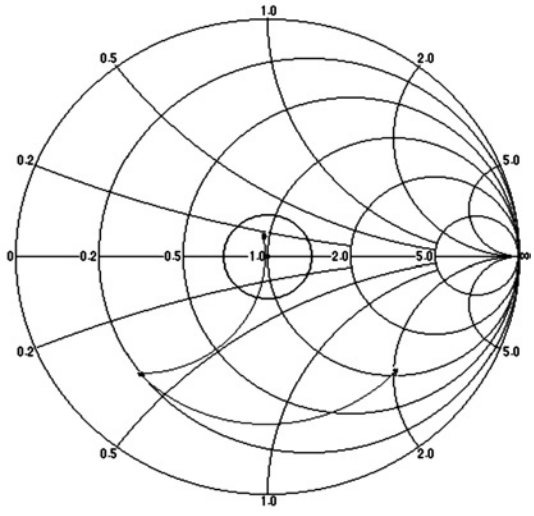

(c) 10dBm

Figure 4-15: Simulation results for the HSMS8202 Matching Circuit Section, $R_L = 2k\Omega$

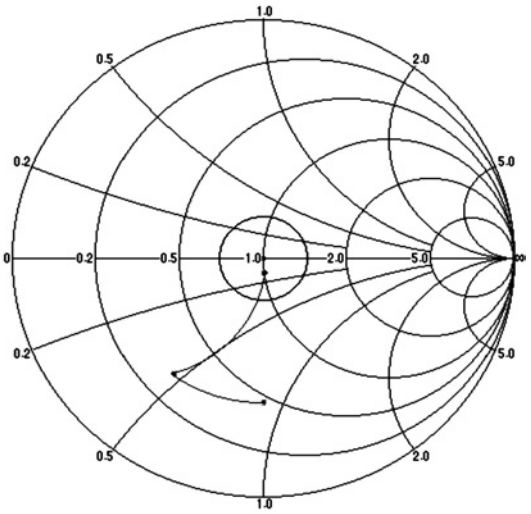

(a) 0dBm

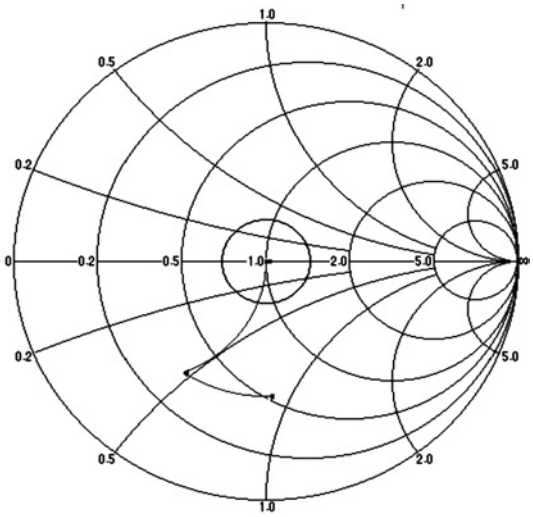

(b) 5dBm

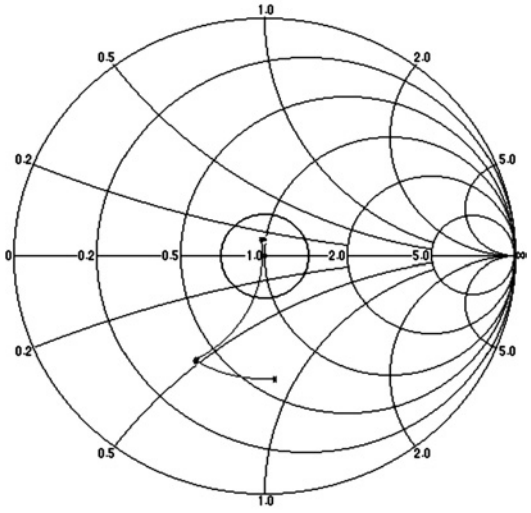

(c) 10dBm

Figure 4-16: Simulation results for the HSMS2852 Matching Circuit Section, $R_L = 2k\Omega$

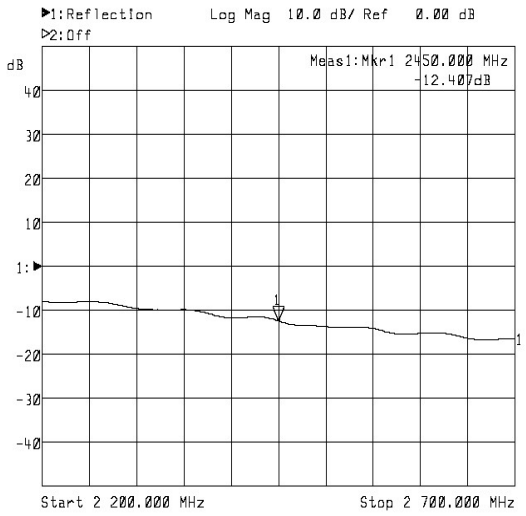

(a) 0dBm

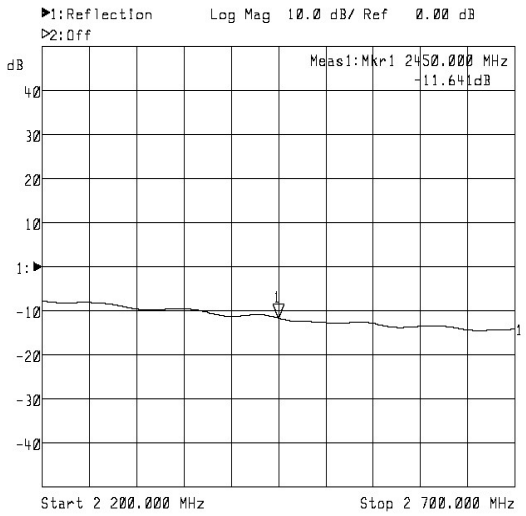

(b) 5dBm

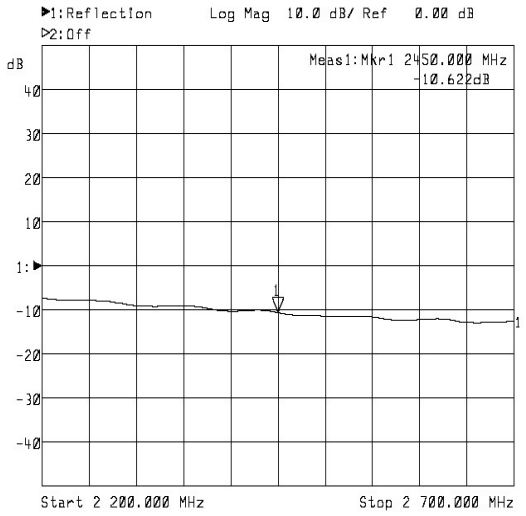

(c) 10dBm

Figure 4-17: Measured Input Return Loss for the HSMS2852 Matching Circuit Section, $R_L = 2k\Omega$

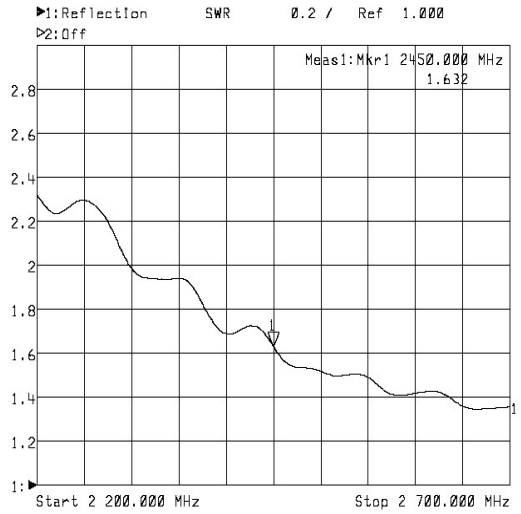

(a) 0dBm

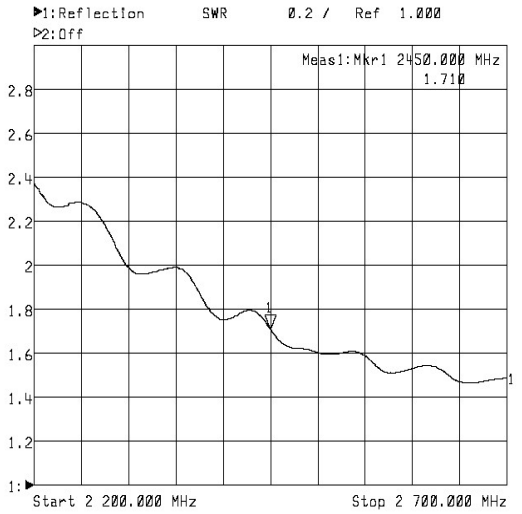

(b) 5dBm

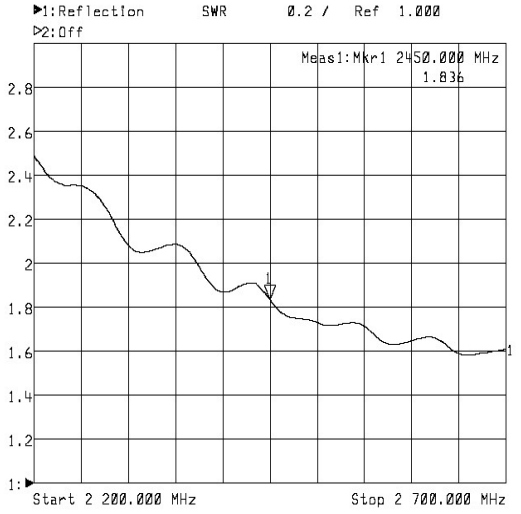

(c) 10dBm

Figure 4-18: Measured VSWR for the HSMS2852 Matching Circuit Section, $R_L = 2k\Omega$

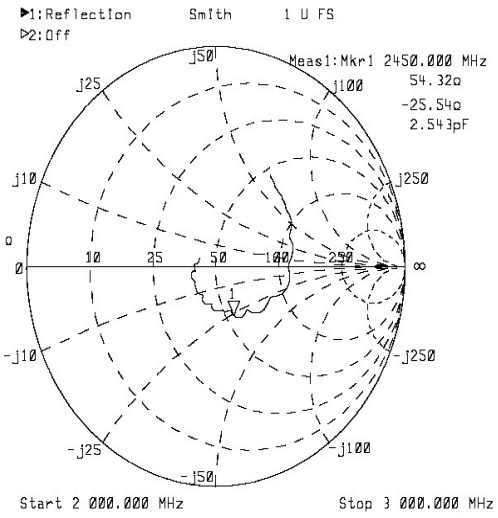

(a) 0dBm

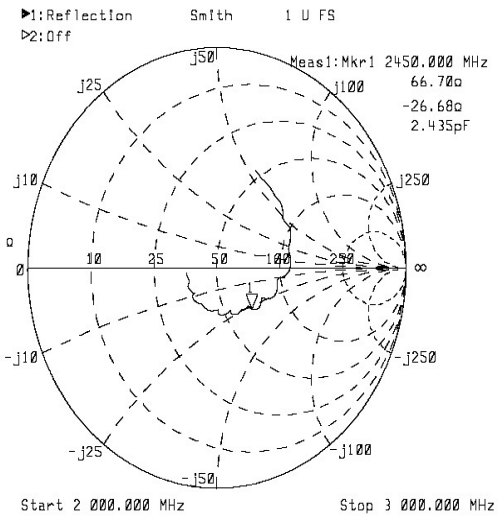

(b) 5dBm

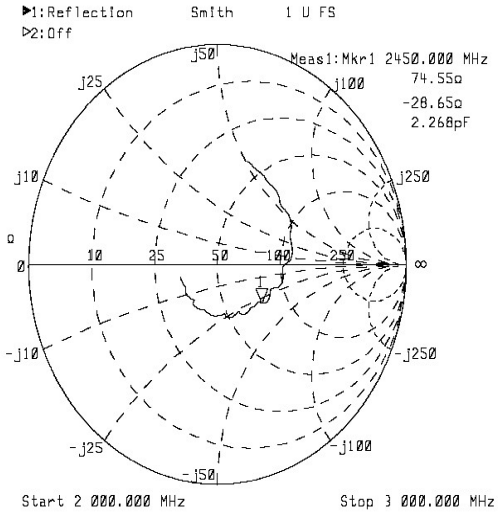

(c) 10dBm

Figure 4-19: Measured Input Impedance for the HSMS2852 Matching Circuit Section, $R_L = 2k\Omega$

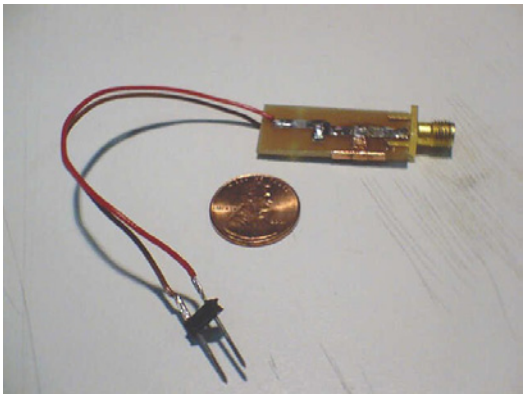

(a) Rectifier circuit

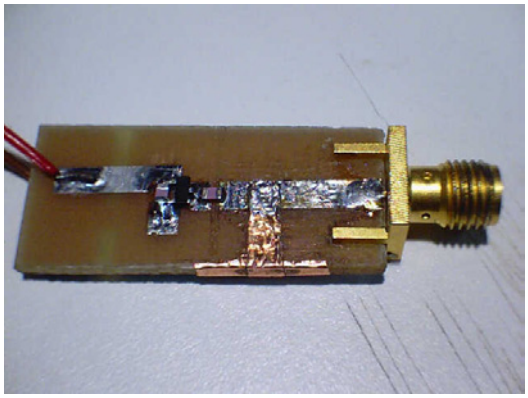

(b) Detail of the Matching Section

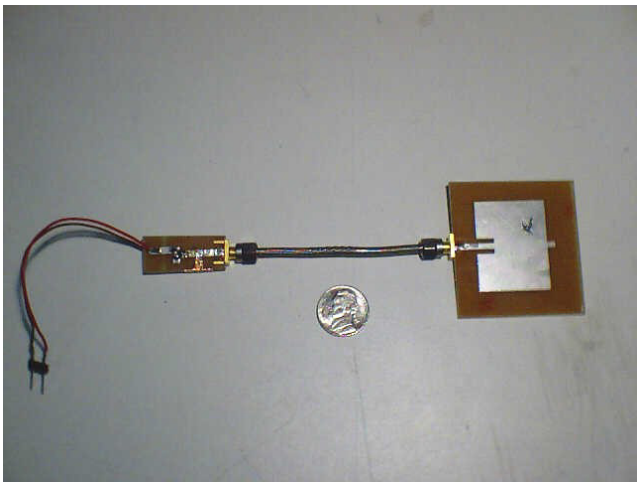

(c) Complete Rectenna

Figure 4-20: Rectification Circuit Board for the HSMS8202 and Final Rectenna System.

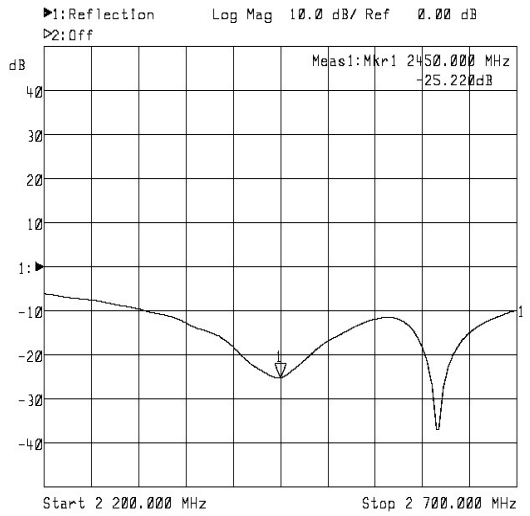

(a) 0dBm

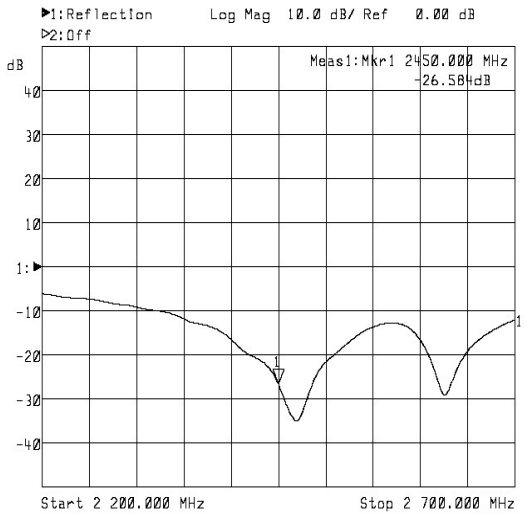

(b) 5dBm

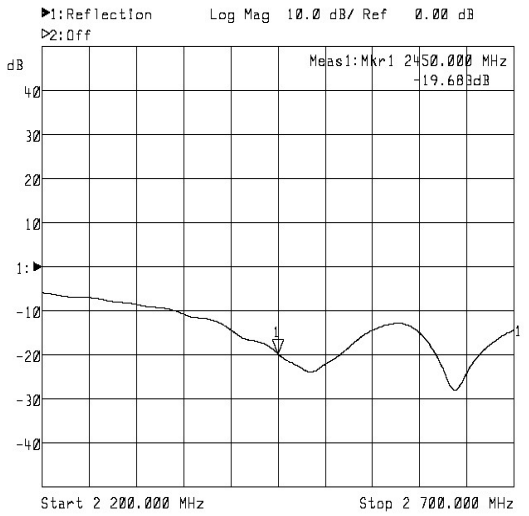

(c) 10dBm

Figure 4-21: Measured Input Return Loss for the HSMS8202 Matching Circuit Section, $R_L = 2k\Omega$

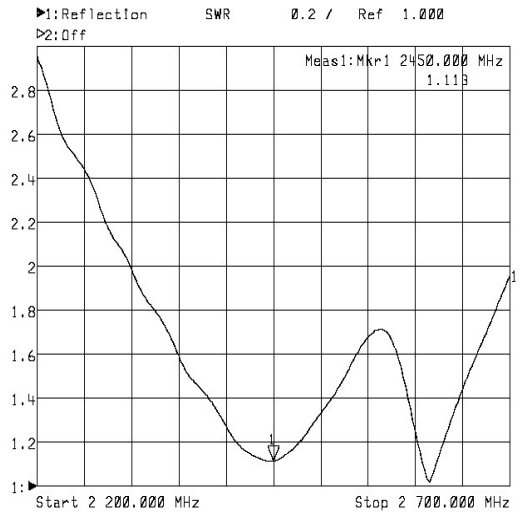

(a) 0dBm

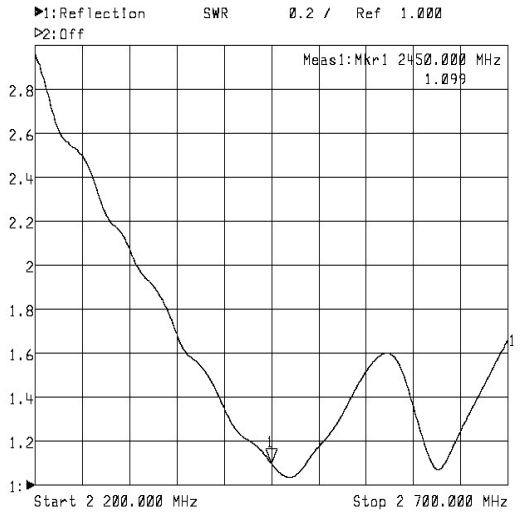

(b) 5dBm

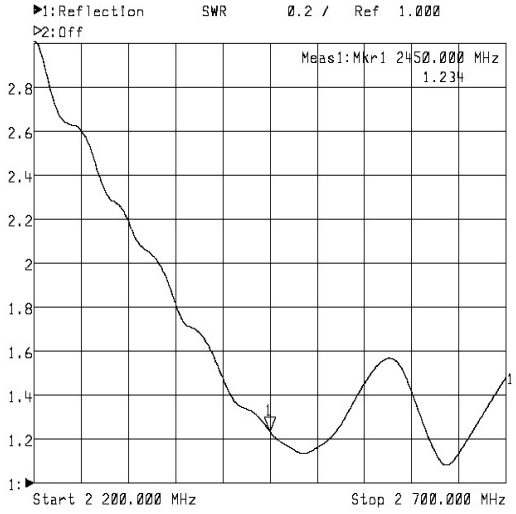

(c) 10dBm

Figure 4-22: Measured VSWR for the HSMS8202 Matching Circuit Section, $R_L = 2k\Omega$

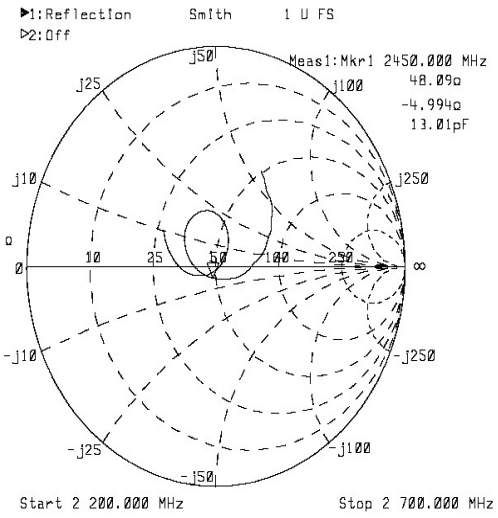

(a) 0dBm

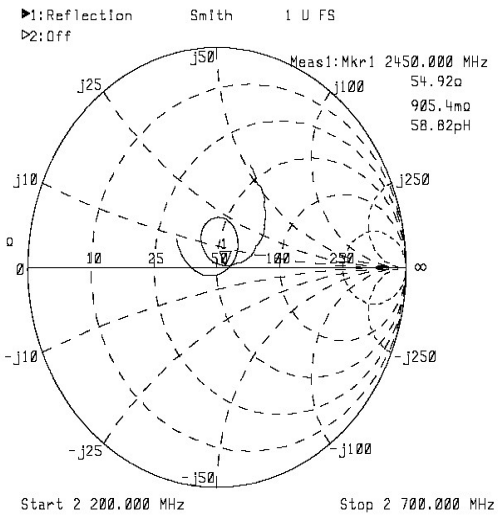

(b) 5dBm

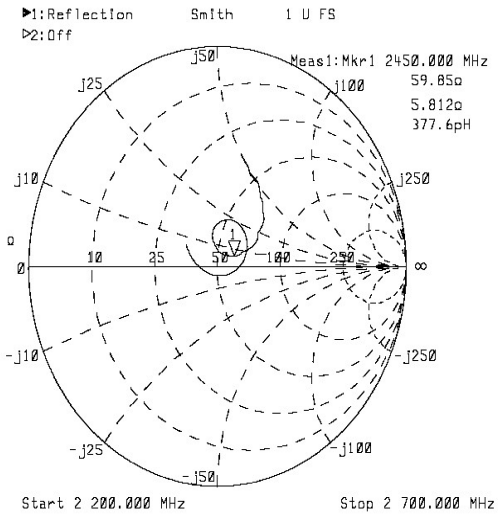

(c) 10dBm

Figure 4-23: Measured Input Impedance for the HSMS8202 Matching Circuit Section, $R_L = 2k\Omega$

P_{in} [dBm]	P_{in} [mW]	V_{out} [V]	P_{out} [mW] $R_L = 2k\Omega$	P_{out} [dBm]	Efficiency [%] $\eta = (P_{in}/P_{out})\times 100$
0	1.0000	0.36	0.0648	-11.8842	6.4800
2	1.5849	0.44	0.0968	-10.1412	6.1077
4	2.5119	0.56	0.1568	-8.0465	6.2423
6	3.9811	0.70	0.2450	-6.1083	6.1541
8	6.3096	0.90	0.4050	-3.9254	6.4188
10	10.0000	1.16	0.6728	-1.7211	6.7280
12	15.8489	1.32	0.8712	-0.5988	5.4969
14	25.1189	1.63	1.3285	1.2335	5.2887
16	39.8107	1.92	1.8432	2.6557	4.6299
18	63.0957	2.16	2.3328	3.6788	3.6972
20	100.0000	2.16	2.3328	3.6788	2.3328

Table 4.7: Measured Voltages for the HSMS2852 rectification circuit

P_{in} [dBm]	P_{in} [mW]	V_{out} [V]	P_{out} [mW] $R_L = 2k\Omega$	P_{out} [dBm]	Efficiency [%] $\eta = (P_{in}/P_{out})\times 100$
0	1.0000	1.00	0.5000	-3.0103	50.0000
2	1.5849	1.33	0.8845	-0.5333	55.8050
4	2.5119	1.70	1.4450	1.5987	57.5265
6	3.9811	2.22	2.4642	3.9168	61.8979
8	6.3096	3.00	4.5000	6.5321	71.3202
10	10.0000	3.84	7.3728	8.6763	73.7280
12	15.8489	4.56	10.3968	10.1690	65.5994
14	25.1189	5.60	15.6800	11.9535	62.4232
16	39.8107	6.63	21.9785	13.4200	55.2074
18	63.0957	7.56	28.5768	14.5601	45.2912
20	100.0000	7.56	28.5768	14.5601	28.5768

Table 4.8: Measured Voltages for the HSMS8202 rectification circuit

achieved during the laboratory tests. This can be seen in the low efficiencies stated in Table 4.7. In previous literature [26] the same behavior was observed, even with a better matching section. Thus, as a final decision for the rectenna, the HSMS8202 will be used as part of the rectification section. The complete rectenna system can be seen in 4-20(c).

4.3 Radio Link calculation

The calculations for the basic radio link that will provide the wireless power to the receiver are presented. The basic Friis equation explained in section 2.3 has been used to calculate the expected radio link power levels at different distances between the transmitter and receiver.

First, it is important to notice the constraints given by the IEEE [10] and FCC [33] concerning the amount of power and power densities a transmitter in the ISM band can handle. According to FCC regulations, the maximum transmitter power is 1W, therefore in all foregoing calculations $P_t = 1W$. Also, the design must be made taking into account that the power density has to be within regulations, that is $2mW/cm^2$, or equivalently $20W/m^2$. For this purpose, equation 2.2 is used so the minimum safety distance where the power density is within specification can be calculated. Thus, solving for R

$$R_{min} = \sqrt{\frac{G_t P_t}{4\pi S_{avg}}}[m]$$

According to the antenna design, the patch antenna has a gain of 6dB. This, in linear quantities, is equal to $10^{6/10} = 3.98$. In this first approach, let's consider that both the transmitting and receiving antenna are the same. Therefore

$$
\begin{aligned}
R_{min} &= \sqrt{\frac{G_t P_t}{4\pi S_{avg}}}[m] \\
&= \sqrt{\frac{(3.98)\cdot(1W)}{(4\pi)\cdot(20W/m^2)}} \\
&= 0.126m \\
&= 12.6cm
\end{aligned}
$$

As it can be seen, the minimum distance is 12.6cm. Shorter distances imply higher densities.

The ends of the ISM band will give the shortest and longest wavelengths that can be used in the system. For the low frequency end (long wavelength)

$$
\begin{aligned}
\lambda &= \frac{c}{f} \\
&= \frac{3 \times 10^8[m/s]}{2.4 \times 10^9[1/s]} \\
&= 0.125m \\
&= 12.5cm
\end{aligned}
$$

For the high frequency end (short wavelength)

$$
\begin{aligned}
\lambda &= \frac{c}{f} \\
&= \frac{3 \times 10^8[m/s]}{2.5 \times 10^9[1/s]} \\
&= 0.12m \\
&= 12cm
\end{aligned}
$$

For simplicity, further calculations are made using the wavelength mean of 12.25cm that corresponds to a frequency of 2.45GHz.

Plugging all the previous values into the Friis equation, the maximum power at

the receiver's end, obtained with the receiver closest to the transmitter, is

$$\begin{aligned} P_r &= \frac{G_t G_r \lambda^2}{(4\pi R)^2} P_t \\ &= \frac{(3.98)^2 (0.1225m)^2}{(4\pi \cdot 0.126m)^2} \cdot (1W) \\ &= 94.81 \times 10^{-3} W \\ &\doteq 95mW \end{aligned}$$

The minimum amount of power is received at the maximum distance, $R = 1m$. Therefore

$$\begin{aligned} P_r &= \frac{G_t G_r \lambda^2}{(4\pi R)^2} P_t \\ &= \frac{(3.98)^2 (0.1225m)^2}{(4\pi \cdot 1m)^2} \cdot (1W) \\ &= 1.5 \times 10^{-3} W \\ &= 1.5mW \end{aligned}$$

The power range is then from 95mW at short ranges and up to 1.5mW at the maximum specified distance. In a decibels scale, the range goes from ∼20dBm to ∼1.8dBm. This is shown in figure 4-24

If an antenna of bigger gain is used, say an array of two patches on the transmitter's side, it is possible to receive more power within the desired distances. The array equivalent gain will be around 12dB according to the theory associated with antenna arrays [34]. The minimum safety distance will then be modified to:

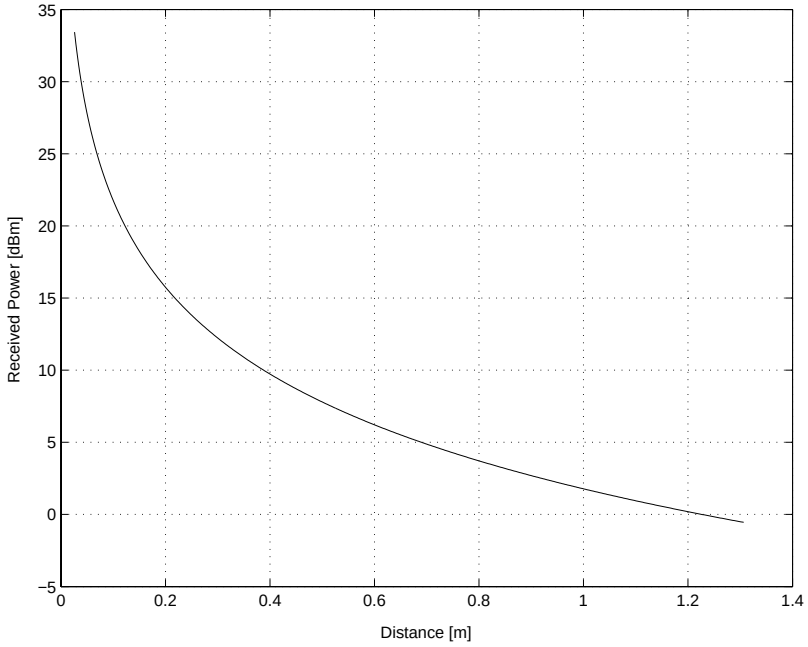

Figure 4-24: Radiolink performance for $P_{tx} = 30dBm$, $G_{tx} = 6dB$

$$\begin{aligned} R_{min} &= \sqrt{\frac{G_t P_t}{4\pi S_{avg}}}[m] \\ &= \sqrt{\frac{(15.85)\cdot(1W)}{(4\pi)(20W/m^2)}} \\ &= 0.25m \\ &= 25cm \end{aligned}$$

And the modified ranges are given by

$$\begin{aligned} P_r &= \frac{G_t G_r \lambda^2}{(4\pi R)^2} P_t \\ &= \frac{(15.85)\cdot(3.98)(0.1225m)^2}{(4\pi\cdot 0.25m)^2}\cdot(1W) \\ &= 95.91 \times 10^{-3} W \\ &\doteq 96mW \end{aligned}$$

$$
\begin{aligned}
P_r &= \frac{G_t G_r \lambda^2}{(4\pi R)^2} P_t \\
&= \frac{(15.85)\cdot(3.98)(0.1225m)^2}{(4\pi\cdot 1m)^2}\cdot(1W) \\
&= 5.99 \times 10^{-3} W \\
&\doteq 6mW
\end{aligned}
$$

Therefore, for this kind of radio link we have a range from ∼20dBm to ∼8dBm, 6dB more than the previous link with a transmitting antenna of lesser gain. Figure 4-25 shows these results.

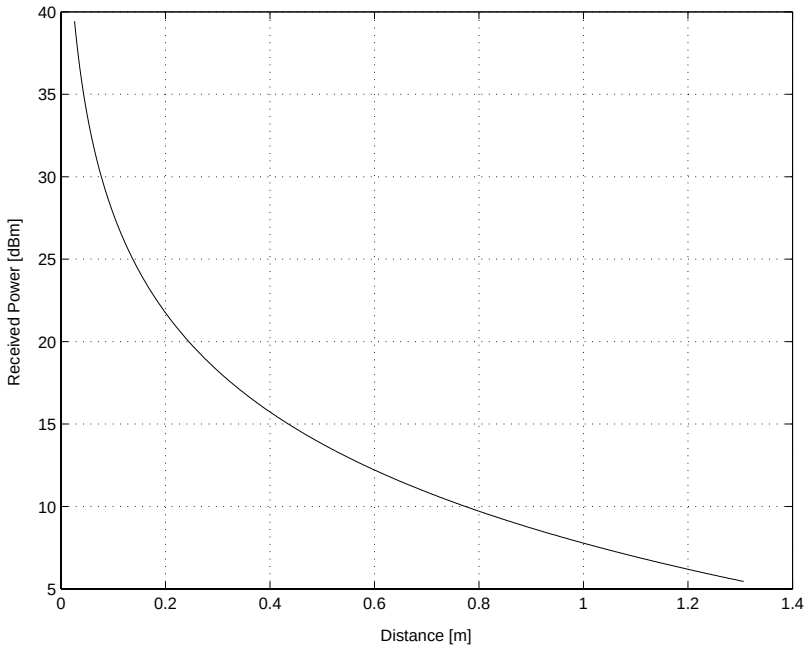

Figure 4-25: Radiolink performance for $P_{tx} = 30dBm$, $G_{tx} = 12dB$

4.3.1 Measured Link Data

The laboratory setup used to characterize the Radio Link is shown in 4-26. The physical length of the test cables restricted the laboratory test to $R_{max} = 40cm$. The amount of transmitted power was also restricted by the laboratory equipment, where the HP Function generator could only provide signal powers up to 20dBm. The

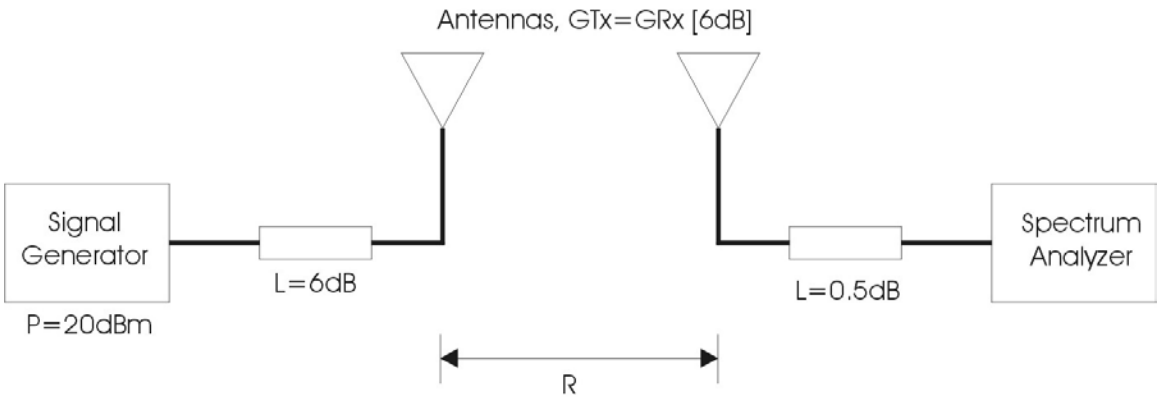

Figure 4-26: Block Diagram for the Power Link Test

obtained values for four fixed distances are summarized in table 4.9.

Distance [cm]	Expected Power [dBm]	Measured Power [dBm]
10	12	7
20	6	-2
30	3	-13
40	0	-7

Table 4.9: Measured and expected Powers for the experimental Radio Link

The Radiolink performance is poor compared to that expected from the theory obtained in 4.3. This can be due to several reasons. Attenuation effects are discarded because the laboratory environment is somewhat free of humidity and particles. One explanation could be that the radiation properties of the antennas used so far are not the expected ones, either these antennas have a lower gain than the expected 6dB value or the radiation efficiency for the FR4 material is very low. Another important consideration is the unexpected high attenuation of the transmitting cable, as shown in 4-26. Also, the radiation patterns of the antennas are broad, and multipath effects could exist that create destructive interference of the signals arriving at the antenna on the receiver's side. It is important to notice that phase plays an important role, this can be seen in the table 4.9 at $L = 30cm$, where we have read a minimum in the power level. For future improvements, a more complete radio link model analysis should be made, where phase delays and multipath are taken into consideration.

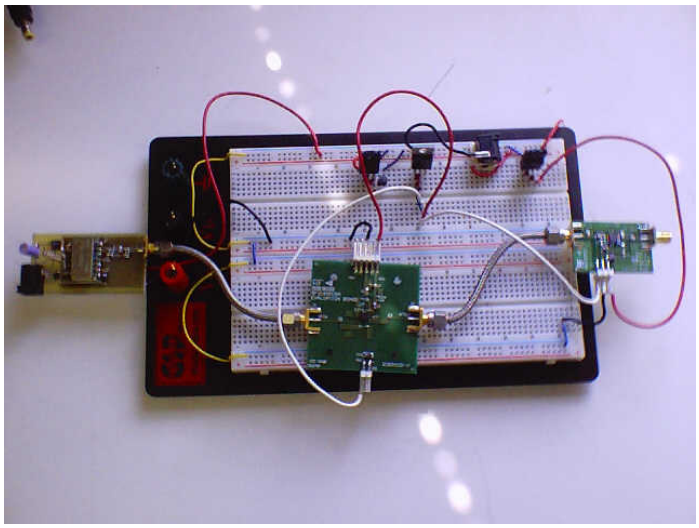

Figure 4-27: Actual Power Transmitter. From left to right: 2.45GHz tuned VCO, RF2189 medium power amplifier and RF2126 high power amplifier

4.3.2 Power Base Station

Using off-the-shelf components, a power station was assembled and tested. The actual transmitter is shown in figure 4-27. This high-gain, high-power base station generates a pure 2.45GHz 30dBm tone that is being broadcasted to the environment. As can be seen in 4-27, the power base station consists of three major elements: a Voltage Controlled Oscillator (VCO) from Mini Circuits® that generates the 2.45GHz tone. The RF2189 is a medium gain, medium power stage with a gain of 20dB and maximum power handling of 25dBm, and the final stage is an RF2126 medium gain, high power stage with 12dB small signal gain and maximum power handling of 31dBm. The manufacturer of both amplifiers is RF Micro Devices®. Both amplifiers also have power control pins that allow control of the gain in each section and also provide a shut-down mode. A microcontroller can make use of those pins to automatically control the power base station.

Chapter 5

Scenario Discussion

5.1 Interactive Necklace

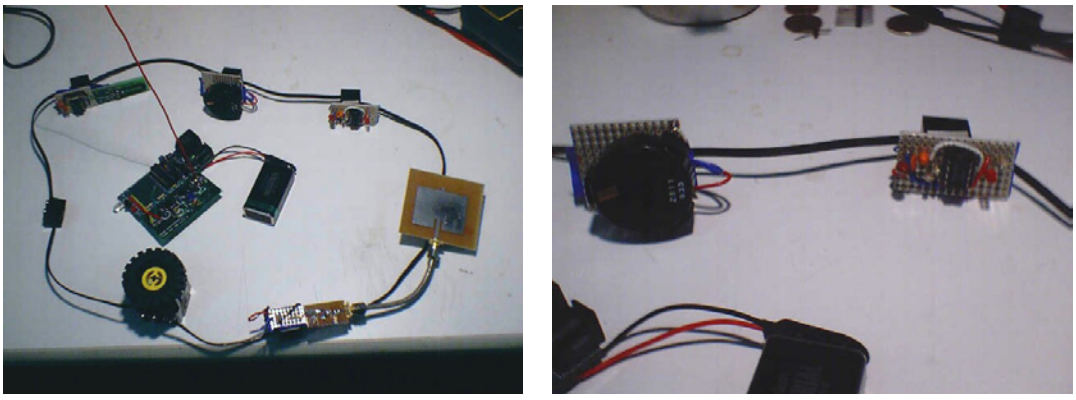

(a) Necklace v2.0 (b) Beads Detail

Figure 5-1: Interactive Necklace System v2.0

As a first application example for the proposed Wireless Transmission of Power discussed through the present dissertation, the platform known as the Interactive Necklace (figure 5-1) will be used. The first version of the necklace was designed by Ted Selker [35] in the year 1999 and consists of a group of electronic beads that make sound and turn lights on when a DC motor wheel is turned. This motor is present as another bead in the necklace. The DC motor provides the energy that the rest of the beads need to operate, so no batteries are present in the necklace. The main objective

is to implement a new series of beads that allow the necklace to have interactions with elements that may be present in the environment, whether they be other necklaces, computers, etc., and also that these external devices can somehow interact with the necklace itself, even at a physical level.

To achieve this objective, as a first step, an RF transmitter bead was implemented. Such transmitter is a modified version of the Tx99 v3.0 transmitter manufactured by Ming Microsystems; the modification was made by Mark Feldmeier [36] in the MIT Media Laboratory Responsive Environments Group. Such a transmitter works within the 300MHz band. Also, a base station was implemented using the RE-99 v3.0A 300MHz receiver from Ming Microsystems and an IRx board [37]. It was decided that, whenever there was activity in the necklace (i.e., the wheel was being turned) the base station would detect this, which gives a bit of information (activity/no-activity) that can be used for some applications. Images of both Transmitter and receiver electronics can be seen in figure 5-2.

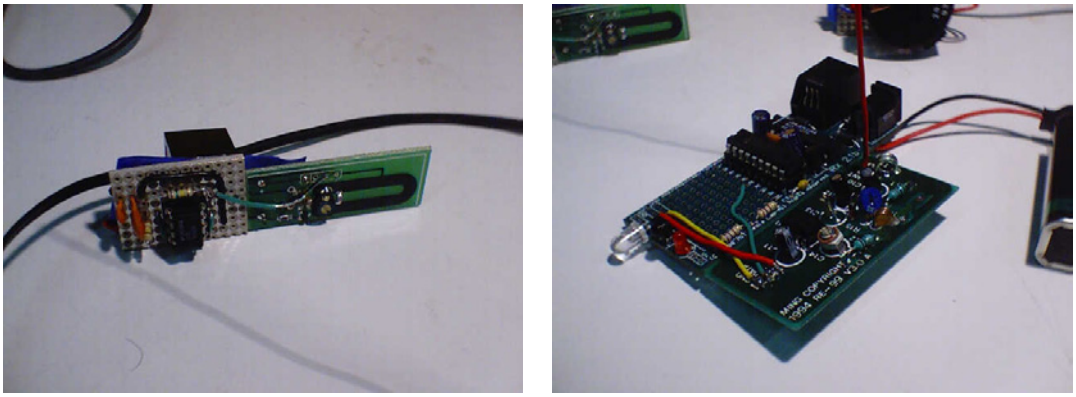

(a) 300MHz Transmitter Bead (b) 300MHz Receiver Station

Figure 5-2: Transmitter and Receiver pair used in the Interactive Necklace Scenario.

One of the intended new applications for the necklace is a basic Friend/Foe game implemented with a computer. This has the purpose of enhancing the social interactions of the necklace bearer, with the computer playing the role of another entity with whom to have interactions. The main idea of this game is that, whenever the necklace is activated in front of a friendly entity (Friend) there won't be any problems

in operating the necklace, this means that the torque of the DC motor wheel would be low; when the necklace is being activated in front of an unfriendly entity (Foe), the wheel will have a higher torque and thus become harder to spin for the user, indicating a certain degree of rejection.

From the electronic point of view, it can be explained like this: whenever there is a friendly entity present in front of the necklace, the impedance between the terminals of the DC motor will be high, thus allowing a normal operation of this DC voltage source. In the presence of a foe, this impedance has to be very low such that there is a short circuit between the motor DC terminals, which blocks the wheel and presents a higher torque. This electrical behavior was done using the circuit shown in 5-3

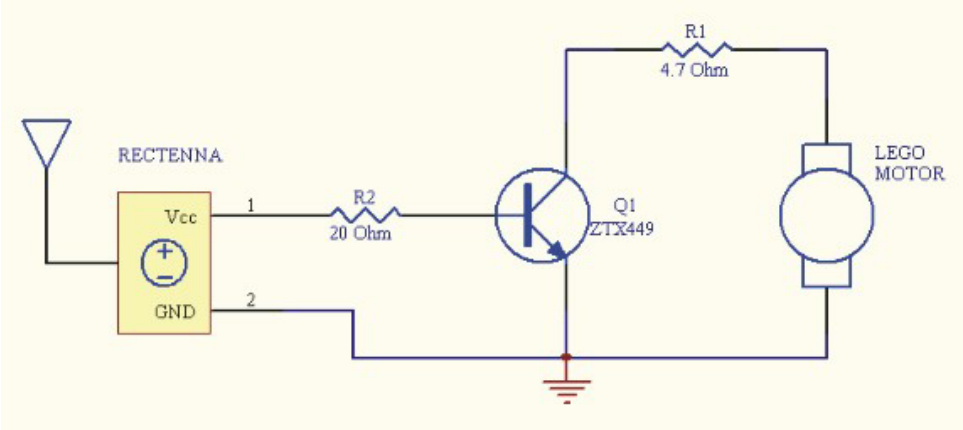

Figure 5-3: Electronic Switch Schematic

As one can see, the circuit is a very basic transistor-based electronic switch. The explanation of its operation follows. As long as there is no current present in the base of the transistor Q1, the Collector and Emitter will be operating in the Cutoff region, hence no current can circulate through them and the DC motor will see a high impedance that will not interfere with its normal operation. This only happens in a given spinning direction, due to the fact that the collector–emitter junction can be treated as a diode in the sense that current can just flow in one direction, collector–emitter, and not the other way around. This implies that the DC motor will now have a sort of polarity.

Now, when there's a current flowing through the transistor's base, the collector–

emitter junction enters into the Saturation region. This will make the motor terminals to be close to a zero volt potential, and now all the current from the DC motor will tend to flow through this new low impedance path which will automatically turn off all the associated electronics present in the necklace. There are also repercussions on the mechanical level, because the low impedance path will force the wheel to present a much higher torque than in the free operation state, thus for the user it will imply a sensible physical blockage (braking) of the wheel.

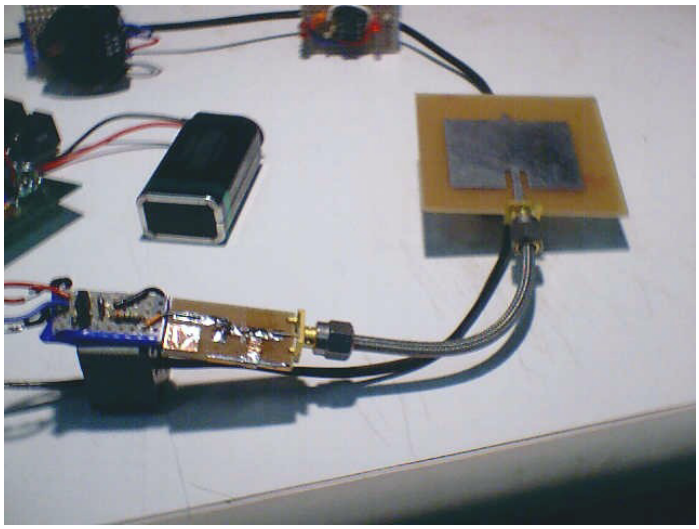

Figure 5-4: Rectenna Implemented in the Interactive Necklace.

The energy source that will power the transistor's base is the rectenna system that has been proposed and characterized in the present thesis. Due to the fact that the base–emitter junction turns on at 0.7V and the nature of such junction is basically a diode, this voltage will be constant. That implies that most of the power delivered from the rectenna to the transistor will be in the form of electrical current, which makes the rectenna a Power Controlled Current Source.

The free spinning of the motor (i.e. no load connected) generates peak voltages of about 18V, with associated peak currents of about 8mA, which means that the motor can deliver to a load as much as 144mW of power at maximum spinning. To provide a quantitative measurement of the switch operation, when the base-emitter junction voltage reaches 0.75V and the base current is about $700\mu A$, the motor's voltage performance is reduced about 60%, with output voltages of 2.5V and currents about

60mA. With base currents of about 3mA the voltage performance is further reduced to 90%, that is 1.8V at 85mA. In both cases, the mechanical equivalence is an increase of the motor's torque. From a qualitative point of view, the wheel is harder to turn when there's more current flowing into the transistor, compared to the open switch state (no base current flowing). It was observed that the maximum distance for power transmission where there still was a significant torque were 50cm.

The complete scenario is the following. The 300MHz base station connects to a host computer using the serial port and also to a 2.4GHz base station that provides the Wireless Power. When the necklace has the 300MHz transmitter attached to it, it generates a beacon that is detected by the base station, and this beacon is associated with the Foe state. Then the computer displays an alarm and a rejection message; also it activates the 2.4GHz wireless power source. The rectenna attached to the necklace then harvests the power from the wireless power source and thus blocks the necklace. After a programmable period of time (between 6 to 10 seconds) the base station deactivates the wireless power source and the computer presents to the user information available only to "New" Friends.

5.2 Wireless Sensors

The next step is to create a group of wireless and battery-less sensors that would be installed in different environments. This way, the sensors relay the information of the sensed variables, output can range from visual feedback using LEDs, audio feeback using buzzers, and other types of alarms. The sensors can even wirelessly relay the information to somewhere else.

The first example is a stapler sensor. The circuit is a low power CMOS 555 timer, programmed to generate a square signal of a fixed 10Hz frequency and 10% duty cycle. This signal is used to turn on or off an LED. The mechanism inside the stapler that pushes the staples forward is the mechanical switch of this system. A pair of connectors was placed inside the stapler, one on the front inner side of it and the other on the sliding piece of metal that pushes the staples. When the stapler runs out of

staples, both connectors make contact and the LED starts flashing, giving a visual feedback to the user that indicates a refill state. This flashing circuit drains power that can be as low as $500\mu W$, with $1V@500\mu A$ for assured operation. The power peaks present whenever the LED flashes, where the circuit drains $1.5mW$ $(1.5V@1mA)$. These low power levels can be easily handled by the designed rectenna. In a laboratory setup, the maximum observed distance where the sensor's LED stopped blinking were near 60cm when using the rectenna system as a power source. Figure 5-5 shows the complete Circuit Schematic.

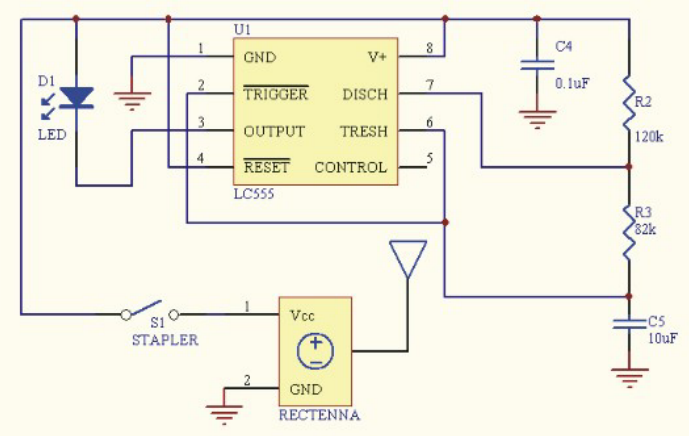

Figure 5-5: CMOS Timer implemented in the Staples Sensor

The same principle can be applied to a piezo-buzzer. The circuit is shown in figure 5-6. The power demand of such a circuit is extremely low, with an weak but audible tone starting at just about $225\mu W$ $(1V@225\mu A)$, reaching a high audible level at a mere $1.4mW$ $(2V@700\mu W)$. The maximum distance of operation with the rectenna as a feeding element was the longest one achieved from all the sensors, 80cm.

Another more elaborate sensor is a humidity sensor. This sensor is placed in a flowerpot, and it senses the humidity level of the soil. The sensor is basically a variable capacitor made with two copper electrodes separated by a hygroscopic material (special paper used to clean lenses). The complete Schematic is shown in 5-7(a). When the sensing capacitor is dry, the capacitance value is about 4-6pF; when the piece of paper that separates the electrodes is wet the value jumps to about 20-30pF. This capacitor is part of a tank circuit in the 300MHz transmitter

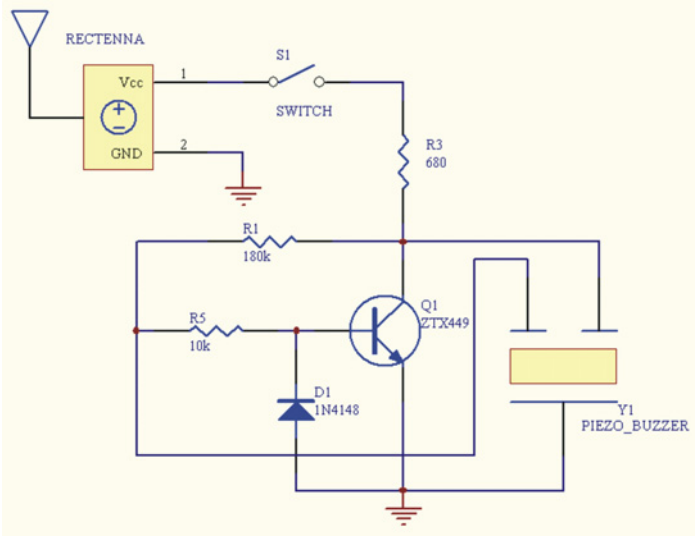

Figure 5-6: Piezo-buzzer circuit implemented

discussed previously. Thus when the sensor is dry, the tank circuit will be tuned to the desired frequency of 300MHz and the signal generated by the oscillator can be detected by a wireless station tuned to the same frequency. When the sensor is wet the frequency drops around 200MHz due to the higher capacitance value, and given the fact that the base station only can be tuned to detect signals around 290-310MHz, the generated beacon will not be detected. The base station can be programmed such that, whenever it detects the 300MHz beacon, a signal is sent to the host computer, using the IRx [37] 232 serial port or maybe other means, so it can alert the user about the state of the plant (i.e. sending the user a courtesy notice email).

Laboratory tests have shown that the 300MHz transmitter can operate as low as with $1.2V@1.5mA$, which means a power demand of $1.8mW$. The associated square wave generator (the same low-power CMOS timer used for the stapler) only drains $500\mu W$; taking both circuits into account, the transmitter needs only 2.3mW to operate. The rectenna system provided enough energy to make the circuit to work at a distance ranging up to 45 cm. At longer distances, the signal's level was so weak that the base station could not detect the beacon. This distance could be improved if the base station is designed to have a higher sensitivity.

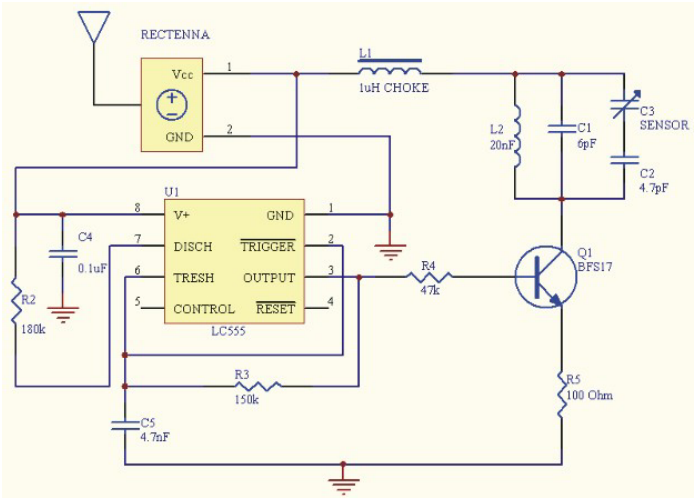

(a) Schematic Circuit

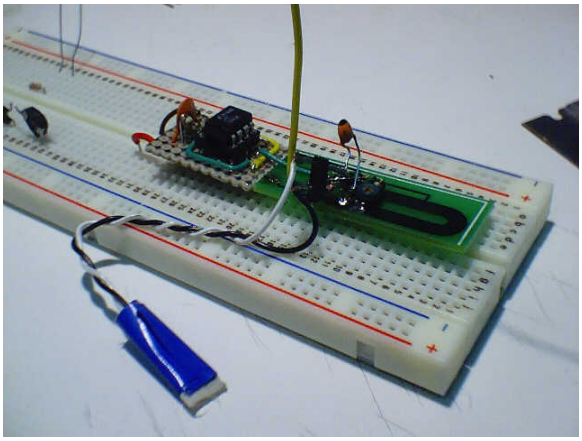

(b) Actual Sensor

Figure 5-7: Humidity Sensor.

Chapter 6

Conclusions

A Wireless Transmission of Power for Sensors (WTPS) system has been analyzed, discussed, designed, and tested in the present dissertation, to explore the idea of getting rid of cables and batteries.

First, a low profile antenna with compact size was designed, simulated and implemented. It was observed that the theoretical design procedure was straightforward; the simulations obtained from this design shown very acceptable performances in the frequency band of interest. In the implementation level, a manual tuning of the antenna had to be done to obtain the desired radiation properties at the frequency objective of 2.45GHz. A very simple procedure for tuning followed, where, with the addition of a small tuning flag, a direct control of the antenna's resonant frequency was obtained. The fine segmentation of this short tuning flag allowed precise frequency tuning, with an accuracy of a few megahertz.

Without the proper equipment and facilities to measure the radiation properties of the antenna, the design and testing relied entirely on other properties of the antenna such as Voltage Standing Wave Ratio (VSWR) and Input Impedance. The resulting measurements of these properties were more than satisfactory. In a qualitative way, the radiation properties were obtained for the microstrip antenna by means of a small laboratory radio link setup. It was observed that the FR4 material selected as the dielectric of the antenna had a poor radiation performance, presenting high radiation losses. Future improvements of the antenna can take this into account, and

other materials can be used, such as duroid or GML1000, to improve the radiation properties and thus obtaining better performance. It is important to note that if the substrate material is changed, the final design presented in this dissertation cannot be used and changes in the antenna's dimensions have to be made, following the procedure shown in section 3.1.

Little or no attention was paid to the associated ground plane of the antenna. Increasing its size will definitely improve the front-to-back ratio of the antenna, which can increase the endfire properties and provide higher gains in the direction of interest.

The theoretical radiation pattern presents a fan-beam shape, which is desired for the type of applications sought here, which have a set of sensors extended all over a wide area, with each sensor will be harvesting the incoming energy from a power base station. Nonetheless, a more directive antenna with a narrower beam could be used to concentrate more energy within a small area, thus having a high power density that the designed rectennas can convert to usable DC power. The use of such a directional antenna can add directionality to the WTPS system, hence certain applications that can take advantage of this property should have to be analyzed in any future work.

A 2.4GHz rectifier was also analyzed, designed, and implemented. Two different types of diode pairs were used. It was observed that, from the theoretical point of view, both diodes presented very similar rectification properties. In the coupling section, the obtained stub length values for the HSMS2852 were low, so their manual implementation in the lab presented certain complications that didn't allow a proper match to be achieved. On the other hand, the HSMS8202 diode pair had better performance in that sense. The stub lengths were acceptable, and in the lab bench, the match was achieved with very good results. The impedance match of both diodes was key when measuring their rectification properties. The HSMS8202 got the higher efficiencies, some of them above 70% as stated in 4.8. Note, however, that the diode entered into saturation with moderately high inputs (20dBm), which places a top boundary on the whole range of operation of the rectenna system.

A set of low-power circuits was also designed to serve as a test platform of the whole WTPS system. Very basic sensors where designed and implemented in common

environments, such as staplers and flowerpots. The information obtained from the sensors provided just one bit, but given the intended applications for these sensors, that proved to be enough to give the user meaningful information. More complex sensors can extent the capabilities of the WTPS system. A design of more evolved sensors can follow in the future, allowing more information to be extracted from the environment and thus gaining more complex knowledge of the sensors' surroundings. Because of the nature of the microwave power links, these sensors have to operate under low power conditions, hence a limit of $P < 5mW$ is suggested to take good advantage of the system presented in this dissertation.

Finally, the complete WTPS system was used to energize this set of sensors in a remote fashion, which was the primary objective of the system. The maximum distances obtained in lab tests ($\leq 1m$) certainly were less than those expected in theory. This could be explained given the very basic link model that was used, where multipath effects and fading due to elements in the line-of-sight were not taken into account. A more complex model that considers all these effects can be realized and used to predict the real performance of a system like the WTPS.

6.1 Future Work

Every day more information is going into computational systems. Accordingly, information coming from sensors deployed in the external world is in high demand, and such sensor systems can help the computer to make important decisions on what the user needs are. By following somewhat complex rules and user-task models, computers can become more aware of their context and also the user's context as well. To obtain reliable user task models, the sensors have to be simple yet provide useful information to the system.

If one thinks about the possible future of a wireless power system like the one presented in this dissertation, the possibilities appear attractive when focused on electronic sensors systems. First, one could think of a world where low power batteries, like the coin-cell type ones, have evolved in a way such that there is no need

to replace them. They could become permanent recharging batteries thanks to an existing wireless power source in the surroundings. This has important repercussions in different fields; from an economic point of view there would be no need to buy new batteries, and from the environmental point of view less disposed batteries mean less pollution and less poisonous materials exposed to Nature.

Also, getting rid of cables is an attractive option for the automotive industry. Current research and discussions with representatives in the field have expressed their interest in using wireless power to feed the electronic door switches of an automobile. In an enclosed space, such as an automobile's door, the electromagnetic fields could certainly be more easily guided to the area of interest, thus allowing larger concentrations of energy within the rectenna's area and, as a consequence, better performance can be achieved for not only activating door switches, but for possibly allowing the existence of sensors inside the door that can provide useful information to the user. As a few examples of this concept are door temperature sensors that could help regulate the driver's environment and water sensors that could trigger the side windows when it is raining.

It would also be interesting to explore the idea of an array of power transmitters, such that within a specific area, a uniform power distribution can be obtained. This idea can be applied in household environments or even in office environments. For example, to have entire walls covered with power transmitters (or even floor mats) could provide a good platform to power and implement sensors in diverse low-tech devices like chairs and tables [38].

The WTPS system could extend the capabilities of modern RFID systems, allowing more active electronics to be embedded in different appliances that could extent their native capabilities and thus provide a test-bed for future more complex Context Aware Spaces. Right now, RFID systems do not have the capabilities of enabling active electronics to perform common tasks because of the low power levels involved. By creating sounds with off-the-shelf components, by having visual feedback with lights and, even more, by having active sensorial systems relaying the information they generate one can envision a first step towards a new extended RFID system.

It must be noted that various obstacles exist to this scenario, including a public that (justified or not) is very wary of the low power levels coming from cell phones, power lines, and microwave oven leakage.

Bibliography

[1] H Hertz. Dictionary of scientific biography. New York: Scribner, 340-349.

[2] J. J. O'Neill. Prodigal genius – the life of nikola tesla, 1944. New York: Washburn.

[3] M. Cheney. *Tesla, Man Out of Time*. Prentice Hall, Englewood Cliffs, NJ, 1981.

[4] Robert Buderi. *The Invention That Changed the World : How a Small Group of Radar Pioneers Won the Second World War and Launched a Technical Revolution*. Touchstone Books, March 1998.

[5] K.V.S. Rao. An overview of back scattered radio frequency identification systems (RFID). *IEEE Transactions*, pages 746–749, 1999.

[6] W.C. Brown. *The History of Power Transmission by Radio Waves*, volume MTT-32 no 9. IEEE Press, Sept 1984.

[7] G. Goubau and F. Schwering. On the guided propagation of electromagnetic wave beams. *IRE Trans. Antennas Propagat.*, Vol. AP-9:248–256, May 1961.

[8] H . Kogelnik and T. Li. Laser beams and resonators. *Proc. IEEE*, Vol. 54 no. 10, Oct 1966.

[9] Raytheon. Electronic and mechanical improvement of the receiving terminal of a free-space microwave power transmission system. Raytheon Contractor Rep. PT 4964, CR-135194, Aug. 1977.

[10] IEEE Standards Board. IEEE standard for safety levels with respect to human exposure to radio frequency electromagnetic fields, 3kHz to 300GHz. Technical Report IEEE C95.1-1992, IEEE Standards Coordinating Committee 28, 1992.

[11] Eleanor R. Adair. Biological effects of radio-Frequency/Microwave radiation. *IEEE Transactions On Microwave Theory And Techniques*, Vol. 50, No. 3:953–962, March 2002.

[12] James J. and P.S. Hall. *Handbook of Microstrip Antennas*. Peter Peregrinus, 1989.

[13] D.M. Pozar. Considerations for millimeter wave printed antennas. *IEEE Trans. on Antennas and Propagation*, AP-31:740–747, 1983.

[14] Y.T. Lo Richards W.F. and D.D. Harrison. An improved theory for microstrip antennas and applications. *IEEE Transactions on Antennas and Propagation*, AP-29:38–46, 1981.

[15] D. Solomon Y. T. Lo and W.F. Richards. Theory and experiment on microstrip antennas. *IEEE Trans. on Antennas and Propagation*, AP-27:137–145, 1979.

[16] Jin Au Kong. *Electromagnetic Wave Theory*. EMW Publishing, 2000.

[17] E.O. Hammerstad. Equations for microstrip circuit design. *5th European Microwave Conference*, pages 268–272, 1975.

[18] M. Kara. The resonant frequency of rectangular microstrip antenna elements with various substrate thicknesses. *Microwave and Opt. Technol. Lett.*, vol 11:55–59, 1996.

[19] D.R. Jackson and N.G. Alexopoulos. Simple approximate formulas for input resistance, bandwidth and efficiency of a resonant regular patch. *IEEE Trans. on Antennas and Propagation*, Vol. AP-39:407–410, 1991.

[20] Perlmutter P. Shritkman S. and D. Treves. Electric surface current model for the analysis of microstrip antennas with application to rectangular elements. *IEEE Trans. on Antennas and Propagation*, AP-33:301–311, 1985.

[21] M. Kara. Calculation of the radiation patterns of rectangular microstrip antenna elements with various substrate thicknesses. *Microwave and Optical Technol. Letters*, Vol. 13:221–226, 1996.

[22] D. Thoroude. CAD-oriented cavity model for rectangular patches. *Electron. Lett.*, Vol. 13:842–844, 1990.

[23] D.M. Pozar. Rigorous closed-form expressions for the surface wave loss of printed antennas. *Eletronic Letters.*, Vol. 26:954–956, 1990.

[24] Ramesh Garg. *Microstrip Antenna Design Handbook*. Artech House, 2001.

[25] M. Kara. Formulas for the computation of the physical properties of rectangular microstrip antenna elements with various substrate thicknesses. *Microwave and Opt. Technol. Lett.*, Vol 12:234–239, 1996.

[26] Agilent Technologies. Designing the virtual battery. Technical Report Application Note 1088, Aggilent Technologies, 1999.

[27] Ansoft Ensemble SV. Maxwell 2d ver. 2.0.57. http://www.ansoft.com.

[28] Agilent Technologies. Designing detectors for RF/ID tags. Technical Report Application Note 1089, Agilent Technologies, 1999.

[29] Agilent Technologies. Impedance matching techniques for mixers and detectors. Technical Report Application Note 963, Agilent Technologies, 1999.

[30] Agilent Technologies. The zero bias schottky detector diode. Technical Report Application Note 969, Agilent Technologies, 1999.

[31] R. Boylestad and L. Nashelsky. *Electronic Devices and Circuit Theory*. Prentice-Hall, 1987.

[32] W.C. Brown. An experimental low power density rectenna. *IEEE MTT-S Digest*, April:197–200, 1991.

[33] Federal Communications Commission Office of Engineering & Technology. Questions and answers about biological effects and potential hazards of radiofrequency electromagnetic fields, OET bulletin 56 Fourth Edition August 1999.

[34] Constantine Balanis. *Antenna Theory: Analysis and Design*. Bk & Dk 2^{nd} edition, May 1996.

[35] Ted Selker and Win Burleson. Context-aware design and interaction in computer systems. *IBM Systems Journal*, Vol. 39, no. 3 & 4, 2000.

[36] Mark Feldmeier and Joe Paradiso. Ultra-low-cost wireless motion sensor for musical interaction with very large groups. *UBICOMP 2001 Workshop on Designing Ubiquitous Computing Games*, ACM UBICOMP Conference Proceedings, 2001.

[37] Rob Poor. irx2 prototyping board programming seminar. http://web.media.mit.edu/ r/projects/picsem/.

[38] E. Arroyo W. Burleson, T. Selker. Chameleon tables: Using context information in everyday objects. *Conference on Human Factors in Computing Systems*, Extended Abstracts:580–581, 2002.

[39] Agilent Technologies. Surface mount microwave schottky mixer diodes. Technical Report Technical Data HSMS–820x Series, Agilent Technologies, 2001.

[40] Matthew M. Radmanesh. *Radio Frequency and Microwave Electronics*. Prentice Hall, 2001.

[41] Agilent Technologies. Surface mount RF schottky diodes. Technical Report Technical Data HSMS–282x Series, Agilent Technologies, 2000.

[42] Association of the Automatic Identification and Data Capture Industry. Draft paper on the characteristics of RFID systems. Technical Report AIM FF 2000:001, AIM Frequency Forums, 2000.

[43] Agilent Technologies. Square law and linear detection. Technical Report Application Note 986, Agilent Technologies, 1999.

[44] Agilent Technologies. Surface mount zero bias schottky detector diodes. Technical Report Technical Data HSMS–285x Series, Agilent Technologies, 1999.

[45] Dong-Gi Youn. A study of the fundamental transmission experiment for wireless power transmission system. *IEEE TENCON*, pages 1419–1422, 1999.

[46] A. Papiernik S. Drabowitch. *Modern Antennas*. Chapman & Hall, 1998.

[47] J. Kymissis C. Kendall J. Paradiso and N. Gershenfeld. Parasitic power harvesting in shoes. *Proc. of the Second IEEE International Conference on Wearable Computing, (ISWC)*, IEEE Computer Society Press:132–139, 1998.

[48] David Pozar. *Microwave Engineering*. John Wiley & Sons, 1997.

[49] David Pozar. *Microstrip Antennas : The Analysis and Design of Microstrip Antennas and Arrays*. IEEE, July 1995.

[50] W.C. Brown. Beamed microwave power transmission and its applications to space. *IEEE Transactions on Microwave Theory and Techniques*, Vol 40 no 6:1239–1250, June 1992.

[51] David K Cheng. *Field and Wave Electromagnetics*. Addison-Wesley, 1989.

[52] Paul Horowitz. *The Art of Electronics*. Cambridge University Press 2^{nd} edition, 1989.

[53] John Kraus. *Antennas*. McGraw Hill 2^{nd} edition, 1988.

[54] W.C. Brown. Experiments involving a microwave beam to power and position a helicopter. *IEEE transactions Aerosp. Electron. Sys.*, AES-5:692–702, 1969.